

TABLE OF CONTENTS

RÉSUMÉ	i
ABSTRACT	iv
ACKNOWLEDGMENTS	vii
TABLE OF CONTENTS	viii
LIST OF FIGURES	xi
LIST OF TABLES	xvi
CHAPTER 1	
DEFINING THE PROBLEM	1
1.1 INTRODUCTION	2
1.2 OBJECTIVES	8
CHAPTER 2	
REVIEW OF THE LITERATURE	9
2.1 ALUMINUM-SILICON ALLOYS	10
2.1.1 Al-Si-Cu Alloy System	13
2.2 SOLIDIFICATION OF Al-Si-Cu 319-TYPE ALLOYS	14
2.3 ROLE OF MODIFICATION	15
2.4 ROLE OF MAGNESIUM	20
2.5 INTERMETALLIC PHASES IN Al-Si-Cu ALLOYS	23
2.5.1 Copper Intermetallic Phases	23
2.5.2 Iron Intermetallic Phases	26
2.6 HEAT TREATMENT OF Al-Si-Cu ALLOYS	28
2.6.1 Solution Heat Treatment	28
2.6.2 Quenching	33
2.6.3 Precipitation Heat Treatment (Aging)	33

2.6.4 Incipient Melting	34
2.7 POROSITY	35
2.7.1 Theory of Porosity Formation	35
2.8 MECHANICAL PROPERTIES OF Al-Si ALLOYS	37
2.8.1 Hardness Testing	38
2.8.2 Impact Testing	40
2.8.2.1 Effect of Sample Configuration	43
CHAPTER 3	
EXPERIMENTAL PROCEDURES	47
3.1 INTRODUCTION	48
3.2 ALLOY PREPARATION AND MELTING PROCEDURE	48
3.3 MELTING AND CASTING PROCEDURES	51
3.4 SOLUTION HEAT TREATMENT AND AGING	54
3.5 MECHANICAL TESTING	55
3.5.1 Hardness Testing	55
3.5.2 Impact Testing	56
3.6 METALLOGRAPHY AND MICROSTRUCTURAL EXAMINATION	58
CHAPTER 4	
MICROSTRUCTURE AND HARDNESS OF 319-TYPE	
Al-Si-Cu-Mg ALLOYS	61
4.1 EFFECT OF MODIFICATION	63
4.2 EFFECT OF MAGNESIUM	65
4.3 COMBINED EFFECTS OF MAGNESIUM WITH STRONTIUM	66
4.4 EFFECT OF COOLING RATE	67
4.5 EFFECT OF HEAT TREATMENT	68
4.6 EFFECT OF INTERMETALLIC PHASES	69
4.7 RESULTS AND DISCUSSION	75
4.7.1 Microstructural Analysis	75

4.7.2 Porosity Characteristics	90
4.7.3 Hardness	91
CHAPTER 5	
IMPACT TOUGHNESS AND FRACTOGRAPHY OF 319-TYPE Al-Si-Cu-Mg ALLOYS	105
5.1 EFFECTS OF SAMPLE CONFIGURATION	106
5.2 EFFECTS OF MODIFICATION	107
5.3 EFFECTS OF MAGNESIUM	109
5.4 COMBINED EFFECTS OF MAGNESIUM WITH STRONTIUM	110
5.5 EFFECTS OF COOLING RATES	110
5.6 EFFECTS OF HEAT TREATMENT	113
5.7 EFFECTS OF INTERMETALLIC PHASES	114
5.8 RESULTS AND DISCUSSION	116
5.8.1 Impact Toughness	116
5.9 PRECIPITATION PROCESSES	139
5.10 FRACTOGRAPHY RESULTS	142
5.10.1 Secondary Electron Beam Imaging (SEM Fractography)	142
5.10.2 Backscattered Imaging	151
CHAPTER 6	
CONCLUSIONS	157
RECOMMENDATIONS FOR FUTURE WORK	162
REFERENCES	163

LIST OF FIGURES

CHAPTER 2

Figure 2.1	Part of the Al-Si phase diagram showing composition ranges for various alloy types.	11
Figure 2.2	Rating system for a modified microstructure.	17
Figure 2.3	Depression of the eutectic temperature as a function of magnesium level for unmodified and strontium-modified Al-Si alloys.	21
Figure 2.4	Dark spots observed on the fracture surfaces of test bars of a 319 + 0.5 wt% Mg alloy, solutionized for (a) 12h/510°C, and (b) 12h/520°C. Arrows show the progress in the size of the dark spot.	23
Figure 2.5	(a) Microstructure of a sample from 319.1 alloy: (1) β -Al ₅ FeSi, (2) blocky Al ₂ Cu phase, (3) Al ₅ Mg ₈ Cu ₂ Si ₆ phase, (4) acicular Si phase; (b) secondary electron image of 319 alloy showing the eutectic Al-Al ₂ Cu phase.	24
Figure 2.6	Backscattered image showing the dissolution process of Al ₂ Cu particles in 319 alloys after 8h solution heat treatment at 505°C: (1) separation of the Al ₂ Cu particles from the β -Al ₅ FeSi platelets, (2) necking of the Al ₂ Cu particles, (3) spheroidization of Al ₂ Cu and reduction in the size of Al ₂ Cu fragments.	26
Figure 2.7	Micrographs taken of a 319 alloy automotive component showing: (a) Si particles and (b) Cu-rich phase segregation in the as-cast condition; (c) Si particles and (d) Cu-rich phase segregation after single-step solution treatment; and (e) Si particles and (f) remnants of Cu-rich phases after two-step solution treatment.	32
Figure 2.8	Microstructure of 319 alloy showing the occurrence of incipient melting taking place at grain boundaries.	35
Figure 2.9	The growth process of porosity formation.	37
Figure 2.10	Schematic diagram of Brinell hardness test.	39
Figure 2.11	Typical tension stress-strain curve.	41
Figure 2.12	An idealized load-time trace for an impact Charpy V-notch specimen.	42
Figure 2.13	Schematic representation of relationship between load and time in Charpy impact test. M: Maximum load; I: Crack initiation impulse; II: Crack propagation impulse; OM': Crack initiation time; M'F: Crack propagation time.	43
Figure 2.14	Load-time relationship for Φ -notch and U-notch specimens.	44
Figure 2.15	Dimensions of Charpy test specimens.	45

CHAPTER 3

Figure 3.1	Furnace used for preparing experimental alloys.	50
Figure 3.2	Star-like metallic mold used to prepare impact test bars.	53

Figure 3.3	L-shaped metallic mold used to prepare impact test bars.	54
Figure 3.4	Brinell hardness tester used for hardness measurements.	56
Figure 3.5	Charpy unnotched impact specimen (all dimensions in mm).	56
Figure 3.6	A computer-aided instrumented SATEC SI-1D3 Universal Impact Testing Machine, with a Dynatup IPM/PC impact testing system for data acquisition.	57
Figure 3.7	Optical Microscope - Clemex Image Analyzer system.	60

CHAPTER 4

Figure 4.1	Optical micrographs showing various common iron-containing intermetallics (arrowed) and their typical morphologies in Al-5%Si-1%Cu-0.5%Mg-(Fe) alloys: (a) β -Al ₅ FeSi platelets, (b) script-like α -Al ₈ Fe ₂ Si, (c) π -Al ₈ Mg ₃ FeSi ₆ phase growing from β and (d) script-like π -phase.	74
Figure 4.2	SEM backscattered-electron image of as-cast Sr-modified 603 alloy showing the close association sometimes observed between π -Al ₈ Mg ₃ FeSi ₆ and β -Al ₅ FeSi.	75
Figure 4.3	Optical microstructures observed in D1 experimental base alloy samples obtained from star-like mold castings: (a) as-cast D1 alloy, (b) Sr-modified DS1 alloy, (c) SHT D1 alloy and (d) SHT and Sr-modified DS1 alloy.	77
Figure 4.4	Optical microstructures observed in D6 experimental alloy samples obtained from star-like mold castings: (a) as-cast D6 alloy, (b) Sr-modified DS6 alloy, (c) SHT D6 alloy and (d) SHT and Sr-modified DS6 alloy.	80
Figure 4.5	Optical microstructures observed in D7 industrial alloy samples obtained from star-like mold castings: (a) as-cast D7 alloy, (b) Sr-modified DS7 alloy, (c) SHT D7 alloy and (d) SHT and Sr-modified DS7 alloy.	83
Figure 4.6	Optical microstructures observed in D8 industrial alloy samples obtained from star-like mold castings: (a) as-cast D8 alloy, (b) Sr-modified DS8 alloy, (c) SHT D8 alloy and (d) SHT and Sr-modified DS8 alloy.	84
Figure 4.7	Optical microstructures observed in LD1 experimental base alloy samples obtained from L-shaped mold castings: (a) as-cast LD1 alloy, (b) Sr-modified LDS1 alloy, (c) SHT LD1 alloy and (d) SHT and Sr-modified LDS1 alloy.	85
Figure 4.8	Optical microstructures observed in LD6 experimental alloy samples obtained from L-shaped mold castings: (a) as-cast LD6 alloy, (b) Sr-modified LDS6 alloy, (c) SHT LD6 alloy and (d) SHT and Sr-modified LDS6 alloy.	86

Figure 4.9	Optical microstructures observed in LD7 industrial alloy samples obtained from L-shaped mold castings: (a) as-cast alloy LD7, (b) Sr-modified alloy LDS7, (c) SHT alloy LD7 and (d) SHT and Sr-modified alloy LDS7.	87
Figure 4.10	Magnified micrographs of the regions marked 1, 2, and 3 in Figure 4.9(d) of SHT Sr-modified LDS7 showing an ultrafine β -Al ₅ FeSi platelets in (1), ultrafine Si particles within the Al ₂ Cu eutectic phase in (2), and fine remnants of mostly dissolved π -Al ₈ Mg ₃ FeSi ₆ phase.	88
Figure 4.11	Optical microstructures observed in LD8 industrial alloy samples obtained from L-shaped mold castings: (a) as-cast LD8 alloy, (b) Sr-modified LDS8 alloy, (c) SHT LD8 alloy and (d) SHT and Sr-modified LDS8 alloy.	89
Figure 4.12	Hardness of T6-tempered experimental 319 alloys (aging temperature 180°C) as a function of aging time, using the star-like mold samples: (a) non-modified alloys, and (b) Sr-modified alloys.	95
Figure 4.13	Hardness of T6-tempered experimental 319 alloys (aging temperature 180°C) as a function of aging time, using the L-shaped mold samples: (a) non-modified alloys, and (b) Sr-modified alloys.	96
Figure 4.14	Hardness of T7-tempered experimental 319 alloys (aging temperature 220°C) as a function of aging time, using the star-like mold samples: (a) non-modified alloys, and (b) Sr-modified alloys.	98
Figure 4.15	Hardness of T7-tempered experimental 319 alloys (aging temperature 220°C) as a function of aging time, using the L-shaped mold samples: (a) non-modified alloys, and (b) Sr-modified alloys.	99
Figure 4.16	Hardness of T6-tempered industrial non-modified and Sr-modified 319 alloys (aging temperature 180°C) as a function of aging time for: (a) star-like mold samples, and (b) L-shaped mold samples.	100
Figure 4.17	Hardness of T7-tempered industrial non-modified and Sr-modified 319 alloys (aging temperature 220°C) as a function of aging time for: (a) star-like mold samples, and (b) L-shaped mold samples.	101
Figure 4.18	Schematic of the structures observed at the aging peak (coherent fine precipitates) and in the valley between two peaks (incoherent coarse precipitates): (1) first GP zone for phase 1; (2) coherent structure of phase 1; (3) incoherent structure of phase 1; (4) coherent structure of phase 2 and incoherent structure of phase 1; and (5) incoherent structure of both phases 1 and 2.	103

CHAPTER 5

Figure 5.1	Impact strength of strontium-treated 413 alloy; as-cast ● and heat-treated ■ (13 hours/538°C and water quenched).	108
Figure 5.2	The effects of solidification time on the load-time relationship in the AC4C (356) and AC2B (B319) alloys (T6 treatment).	111

Figure 5.3	Impact toughness of eutectic Al-Si alloy as a function of Sr-content and solidification time.	112
Figure 5.4	Total absorbed energy of experimental alloys in the T6-tempered condition (aging temperature 180°C): (a) non-modified alloys, and (b) Sr-modified alloys (samples obtained from the star-like mold).	120
Figure 5.5	Total absorbed energy of experimental alloys in the T6-tempered condition (aging temperature 180°C): (a) non-modified alloys, and (b) Sr-modified alloys (samples obtained from the L-shaped mold).	121
Figure 5.6	Undissolved Al ₂ Cu in solution heat-treated alloys: (a) alloy D1, (b) alloy LD1, (c) Sr-modified alloy DS1, and (d) Sr-modified alloy LDS1.	123
Figure 5.7	Total absorbed energy of experimental alloys in the T7-tempered condition (aging temperature 220°C): (a) non-modified alloys, and (b) Sr-modified alloys (samples obtained from the star-like mold).	126
Figure 5.8	Total absorbed energy of experimental alloys in the T7-tempered condition (aging temperature 220°C): (a) non-modified alloys, and (b) Sr-modified alloys (samples obtained from the L-shaped mold).	127
Figure 5.9	Crack initiation energy of experimental alloys in the T6-tempered condition (aging temperature 180°C): (a) non-modified alloys, and (b) Sr-modified alloys (samples obtained from the star-like mold).	130
Figure 5.10	Crack initiation energy of experimental alloys in the T6-tempered condition (aging temperature 180°C): (a) non-modified alloys and (b) Sr-modified alloys (samples obtained from the L-shaped mold).	131
Figure 5.11	Crack initiation energy of experimental alloys in the T7-tempered condition (aging temperature 220°C): (a) non-modified alloys and (b) Sr-modified alloys (samples obtained from the star-like mold).	132
Figure 5.12	Crack initiation energy of experimental alloys in the T7-tempered condition (aging temperature 220°C): (a) non-modified alloys, and (b) Sr-modified alloys (samples obtained from the L-shaped mold).	133
Figure 5.13	Impact toughness energy (total absorbed energy, E _t , and crack initiation energy, E _i) in industrial alloys after T6-temper treatment (180°C): (a) non-modified alloys, and (b) Sr-modified alloys (star-like mold samples).	135
Figure 5.14	Impact toughness energy (total absorbed energy, E _t , and crack initiation energy, E _i) in industrial alloys after a T6-temper treatment (180°C): (a) non-modified alloys, and (b) Sr-modified alloys (L-shaped mold samples).	136
Figure 5.15	Impact toughness energy (total absorbed energy, E _t , and crack initiation energy, E _i) in industrial alloys after a T7-temper treatment (220°C): (a) non-modified alloys, and (b) Sr-modified alloys (star-like mold samples).	137

- Figure 5.16 Impact toughness energy (total absorbed energy, E_t , and crack initiation energy, E_i) in industrial alloys after a T7-temper treatment (220°C): (a) non-modified alloys, and (b) Sr-modified alloys (L-shaped mold samples). 138
- Figure 5.17 Fracture surface of : (a) D1 alloy, (b) LD1 alloy, and (c) LD1 alloy at high magnification. 143
- Figure 5.18 Fracture surface of DS1 alloy: (a) general view, (b) high magnification view, and (c) EDS spectrum corresponding to (b). 144
- Figure 5.19 Fracture surface of LDS1 alloy showing: (a) crack initiation area, and (b) crack propagation across the sample surface. Note the presence of the secondary crack (arrowed) in (b). 145
- Figure 5.20 Fracture surfaces of D6 alloy showing: (a) crack initiation area, (b) crack propagation across the sample, and (c) fracture of an Al_2Cu particle. 146
- Figure 5.21 Fracture surface of LD6 alloy showing: (a) crack initiation area, (b) crack propagation across the sample, and (c) fracture of Q-phase. 147
- Figure 5.22 Fracture surface of D6 alloy showing: (a) crack initiation area, (b) fracture of Q-phase, and (c) EDS spectrum corresponding to (b). 148
- Figure 5.23 Fracture surface of LDS6 alloy showing: (a) crack initiation area, (b) fracture of a mixture of Q- and π - phase particles, and (c) EDS spectrum corresponding to (b). 149
- Figure 5.24 Fracture surfaces of T7-tempered alloys: (a) D1, (b) LD1, (c) DS1, and (d) LDS1 alloys. 150
- Figure 5.25 Fracture surfaces of T7-tempered alloys: (a) D6, (b) LD6, (c) DS6, and (d) LDS6 alloys. Note the difference in the size of Si particles in (a) and (b), corresponding to high and low cooling rates. 151
- Figure 5.26 Backscattered image of the fracture surface of the D1 alloy sample: (a) general view; arrow points the presence of Al_2Cu particles, and (b) corresponding EDS spectrum. 152
- Figure 5.27 Backscattered image of the fracture surface of the DS1 alloy sample: (a) general view; arrows point to massive areas of Al_2Cu , and (b) corresponding EDS spectrum. 152
- Figure 5.28 Backscattered image of the fracture surface of the D6 alloy sample: (a) general view, and (b) EDS spectrum of Q-phase particle (arrowed) observed in (a). 153
- Figure 5.29 Backscattered images of the fracture surface of the DS6 alloy sample showing: (a) crack initiation area, (b) crack propagation; arrow shows the fracture of the π -phase, (c) EDS spectrum corresponding to (a), and (d) EDS spectrum corresponding to (b). 154
- Figure 5.30 Backscattered images of the fracture surface of the: (a) LD6 alloy sample showing β -Fe platelets, (b) LDS6 alloy sample showing precipitation of π -phase (solid arrow) together with undissolved Mg_2Si (broken arrows), and (c) EDS spectrum corresponding to Mg_2Si . 155

LIST OF TABLES

CHAPTER 2

Table 2.1	Classification of aluminum casting alloys.	12
Table 2.2	Chemical composition of 319 alloys (wt %).	14
Table 2.3	Sequence of phase precipitation in hypoeutectic Al-Si alloys.	15

CHAPTER 3

Table 3.1	Chemical composition of the industrial B319 alloy.	49
Table 3.2	List of the alloys used in the present work and their respective codes.	49
Table 3.3	Average chemical composition (wt%) of the experimental alloys and industrial alloys studied.	51
Table 3.4	Grinding and polishing procedures for metallographic samples.	59

CHAPTER 4

Table 4.1	Silicon particles measurements for the D1 experimental alloy using the star-like mold (24 μm DAS).	76
Table 4.2	Silicon particles measurements for the LD1 experimental alloy using the L-shaped mold (50 μm DAS).	78
Table 4.3	Silicon particles measurements for the D7 industrial alloy using the star-like mold.	78
Table 4.4	Silicon particles measurements for the LD7 industrial alloy using the L-shaped mold.	79
Table 4.5	Porosity measurements for the as-cast alloys using the star-like mold.	91
Table 4.6	Porosity measurements for the as-cast alloys using the L-shaped mold.	91
Table 4.7	Hardness of the as-cast experimental and industrial 319 alloys.	93

CHAPTER 5

Table 5.1	Total absorbed energy of the as-cast experimental and industrial 319 alloys.	117
Table 5.2	Crack initiation energy of the as-cast experimental and industrial 319 alloys.	118
Table 5.3	Volume fraction of Al_2Cu (%) for the base alloy.	124
Table 5.4	Age-hardening behavior of Al-Si-Cu-Mg alloys.	140

CHAPTER 1

DEFINING THE PROBLEM

CHAPTER 1

DEFINING THE PROBLEM

1.1 INTRODUCTION

Aluminum-silicon alloys are popularly used for a wide range of applications. These alloys are characterized by their low specific gravity, low melting point, negligible gas solubility (with the exception of hydrogen), excellent castability, and good corrosion resistance; such characteristics thus make them excellent candidates for the type of applications mentioned below. Also, because of their high strength-to-weight ratio, high wear resistance, high reflectivity, and excellent conductivity of heat and electricity, aluminum alloys are now widely used in numerous areas, particularly in the automobile, marine, and aerospace industries.

Aluminum alloys can generally be classified into two categories: wrought alloys and casting alloys. Aluminum casting alloys constitute a group of cast materials which, in tonnage terms, is second only to ferrous castings,^[1] this is mainly because aluminum casting alloys are among the most versatile of foundry alloys. As casting materials, they display favorable characteristics such as suitable fluidity for filling thin sections, and chemical stability combined with a low melting point when compared with a number of other metals or alloys. The capability of rapid heat transfer from the molten aluminum to the mold also provides for much shorter casting cycles. In addition, many aluminum alloys are relatively free of hot short cracking and tearing tendencies, while at the same time

yielding a good as-cast surface finish with few blemishes or none at all.^[2]

Copper (Cu) and magnesium (Mg) are often added as alloying elements to increase strength and hardenability values, whereas iron (Fe), manganese (Mn), nickel (Ni), and chromium (Cr) are usually present as impurity elements.

The excellent castability and mechanical properties of Al–Si–Cu–Mg cast alloys make them popular foundry alloys for industrial applications. These alloys are usually heat-treated in order to obtain an optimum combination of strength and ductility. Critical automotive applications using these heat-treatable alloys are designed for high impact toughness which can be improved using a specified heat treatment or temper. The relevant heat treatment/temper consists of solution treatment and quenching, followed by artificial aging. Solution heat treatment is carried out so as to obtain maximum dissolution of the magnesium and copper in the aluminum matrix. The dissolution rate of intermetallic compounds is temperature sensitive; thus even a 10°C increase in temperature has the potential for appreciably affecting optimum solution time as well as the mechanical properties.

The mechanical properties, in particular ductility, may also be enhanced by changing the morphology of the eutectic silicon particles from their normally acicular brittle form to a more fibrous and rounded form. The desired modification may be obtained through the addition of a chemical modifier such as Na or Sr to the alloy, or else by means of solution heat treatment during which the Si particles are fragmented and become spheroidized. Long solution treatment times can lead to particle coarsening.

The percentage of Si in Al-Si alloys together with the shape and distribution of the

silicon particles all play an important role in determining mechanical properties; under normal conditions, eutectic silicon displays an acicular or lamellar morphology. Strontium (Sr) is commonly used in Al-Si casting alloys to modify the morphology of eutectic silicon from a coarse, flake-like form to a fine fibrous one so as to improve the mechanical properties of the specific alloy, particularly ductility.

With the addition of Sr, the eutectic temperature of the Al-Si eutectic reaction is depressed; subsequently this depression is often used to estimate the degree of modification which has taken place in the Al-Si alloy. Other alloying elements such as Cu and Mg, together with varying amounts of iron, manganese, and zinc as impurity elements, go into solid solution in the matrix and form intermetallic particles during solidification.

The addition of copper to Al-Si alloys leads to the formation of the copper intermetallic phase, which increases the alloy strength both at room temperature and at high temperatures. This intermetallic phase is present in two forms: eutectic-like Al-Al₂Cu and block-like Al₂Cu. The block-like Al₂Cu phase is much harder to dissolve in the aluminum matrix, and thus the benefits of having Cu as a strengthening agent during heat treatment are diminished.

The presence of Mg leads to an increase in the values for yield strength and tensile strength as well as for impact toughness, although it tends to decrease the ductility noticeably. The presence of Mg also leads to a reduction in the eutectic temperature pertaining to the Cu-containing phases as a result of the precipitation of the Al₅Mg₈Cu₂Si₆ intermetallic phase; this would indicate that the addition of Mg curtails the maximum solutionizing temperature. When the Mg content is less than 0.6 wt%, Mg has a tendency to

refine the eutectic Si particles. The addition of Mg also leads to segregation of the Cu phase in areas away from the eutectic Si regions. This segregation leads to the formation of the block-like Al_2Cu , as well as to that of the $\text{Al}_5\text{Mg}_8\text{Cu}_2\text{Si}_6$ phase which forms out of the Al_2Cu phase along its edges during the last stage of solidification.

When combined with Sr, Mg negates the effect of Sr modification to such an extent, that a much higher level of Sr is required to achieve full modification of the eutectic Si structure. In the Sr-modified Mg-free alloy, the Al-Si eutectic is better modified than the one in the Mg-containing alloy modified with the same amount of Sr. Strontium modification, however, also results in a large volume fraction of the interdendritic block-like Al_2Cu structure in 319 alloys. This interdendritic Al_2Cu structure is much harder to dissolve during solution heat treatment, thus increasing the possibility of incipient melting and the consequent formation of porosity; this is significant in that the increased porosity can adversely affect mechanical properties.^[3]

Impact toughness as a property is one of the many significant mechanical properties which are routinely evaluated and used in design calculations. Impact behaviour, or impact toughness, is usually defined by the total energy absorbed by a specimen in fracturing it. This fracture occurs under an impact test at a high strain rate or rapid rate of loading causing a brittle fracture. Castings which have identical properties when tested under tension or torsion at slow strain rates can show pronounced differences in their tendency for brittle fracture when tested in an impact test. Both the tensile and impact properties can be correlated to the microstructure and to the formation of intermetallic phases and porosity. In general, with an increase in the volume fraction and size of intermetallics and porosity,

the tensile and impact properties tend to decrease.

Heat-treatable aluminum alloys are those whose mechanical properties may be improved by using a specified heat treatment or temper. Heat treatment is an elevated temperature process designed to allow soluble elements such as Mg and Cu to become supersaturated in solid solution, followed by cooling which is rapid enough to cause the excess solute to precipitate. The T6 heat treatment process involves three stages, namely, solution heat treatment, quenching, and aging. The purpose of the solution heat treatment is to put the maximum amount of hardening solutes such as Cu and Mg into solid solution in the aluminum matrix. Thus, the temperature of solution heat treatment in the case of 319 alloys must be as close as possible to the Cu eutectic temperature, although this temperature should, at the same time, be limited to a safe level below the maximum so as to avoid overheating and partial melting of the Al_2Cu phase.

The solution heat treatment process may be carried out either in a single step or in multiple steps. The single-step treatment for 319 aluminum alloys is normally limited to 495°C , because a higher temperature might lead to the incipient melting of the copper phase. On the other hand, heat treatment at temperatures of 495°C , or less, is not sufficient to maximize the dissolution of the copper-rich phases, nor to modify the morphology of silicon particles. In order to overcome this problem, a two-step solution heat treatment was proposed by Sokolowski *et al.*,^[4] where the second-stage is maintained at temperatures below 525°C . In general, only the conventional single-stage solution heat treatment of 8h at 495°C for 319 aluminum alloys is carried out to avoid the incipient melting of the copper phase.

Quenching is the step which follows upon solution heat treatment; it is usually conducted in water, making it possible to freeze the structure for a brief period of time. The purpose of this process is to preserve the solid solution formed at the solution heat treating temperature by means of rapid cooling to some lower temperature, usually close to room temperature.

Aging treatment is the controlled process of allowing the hardening constituents to re-precipitate either at room temperature (natural aging) or at an elevated temperature (artificial aging), thereby producing a hardening effect. The highest strength values may thus be obtained by the proper combination of solution heat treatment, quenching, and artificial aging.

1.2 OBJECTIVES

Experimental and industrial 319 alloys in both the non-modified and Sr-modified conditions were used for this study; these alloys contained different Mg levels of 0, 0.1, 0.2, 0.3, 0.4, and 0.6 wt%. Single-step solution heat treatment was also applied to them.

The main purpose of the study was to investigate the effects of magnesium content and aging conditions on the impact toughness of both the non-modified and Sr-modified 319-type alloys, including the subsequent effects on hardness values. These objectives were accomplished by examining the following factors:

- (i) the effects of Mg addition on the various aspects of impact energy, hardness, and microstructure for each alloy;
- (ii) the effects of cooling rate on both experimental and industrial alloys as well as on both non-modified and Sr-modified alloys;
- (iii) the effects of aging conditions, namely time and temperature, on the impact toughness, hardness, and fracture behavior of each alloy;
- (iv) a study of the alloying and melt processing parameters involved in impact behavior with a view to minimizing the harmful effects of porosity and intermetallics.

CHAPTER 2
REVIEW OF THE LITERATURE

CHAPTER 2

REVIEW OF THE LITERATURE

2.1 ALUMINUM-SILICON ALLOYS

Worldwide, aluminum-silicon (Al-Si) base casting alloys are widely used in automotive applications on account of their low density and capacity for being cast in complex shapes. Nowadays, Al-Si alloys are used extensively in the automobile industry for engine components including engine blocks, cylinder heads, pistons, intake manifolds, and brackets; these alloys have even replaced cast iron components in many cases.^[5]

Silicon has a lower density compared to aluminum, and is one of the few elements which may be added to it without the loss of a weight advantage.^[6] Only a few elements such as silicon, zinc, magnesium, and copper are endowed with sufficient capacity for solubility making it possible for them to be used as major alloying additions. Alloys with silicon as a major alloying element are of significance in the industry and are widely used because of their superior casting characteristics. These Al-Si base alloys constitute 85% to 90% of all aluminum castings. Their other outstanding features include high corrosion resistance, a low thermal expansion coefficient, weldability, and heightened mechanical properties.

With the increasing demands of the automotive industry for smaller, lighter-weight high-performance components, Al-Si alloys have today replaced iron and steel in many

components such as transmission cases, intake manifolds, and even in more critical components such as engine blocks, cylinder-heads and wheels. Such applications require that the casting parts exhibit consistent strength-ductility properties throughout the casting.

Depending on the percentage of silicon-content, Al-Si alloys are divided into three groups: hypoeutectic alloys with a Si content of between 5 and 10%, eutectic alloys with 11-13% Si, and hypereutectic alloys, commonly revealing a Si content of between 14 and 20%, as shown in Figure 2.1.^[7]

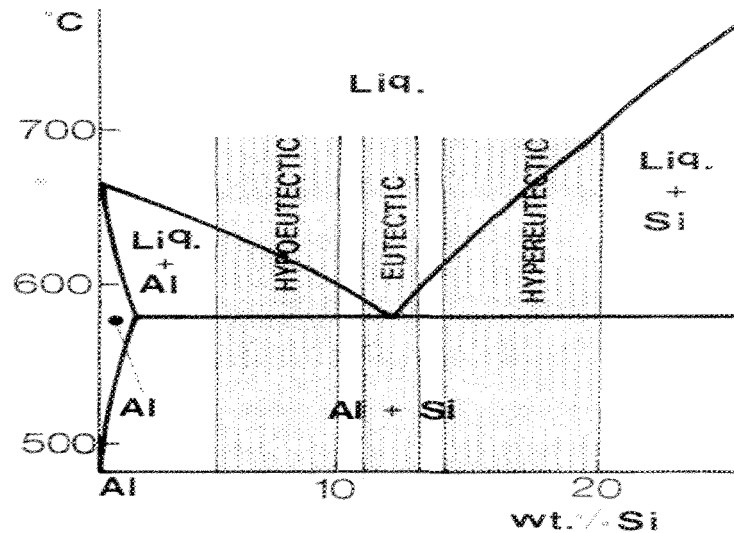


Figure 2.1 Part of the Al-Si phase diagram showing composition ranges for various alloy types.^[7]

The solidification process of Al-Si alloys involves the following main reactions:

- (i) Formation of a dendritic network of the α -aluminum phase.
- (ii) Aluminum-silicon eutectic reaction when the Al-Si eutectic precipitates.
- (iii) Precipitation of a secondary eutectic phase such as Mg_2Si and Al_2Cu .

In addition to the occurrence of these reactions, a number of intermetallic phases are

also liable to precipitate during solidification as a result of the presence of certain impurity elements such as Fe and Mn. The iron intermetallics Al_5FeSi and $Al_{15}(Mn,Fe)_3Si_2$ are two phases which may often be observed in Al-Si alloys.

Casting alloys are defined by their chemical composition; each of the major countries has developed its own nomenclature and designations. In the United States, the three-digit registration system of the Aluminum Association is the one used widely.

In the Aluminum Association (AA) system, casting alloys are divided into nine series according to the major alloying elements present in the alloy. These are shown in Table 2.1.^[8]

Table 2.1 Classification of aluminum casting alloys^[8]

Series	Alloy Family
1XX	99.0% min Al
2XX	Al-Cu
3XX	Al-Si-Mg, Al-Si-Cu, Al-Si-Cu-Mg
4XX	Al-Si
5XX	Al-Mg
6XX	Unused
7XX	Al-Zn
8XX	Al-Sn
9XX	Unused

No commercial alloys are currently established in the 6XX and 9XX series. The classification XXX.0 represents the chemical composition limit for castings, while XXX.1 and XXX.2 represent those for ingots. Aluminum-silicon base alloys belong to the 3XX

and 4XX series of aluminium casting alloys. The three major alloy systems in the 3XX series comprise Al-Si-Mg, Al-Si-Cu, and Al-Si-Cu-Mg, where Mg and Cu are two significant alloying additions acting as effective strengtheners. Some alloys include a prefix letter in their denomination. Different letters used with the same alloy number distinguish alloys of a general composition which differ in the percentage of impurities present in the form of minor alloying elements; examples of this may be observed with alloys 356 and A356, or 380, A380 and B380.^[8]

2.1.1 Al-Si-Cu Alloy System

The Al-Si-Cu alloys are employed extensively in a wide variety of applications on account of their excellent castability, high thermal conductivity and low thermal expansion coefficient.^[9] Furthermore, they can be heat-treated to obtain an optimum combination of strength and ductility. With heat treatment, Al-Si-Cu alloys are capable of producing a wide range of physical and mechanical properties. The heat treatment which is applied includes the processes of solution heat treatment, quenching, and natural or artificial aging. In this particular group of alloys, silicon produces favorable casting characteristics while copper yields high strength and machinability. One of the most well-known alloys belonging to the Al-Si-Cu alloy system is the 319 alloy. The chemical compositions for various 319-type alloys are presented in Table 2.2.^[10]

The 319 alloys contain both copper and magnesium as the hardening elements, together with various impurities such as Fe, Mn or Zn. During solution heat treatment, copper forms an intermetallic phase with aluminum which precipitates during solidification in the form of block-like Al_2Cu or in the form of the eutectic (Al- Al_2Cu) phase. Silicon-

particle characteristics also influence the mechanical properties; thus, with a successful strontium modification treatment, the silicon can assume a fine fibrous structure which leads to an improvement in the mechanical properties.

Table 2.2 Chemical composition of 319 alloys (wt %)^[10]

AA Designation	Si %	Fe %	Cu %	Mg %	Mn %	Zn %	Ti %	Ni %
319.0	5.5-6.5	1.0	3.0-4.0	0.10	0.5	1.0	0.25	0.35
319.1	5.5-6.5	0.8	3.0-4.0	0.10	0.5	1.0	0.25	0.35
319.2	5.5-6.5	0.6	3.0-4.0	0.10	0.1	1.0	0.20	0.10
A 319.0	5.5-6.5	1.0	3.0-4.0	0.10	0.5	3.0	0.25	0.35
A 319.1	5.5-6.5	0.8	3.0-4.0	0.10	0.5	3.0	0.25	0.35
B 319.0	5.5-6.5	1.2	3.0-4.0	0.10-0.5	0.8	1.0	0.25	0.5
B 319.1	5.5-6.5	0.9	3.0-4.0	0.10-0.5	0.8	1.0	0.25	0.5

2.2 SOLIDIFICATION OF Al-Si-Cu 319-TYPE ALLOYS

All commercial solidification processes involve some non-equilibrium effects, particularly in view of the fact that true stable equilibrium conditions seldom exist during casting. The study of equilibrium systems is extremely valuable, however, since it constitutes a limiting condition from which actual conditions can be estimated.^[11] In real casting processes, the extent of deviation from equilibrium conditions has a significant effect on the actual microstructure observed.

During the solidification of the unmodified 319 alloy, the following main sequence of phase precipitation will occur:

- (i) the formation of primary aluminum at about 608°C;
- (ii) the main silicon-forming eutectic reaction at about 563°C;
- (iii) the CuAl_2 -forming reaction at about 550°C; and
- (iv) the complex eutectic reaction at about 525°C.

The solidification rate during casting is of importance in that it affects almost all the microstructural parameters, such as dendrite arm spacing, the degree of eutectic silicon modification, and the porosity and intermetallics which occur in the microstructure.

At the end of the solidification process, Mg_2Si , Al_2Cu and other more complex phases precipitate from the remaining liquid. Table 2.3 summarizes the sequence of phase precipitation in hypoeutectic Al-Si alloys.^[12]

Table 2.3 Sequence of phase precipitation in hypoeutectic Al-Si alloys^[12]

Temperature (°C)	Phases Precipitated	Reaction Type
650	Primary $\text{Al}_{15}(\text{Mn,Fe})_3\text{Si}_2$ (sludge)	Pre-dendritic
600	Aluminum dendrites and $(\text{Al}_{15}(\text{Mn,Fe})_3\text{Si}_2)$ and/or Al_5FeSi	Dendritic Post-dendritic Pre-eutectic
550	Eutectic Al + Si and Al_5FeSi Mg_2Si	Eutectic Co-eutectic
500	Al_2Cu and more complex phases	Post-eutectic

In the current study a graphite mold which had been preheated to 600°C was used for casting for the purposes of the characterizing the microstructures involved. This preheating temperature produced close-to-equilibrium cooling conditions with sufficient time for the precipitating phases to grow, so as to facilitate their identification using electron microscopy techniques. Thermal analysis may also be carried out simultaneously

with the graphite mold set-up; this will contribute appreciably to determining the precipitation reactions taking place during solidification.

2.3 ROLE OF MODIFICATION

As mentioned previously, Al-Si alloys are widely used in applications where strength and light weight are required, or where corrosion resistance and castability are desired qualities. The commercial application of these alloys, however, often depends on the successful modification of eutectic silicon. Modification is one of the melt treatments carried out so as to alter the structure of the eutectic silicon particles, and ultimately to improve the mechanical properties.

A non-modified alloy displays an acicular eutectic silicon structure. Such brittle, acicular Si particles act as internal stress raisers in the microstructure and provide easy paths for fracture. With modification, the eutectic structure becomes finer and the silicon displays increasingly more rounded characteristics, thereby contributing to higher values of ultimate tensile strength and significantly increased values for ductility. It should be noted that during modification, the aluminum phase is not affected structurally, whereas for the silicon phase, modification results in a change from a faceted to a fibrous growth morphology.

The eutectic silicon can also be 'modified' through solution heat treatment or the use of high cooling rates. Fast cooling rates are used to reduce the size and the distance between eutectic silicon particles, rather than to reduce their shape or morphology.^[13] Full modification is difficult to achieve, however, by simply increasing the solidification rate of

the casting alone, and thus Al-Si alloys are generally modified chemically using modifying agents.^[14] These modifiers are normally added to the alloy melt in the form of master alloys in the quantities required to obtain a well-modified eutectic structure.

Apelian *et al.*^[15] assessed the grain refinement and modification of Al-Si foundry alloys using thermal analysis. Figure 2.2 depicts the range of microstructures observed by the authors on the polished surfaces of a modified hypoeutectic Al-Si alloy. The structures are divided into six classes, with the unmodified structure represented by Class 1; lamellar by Class 2; undermodified by Classes 2-4; well-modified structures by Class 5; and overmodified structures by Class 6.

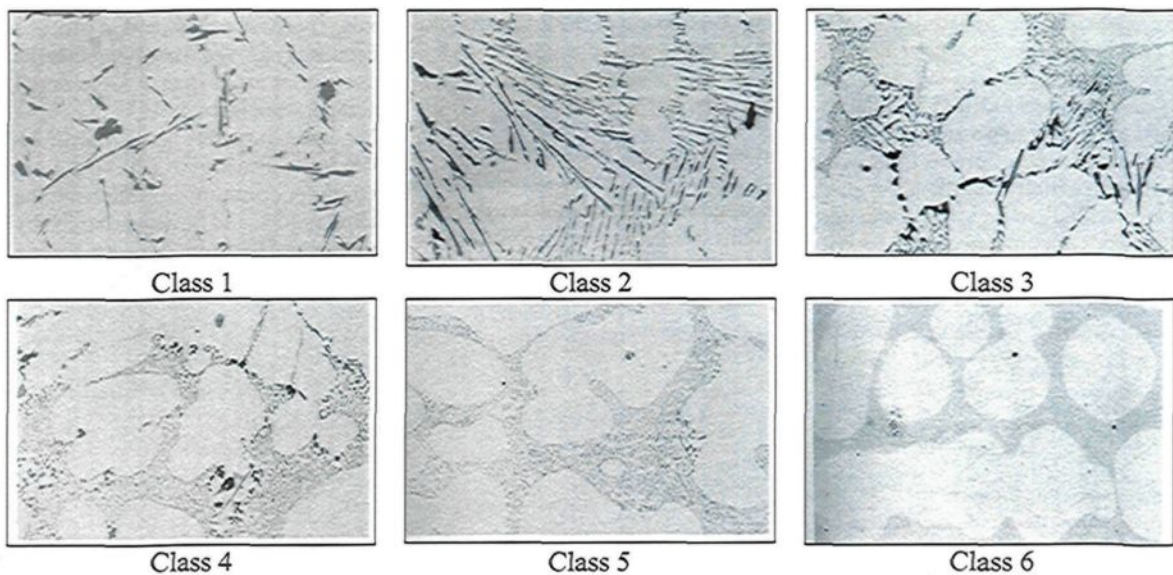


Figure 2.2 Rating system for a modified microstructure.^[15]

Five variables determine the exact microstructure which will form: (i) the type of modifier used; (ii) the impurities present in the melt; (iii) amount of modifier used; (iv) the freezing rate; and (v) the silicon content of the alloy. These five variables interact in a

highly complex manner, such that an exact quantitative prediction of the microstructure in terms of a modification rating is made difficult.

In 1921, Pacz^[16] discovered that Al-Si alloys containing 5 to 15% Si could be treated with an alkaline fluoride, namely, sodium fluoride, to improve their ductility and machinability. A number of researchers^[17,18] found that modification by sodium addition results from a combination of two effects: the first is the neutralization of aluminum-phosphorus (AlP) so that a too easy nucleation of silicon would be prevented; the second is a change in the mode of solidification of the eutectic so that the modified eutectic crystallizes with the aluminum crystals and not with the silicon crystals, as in the case of non-modified alloys. It should be remembered that in the 1970s, Hess and Blackmun^[19] reported strontium to be an effective modifying agent for hypoeutectic Al-Si alloys. Several elements, such as arsenic (As), antimony (Sb), selenium (Se), and cadmium (Cd), are known to cause silicon modification. Only Na, Sr, and Sb however, are currently the most effective within economic constraints. Of these elements, Sb is not used in North American foundries due to its toxic effects. The amount of each modifying element required depends on alloy composition, in that a higher silicon content requires a larger amount of the modifier.

It is a well known fact that sodium has the capacity for greatly modifying the eutectic structure. Due to its low melting point, this element is easily incorporated into Al-Si melts, although its high vapor pressure makes it boil off almost immediately as a result of a phenomenon called “fading”. As sodium is also sensitive to porosity and has an adverse effect in terms of oxidation and aggressiveness against mold coatings, and so

forth,^[20] it is difficult to control the Na-modification process, thereby making it of limited usefulness in this regard.

Compared with Na, Sr as a modifier has been widely used because of its greater stability in the melt. The addition of Sr neutralizes the effect of phosphorus and promotes the formation of a fibrous silicon structure by retarding the growth rate of silicon.^[21,22] The eutectic structure thus becomes finer and the silicon particles become increasingly more rounded, a state which contributes to producing higher values for the ultimate tensile strength and greatly increased values for ductility. Also, because of its low vapor pressure and tendency for oxidation, the loss rate for strontium is distinctly less than it is for sodium.

It has also been reported that an initial incubation period is required for maximum modification. Strontium retains its modifying action longer than Na in spite of a continual loss of Sr during holding, provided a sufficient amount of this element remains in the alloy. The modifying effect of Sr actually appears to improve with holding time, again provided a sufficient amount remains in the melt.^[19] Although the presence of strontium can change the morphology of the silicon particles, when the Al-Si alloy contains more than 0.05 wt% Sr, the formation of undesirable Sr-compounds such as Al_2SrSi_2 contributes to a decrease in mechanical properties.^[23]

Modification with Sr can contribute considerably to lowering the actual eutectic temperature.^[24,25] The depression in the eutectic temperature can be used as an indicator of the extent of modification expected in the Si structure within the casting: the lower the eutectic temperature, the greater the modification effect. Sokolowski *et al.*^[26] have reported that additional strontium raises the eutectic temperature of the copper-rich phases. It is

likely that high strontium melts will need to be subjected to higher temperature solution treatments. An additional benefit of Sr modification is that it is capable of considerably lowering the solution treatment time necessary to attain the desired property level.^[27] On the other hand, Sr modification also results in the segregation of the interdendritic blocky CuAl_2 structure in 319 alloys,^[28] in addition to increasing porosity in the modified alloy.^[29]

2.4 ROLE OF MAGNESIUM

Magnesium is already being used extensively in Al-Si alloys to improve the mechanical properties. The addition of this element increases strength values during aging as a result of the precipitation of submicroscopic and metastable phases containing Mg and Si which provide distinct obstacles to dislocation movement.

In their investigation of the influence of alloying elements in the thermal analysis of Al-Si cast alloys, Heusler and Schneider^[25] observed that any Sr-modified microstructure is clearly affected when magnesium is present. Microstructural parameters as obtained from image analysis, such as silicon particle size and aspect ratio, were found to increase with an increasing Mg content, subsequently becoming increasingly inhomogeneous. The reason for the deterioration in modification is believed to be the formation of intermetallic phases of the type $\text{Mg}_2\text{SrAl}_4\text{Si}_3$, where the addition of Mg also lowers the eutectic temperature; as may be seen in Figure 2.3, the eutectic temperature decreases with increasing Mg content. It was also reported, however, that a magnesium content of ~1 wt% itself acts as a refiner for the eutectic silicon in unmodified Al-Si alloys.^[30]

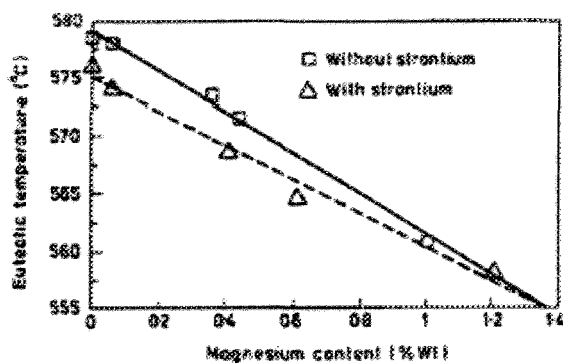


Figure 2.3 Depression of the eutectic temperature as a function of magnesium level for unmodified and strontium-modified Al-Si alloys.^[25]

De la Sablonnière and Samuel^[31] studied the solution heat treatment of a 319 aluminium alloy containing ~ 0.5 wt% Mg; the results they obtained showed that increasing the Mg content to ~ 0.5 wt% would lead to a significant decrease in the eutectic silicon temperature by about 1.5°C per 0.1 wt% Mg. The addition of Mg also led to the precipitation of the $\text{Al}_5\text{Mg}_8\text{Cu}_2\text{Si}_6$ phase, as well as to the splitting of the temperature range pertaining to the copper phase formation thereby separating it into two explicit peaks representing the precipitation of the Al_2Cu and $\text{Al}_5\text{Mg}_8\text{Cu}_2\text{Si}_6$ phases.

Thus, the addition of Mg is seen to result in an increase in the volume fraction of Cu-containing phases, with a clear tendency for segregation in localized areas, leading to the formation of the block-like phase rather than the fine eutectic-like Al_2Cu .^[31] This segregation makes it more difficult to dissolve the Al_2Cu phase during solution heat treatment. It is also important to avoid such segregation to prevent the occurrence of incipient melting, and ensure that the alloy properties and castings all remain sound.

In another study, Samuel *et al.*^[30] showed that the addition of Mg to molten 319 type alloys, in amounts up to 0.5 wt%, leads to the precipitation of a Mg-rich phase, Mg_2Si ,

which appears in the form of rounded black particles dotted along the sides of the eutectic Si particles. A noticeable fragmentation of the eutectic Si, in other words its modification is also observed, and the transformation of a large proportion of the β -Al₅FeSi iron intermetallic phase into a Chinese script-like phase with a composition close to that of Al₈Mg₃FeSi₆.

In the context of alloy properties, de la Sablonnière and Samuel^[31] obtained some interesting results from the tensile testing carried out for solution heat-treated 319 alloys containing 0.5 wt% Mg. They found that two types of defects can occur during solution heat treatment: firstly, “dark spots” displaying no distinct boundaries between them and the surrounding matrix when the alloy test bars are heat-treated at temperatures close to 520°C irrespective of the Mg level; and secondly, “burn spots” which result from the burning, or fusion, of the molten phases in alloy test bars containing high Mg levels of up to 0.5 wt% after being subjected to solution treatment at higher temperatures than previously, *i.e.* over 520°C.

The dark spots were always observed near the periphery of the test bars, thus indicating that they acted as a source for crack initiation. Also, the size of these dark spots was found to increase with an increase in solution temperature. The occurrence of the ‘burn spots’, however, was not restricted to the fracture surface. Nonetheless, the incipient melting which was related to these burn spots resulted in a deterioration of the tensile properties. Figure 2.4 shows examples of such dark spots observed on the fracture surface of 319 + 0.5 wt% Mg alloy test bars which had been solution heat-treated (a) for 12 h/510°C; and (b) for 12 h/520°C.

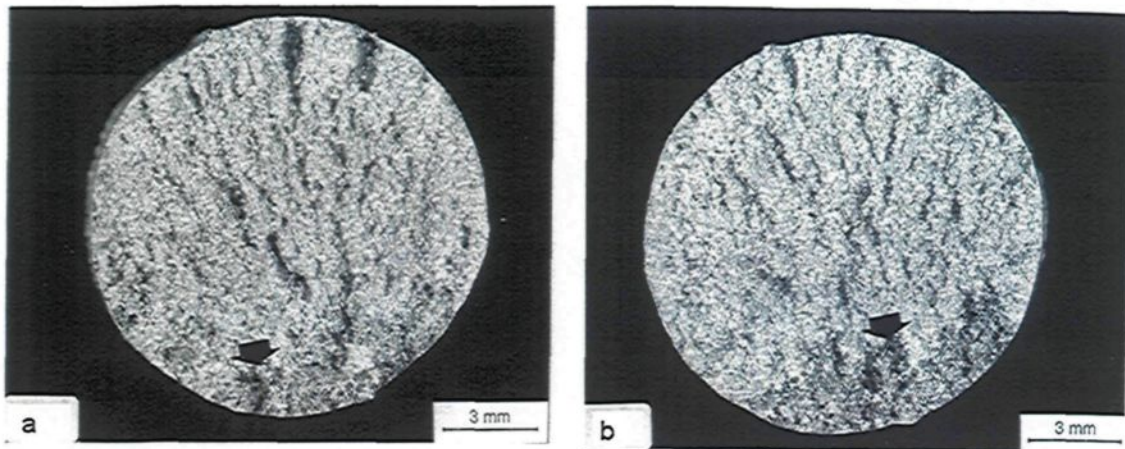


Figure 2.4 Dark spots observed on the fracture surfaces of test bars of a 319 + 0.5 wt% Mg alloy, solutionized for (a) 12h/510°C, and (b) 12h/520°C. Arrows show the progress in the size of the dark spot.^[32]

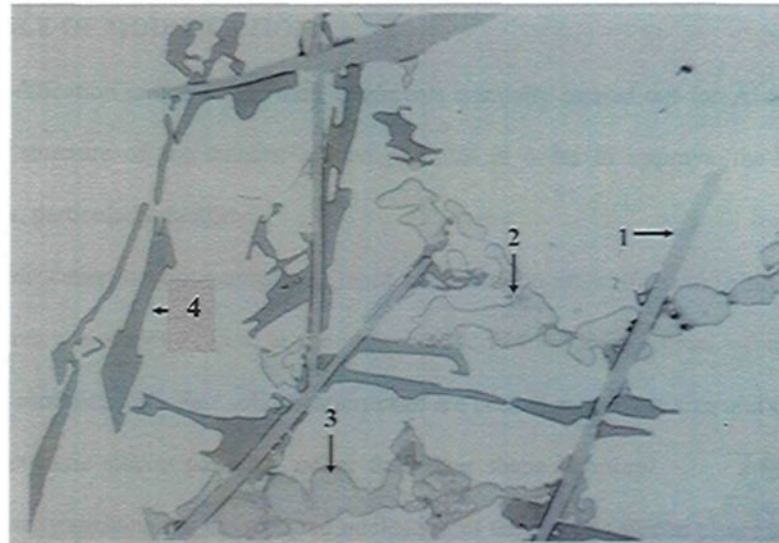
2.5 INTERMETALLIC PHASES IN Al-Si-Cu ALLOYS

The presence of copper in Al-Si-Cu alloys leads to the formation of the copper intermetallic, Al_2Cu . If iron is also present in the alloy, then this element goes partly into solid solution in the matrix and, in part, forms intermetallic compounds during solidification together with other alloying elements; among these will be found the plate-like $\beta\text{-Al}_5\text{FeSi}$ and the script-like $\alpha\text{-Al}_{15}(\text{Mn,Fe})_3\text{Si}_2$ phases. In the solidification process, $\beta\text{-Al}_5\text{FeSi}$ platelets are very active sites for the nucleation of the Al_2Cu phase. These copper and iron intermetallic compounds are discussed below in further detail.

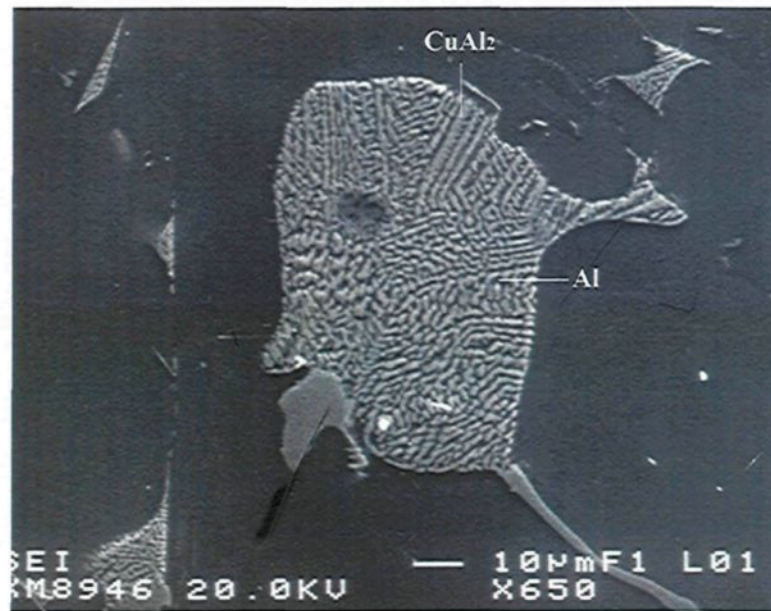
2.5.1 Copper Intermetallic Phases

Three different copper-rich phases are likely to be present in Al-Si-Cu alloys, namely, block-like Al_2Cu , eutectic Al- Al_2Cu , and the $\text{Al}_5\text{Mg}_8\text{Cu}_2\text{Si}_6$ phase, as shown in Figure 2.5.^[33] If the solution heat treatment temperature is not properly controlled, it can induce melting of the copper phases, resulting in the formation of cavities and the lowering

of the casting soundness.



(a)



(b)

Figure 2.5 (a) Microstructure of a sample from 319.1 alloy: (1) β - Al_5FeSi , (2) blocky Al_2Cu phase, (3) $\text{Al}_5\text{Mg}_8\text{Cu}_2\text{Si}_6$ phase, (4) acicular Si phase; ^[33] (b) secondary electron image of 319 alloy showing the eutectic Al- Al_2Cu phase (round).^[34]

The mechanism of Al_2Cu precipitation has been proposed by Samuel *et al.*^[35] as follows. During the first stages of solidification, the formation of the α -Al dendritic network is associated with the segregation of the Si and Cu in the melt ahead of the progressing dendrite interfaces. When the solidification temperature approaches the eutectic temperature, the Si particles precipitate ultimately, leading to a local concentration of Cu in the remaining areas.

The presence of both strontium and magnesium will lead to the segregation of the copper phase to areas free of eutectic silicon particles. Due to this segregation, the Al_2Cu phase precipitates more often in the block-like form rather than in the fine eutectic form. Compared with the eutectic (Al- Al_2Cu) phase, the coarser block-like form of the phase is much more difficult to dissolve in the aluminum matrix. Segregation is also affected by the cooling rate; a high cooling rate is beneficial in contributing to a reduction in the amount of eutectic phase precipitation along the grain boundaries.

According to a study carried out by Li,^[34,36] the mechanism for the dissolution of the Al_2Cu phase during solution heat treatment as shown in Figure 2.6 may be put forward as follows:

- (i) separation of the Al_2Cu particles from the β - Al_5FeSi platelets;
- (ii) necking of the Al_2Cu particles followed by spheroidization;
- (iii) dissolution of the spheroidized particles by radial diffusion of Cu atoms into the surrounding aluminum matrix.

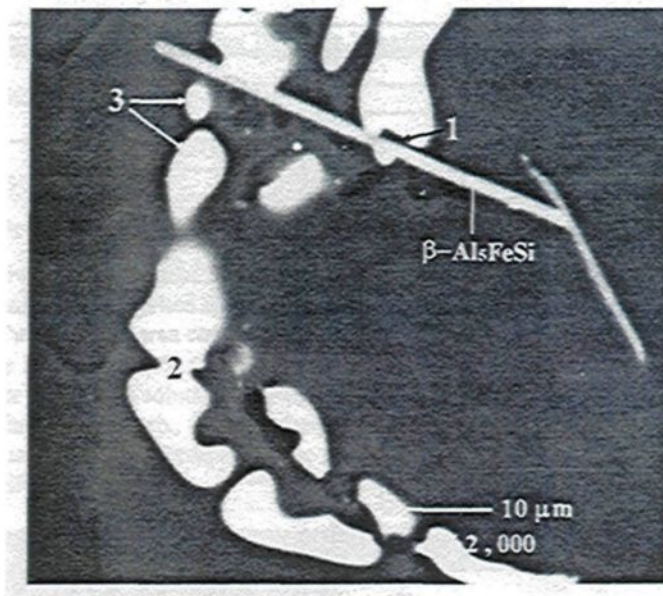


Figure 2.6 Backscattered image showing the dissolution process of Al₂Cu particles in 319 alloys after 8h solution heat treatment at 505°C: (1) separation of the Al₂Cu particles from the β-Al₅FeSi platelets, (2) necking of the Al₂Cu particles, (3) spheroidization of Al₂Cu and reduction in the size of Al₂Cu fragments.^[36]

During solution heat treatment, melting of the Al₂Cu phase may occur if the alloys are subjected to a particularly high solution temperature, ultimately resulting in a structureless form of the phase upon cooling accompanied by porosity formation, all of which can lead to a deterioration of the mechanical properties.

2.5.2 Iron Intermetallic Phases

As mentioned previously, during the solidification of Al-Si base alloys, iron, together with other alloying elements such as Cu, Mg, Zn, Mn, Ti, and so forth, goes partially into solid solution in the matrix and partially forms intermetallic compounds, including the plate-like β-Al₅FeSi phase and the Chinese script-like α-Al₁₅(Mn,Fe)₃Si₂ phase.^[12] Among these, the β-Al₅FeSi phase platelets acting as stress raisers cause iron to

be the most deleterious impurity element present in cast aluminum alloys. These platelets, which appear as needles in the microstructure, also prevent the flow of liquid metal during the solidification process, thereby restricting feedability and causing the formation of porosity in the casting as well as creating general unsoundness. Furthermore, the β - Al_5FeSi plate-like phase also acts as a nucleant for the Al_2Cu phase, which helps to reduce Al_2Cu segregation.

The β - Al_5FeSi platelets are light grey in color when observed under the optical microscope. They grow in a lateral or faceted growth mode, and are bounded by slowly growing planes of low indices. Their surfaces are relatively smooth on the atomic scale, thus atoms from the liquid can find few possibilities to attach themselves at the interface causing their growth to become restricted and slow. This type of growth occurs at low driving forces or slow cooling rates, *i.e.* at low degrees of undercooling, ΔT .

Mondolfo^[37] has summarized the main factors which contribute to the formation of the β -iron Al_5FeSi phase: (a) an Fe/Si ratio close to unity, (b) a low cooling rate of $\sim 0.8^\circ\text{C/s}$, and (c) low concentrations of Mn and/or Cr. The cooling rate has a direct impact on the equilibrium kinetics and quantities of the iron present in the microstructure. A low cooling rate promotes the precipitation of the β -iron Al_5FeSi phase, while rapid solidification favours the crystallization of iron compounds in the form of the α -iron phase.

This other iron intermetallic phase is the Chinese script-like α - $\text{Al}_{15}(\text{Mn,Fe})_3\text{Si}_2$ phase, also light grey in color, and appearing in script form when observed under the optical microscope. This phase grows in an irregular, curved mode; its form is controlled by the temperature gradient and by the diffusion of atoms in the liquid melt. During

crystallization, atoms tend to attach themselves to the solidified part of the α -iron phase particles when they reach the solid/liquid interface. This type of growth occurs at high solidification driving forces or rapid cooling rates, *i.e.* at high undercooling, ΔT . The α -iron phase, due to its compact morphology, is less detrimental to mechanical properties than the β -iron phase.

2.6 HEAT TREATMENT OF Al-Si-Cu ALLOYS

Al-Si-Cu alloys are heat-treatable, which means that their mechanical properties can be enhanced through heat treatment. The temper/heat treatment consists of solution heat treatment, quenching, and a combination of natural and artificial aging processes. The improvement in properties is mainly a result of the precipitation of Al_2Cu within the alloy matrix during the aging process. The changes in the morphology of silicon during the solution treatment also contribute to the improvement in the properties. Solution heat treatment can also minimize the harmful effects of the β -iron phase. Upon solution heat treatment, the β -iron intermetallics undergo dissolution and fragmentation, which subsequently leads to an improvement in the mechanical properties.

2.6.1 Solution Heat Treatment

Solution heat treatment may be obtained by heating the alloy to a suitable temperature, maintaining it at this temperature long enough to allow the constituents to become supersaturated in solid solution, and then cooling it rapidly enough to avoid causing the excess solute to precipitate. The purpose of solution heat treatment is to put the maximum amount of hardening solutes such as Cu and Mg into solid solution in the

aluminum matrix. Solution heat treatment in Al-Si-Cu-Mg alloys is used to homogenize the alloy, change the morphology of the interdendritic phases, and to dissolve precipitation-hardening constituents, such as Al_2Cu , Al_2MgCu , and Mg_2Si .^[38] During the solution heat treatment, the morphology of the eutectic Si particles changes over time, through the fragmentation, spheroidization, and coarsening of the particles. The spheroidization rate increases with the Sr concentrations in the alloy.

In order to dissolve the maximum amount of hardening solutes into solid solution, the temperature of solution heat treatment must be as close as possible to the eutectic temperature while at the same time limiting this same temperature to a safe level below the maximum to avoid overheating and partial melting. Solution temperature and solution time are two of the most important factors in solution heat treatment. The dissolution rate of intermetallic compounds is temperature sensitive and even a 10°C increase in temperature could have an appreciable effect on the optimum solution time and mechanical properties involved.

During solution heat treatment, incipient melting of the Al_2Cu phase at the grain boundaries may occur when the composition exceeds the critical one and the 319 alloy is annealed at a temperature higher than the melting point of eutectic Al- Al_2Cu . This type of melting results in the formation of a structureless form of the Al_2Cu phase with its related porosity upon quenching, and a consequent deterioration of the mechanical properties.

The results obtained by Gauthier *et al.*^[39,40] show that the best combination of tensile strength and ductility is obtained when the as-cast material is solution heat-treated at 515°C for 8 to 16 h, followed by quenching in warm water at 60°C . A higher solution

temperature results in the partial melting of the copper phase at the grain boundaries.

Crowell and Shivkumar^[27] stated that the block-like Cu phase in Al-Si-Cu alloys dissolves with increasing solution time at the recommended solution temperature of 495°C where the rate of dissolution was subsequently observed to increase with Sr concentrations. In their study on the solution heat treatment of 319 alloys containing ~0.5wt% Mg, de la Sablonnière and Samuel^[31,32] reported the appearance of dark spots on the fracture surface of solution heat-treated bars. The size and percentage of the defective test bars obtained increased with an increase in solution temperature.

It is possible to carry out the solution heat treatment process in either a single step or in multiple steps. Single-step treatment is normally limited to about 495°C, because higher temperatures lead to the incipient melting of the copper phase. Unfortunately, heat treatment at temperatures of 495°C or less is not capable of maximizing the dissolution of the copper-rich phases, nor is it able to sufficiently modify the silicon particle morphology.

A two-step solution treatment consisting of conventional solution treatment followed by a high-temperature solution treatment, as suggested by Sokolowski *et al.*,^[41] is reported to reduce the amount of the copper-rich phase in 319 alloys to a significant degree, giving rise to better homogenization prior to aging, and thereby improving the mechanical properties. The holding time of the first stage and the solution temperature of the second stage are significant parameters in this context. The second-stage solution temperature should not be allowed to rise higher than 520°C since this may cause the incipient melting of the copper eutectic phase.

Sokolowski *et al.*^[26] studied the improvement brought about in the durability of 319 aluminium casting alloys as a result of high temperature solution treatment. Their results showed that a two-step solution treatment of 495°C/2h followed by 515°C/4h produced the optimum combination of strength and ductility compared to the traditional single-step solution treatment of 495°C/8h. In both cases, the solution heat treatment was followed by quenching in hot water at 74°C and artificial aging at 250°C/3h. This improvement in the mechanical properties was mainly due to the improvement in homogeneity, as shown in Figure 2.7. Optical micrographs taken of both eutectic Si regions and those containing the Cu-phase revealed the improvement in homogeneity in going from the as-cast to the solution heat-treated samples. As shown in Figure 2.7(b), the as-cast microstructure displays significant copper segregation; whereas the single-step solution treatment of 495°C/8h improves the homogeneity to a considerable extent. Figure 2.7(d) reveals that a number of copper phase regions still remain in the matrix. The two-step solution treatment with its second step applied at 515°C, however, brought about a far greater improvement in homogeneity than the as-cast or single-step solution treatment conditions, *i.e.* only a small amount of the copper-rich phase was present, as shown in Figure 2.7(f). The improvement in Si-particle morphology after solution heat treatment, Figures 2.7(c) and (e), is also evident, compared to the as-cast condition shown in Figure 2.7(a).

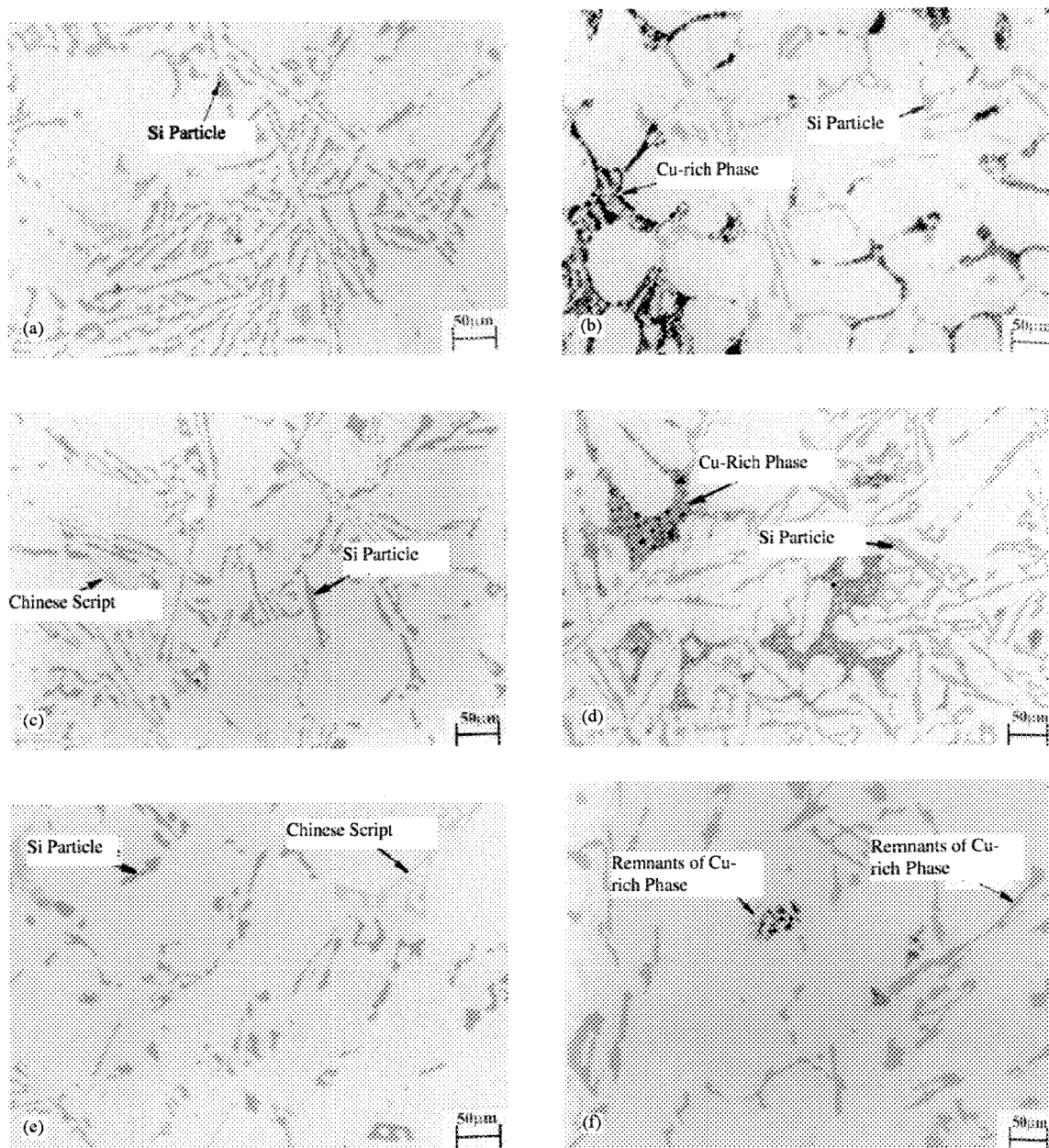


Figure 2.7 Micrographs taken of a 319 alloy automotive component showing: (a) Si particles and (b) Cu-rich phase segregation in the as-cast condition; (c) Si particles and (d) Cu-rich phase segregation after single-step solution treatment; and (e) Si particles and (f) remnants of Cu-rich phases after two-step solution treatment.^[26]

2.6.2 Quenching

Quenching is in many ways the most critical step in the sequence of heat treatment operations. The objective of quenching is to preserve the solid solution formed at the solution heat-treating temperature, by rapidly cooling to some lower temperature, which is usually close to room temperature. This operation is applied not only to retain solute atoms in solution, but also to maintain a certain minimum number of vacant lattice sites to assist in promoting the low temperature diffusion required for GP zone formation. The highest strengths attainable and the best combinations of strength and toughness are those associated with the most rapid quenching rates.^[42]

2.6.3 Precipitation Heat Treatment (Aging)

Aging is the final stage in the heat treatment of cast aluminum alloys. After solution treatment and quenching, strengthening can be completed either at room temperature (natural aging) or by applying a precipitation heat treatment (artificial aging). The effect of precipitation heat treatment on mechanical properties is greatly accelerated by heating the quenched materials in the range of 95°C to 205°C. In certain aluminum alloys, sufficient precipitation occurs in a few days at room temperature to produce stable products with properties which are satisfactory for many applications. These alloys are sometimes precipitation heat-treated to provide increased strength and hardness in wrought or cast products. Other alloys with slow precipitation reactions at room temperature are always precipitation heat-treated before being used. The precipitation heat treatment is also capable of reducing the residual stresses developed during quenching following solution heat treatment. The reduction in residual stresses is determined by the time and temperature of

the precipitation treatment as well as the alloy composition.^[43]

2.6.4 Incipient Melting

During solution heat treatment, when the 319 alloy is observed to exceed the critical composition and is heat-treated at a higher temperature than the copper eutectic temperature, localized partial melting of the Al_2Cu phase will occur at the grain boundaries. This type of melting is called incipient melting, and results in the formation of shrinkage cavities once the alloy samples are quenched after solution heat treatment; this contributes to lowering the casting soundness and diminishing mechanical properties. In Al-Si-Cu alloys, with the segregation of the alloying elements, the composition may exceed the critical one locally, in which case, incipient melting will occur.

Figure 2.8 shows an example of incipient melting taking place at the grain boundaries in a 319 alloy sample (see arrowed sites). Samuel^[32] and Mohamed *et al.*,^[44] noted that the incipient melting of $\text{Al}_5\text{Mg}_8\text{Cu}_2\text{Si}_6$ and Al_2Cu phases of 319-type alloys as well as of near eutectic Al-Si cast alloys took place when the high-Mg version of 319 was solution-treated at temperatures above 505°C for sufficiently long periods. This melting resulted in distortion of the test bars and deterioration of the mechanical properties of the alloy.

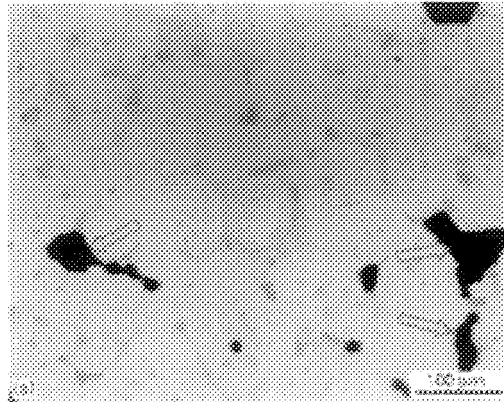


Figure 2.8 Microstructure of 319 alloy showing the occurrence of incipient melting taking place at grain boundaries (arrowed).^[31,32]

2.7 POROSITY

Porosity is one of the critical factors which is central to the quality of the casting. This parameter may be detrimental not only to the surface quality after machining but also to the mechanical properties and corrosion resistance of alloys.

Porosity in castings occurs because of the rejection of gas from the liquid metal during solidification and/or the inability of the liquid metal to feed through the interdendritic regions to compensate for the volume shrinkage associated with solidification. Hydrogen is the only gas capable of dissolving to any significant extent in molten aluminum. The drop in hydrogen solubility during solidification results in outgassing, which leads to the formation of porosity and ultimately to reduced mechanical properties and diminished corrosion resistance.^[45]

2.7.1 Theory of Porosity Formation

The formation of porosity in solidifying metals is the result of two mechanisms: (i) shrinkage, resulting from the volume decrease accompanying solidification; this type of

porosity can also occur as “microshrinkage” or “microporosity”, dispersed in the interstices of dendritic regions, typically found in alloys with a large difference between their solidus and liquidus temperatures. Limited or inadequate liquid metal feeding in the interdendritic regions gives rise to shrinkage; and (ii) gas porosity, resulting from the decrease in the solubility of hydrogen in aluminum during solidification.

According to Campbell,^[46] the growth tendency of pores is described generically by the following equation:

$$P_g + P_s > P_{atm} + P_H + P_{s-t}$$

where P_g = equilibrium pressure of dissolved gases in the melt;

P_s = pressure drop due to shrinkage;

P_{atm} = pressure of the atmosphere over the system;

P_H = pressure due to the metallostatic head;

P_{s-t} = pressure due to surface tension at the pore/liquid interface.

The dissolved gas pressure, P_g , and pressure drop due to shrinkage, P_s , are the major driving forces in the formation of porosity. For a particular casting design, P_{atm} and P_H are constants, and a decrease in P_{s-t} , as observed for modifiers such as sodium or strontium, can lead to the increased probability of pore formation.

The pore growth process has been depicted schematically by Kubo and Pehlke,^[47] as shown in Figure 2.9. In (a), the gas porosity nucleates at the base of the dendrite arms. The synergistic effect between shrinkage and gas pores overcomes the large amount of negative free energy required to form a gas-metal surface, thereby facilitating the nucleation shown in Figure 2.9(a). As solidification proceeds, the degree of porosity

increases as a result of the higher potential for gas evolution. The radius of the porous area becomes large enough to decrease the contribution of interfacial energies, and thus the porosity becomes detached from the dendrites, as shown in (b). At a still further stage of solidification, neighbouring dendrites collide, making interdendritic feeding difficult. At this stage, the porosity is thought to grow so as to compensate for solidification shrinkage, as shown in Figure 2.9(c).

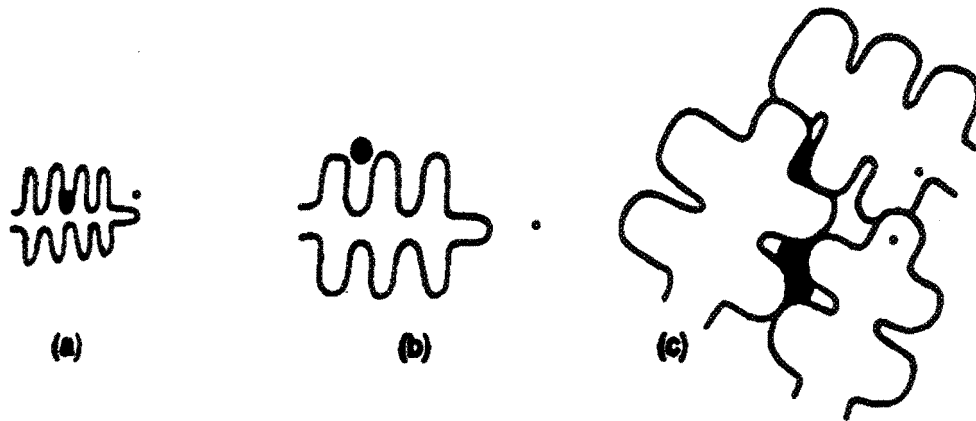


Figure 2.9 The growth process of porosity formation.^[46]

2.8 MECHANICAL PROPERTIES OF Al-Si-Cu ALLOYS

Strength, hardness, toughness, elasticity, brittleness, and ductility are all mechanical properties used to determine how metals behave under load. These properties are described in terms of the types of force or stress that the metal must withstand and the manner in which they are resisted.

Any improvement in mechanical properties is commonly evaluated through the tensile and impact properties of the material. Almost all of the steps in the processing of

aluminum, from establishing the composition to heat treatment, will produce a variation in the mechanical properties. The fact that tensile and impact properties depend on several variables may go far to explain the confusion existing over the properties of cast aluminum alloys. The following may be considered among the most important of the many variables which affect the mechanical properties of the aluminum-silicon alloy castings under investigation here.

- (i) Alloy type and the variation of the chemical composition within the specified limits for that alloy,^[48,49,50,51,52]
- (ii) Metal soundness, which may be affected by gas porosity, shrinkage porosity and non-metallic inclusions;^[53,54]
- (iii) Metallurgical characteristics, examples of which are macro-grain size and micro-constituent distribution;^[55]
- (iv) Solidification rate, which may be related directly to the secondary dendrite arm spacing;^[56,57]
- (v) Heat-treatment, which brings about phase transformation in the solid state of the alloy.^[58]

2.8.1 Hardness Testing

In general, hardness implies resistance to deformation. Hardness has conventionally been defined as the resistance of a material to permanent penetration by another harder material with measurement being made after the applied force has been removed, such that elastic deformation is ignored. Currently, the indentation hardness test is used in practically every metalworking plant as a means of checking the quality and uniformity of metals and

metal parts. Hardness measurements usually fall into three main categories: scratch hardness, static indentation hardness, and dynamic hardness.^[59]

A specific method for the measurement of static indentation hardness is widely used nowadays for determining metal hardness. This universally accepted and standardized indentation hardness test was first proposed by Brinell in 1900. The Brinell Hardness Test consists of indenting a metal surface with a steel ball, 10 mm in diameter, at a load of 3000 kg mass. For soft metals such as aluminum, the load is reduced to 500 kg to avoid deep impression, while for very hard metals a tungsten carbide ball is used to minimize distortion of the indenter.

Figure 2.10 shows a diagram representing the Brinell Hardness Test, where BHN is the Brinell hardness number; F is the imposed load in kg; D is the diameter of the spherical indenter in mm; and D_i is the diameter of the resulting indenter impression in mm.

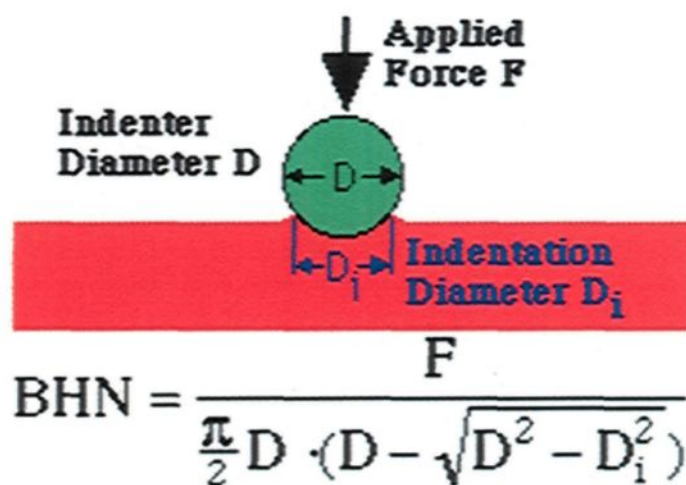


Figure 2.10 Schematic diagram of Brinell hardness test.^[61]

The load is applied for a standard length of time, usually 30 seconds, and the diameter of the indentation is measured with a low-power microscope after removal of the load. The Brinell hardness number is calculated by dividing the load applied by the surface area of the indentation,^[60] as shown in Figure 2.10.^[61]

2.8.2 Impact Testing

Most of the mechanical properties reported for cast Al-Si alloys are the outcome of tensile testing. Considerable scatter is usually observed in the results because this test is highly sensitive to additions of alloying and trace elements to the alloy sample. Furthermore, the test results are not a strong function of silicon morphology. In view of the fact that this study deals with magnesium additions and silicon morphology, a test which is much more sensitive to these parameters was required. Instrumented impact testing was thus chosen since this test is known to be extremely sensitive to the addition of magnesium as an alloying element and to silicon morphology, although data on impact properties is relatively scarce for 319-type alloys.^[59,62]

Impact energy normally means the total energy absorbed by a specimen undergoing fracture when it is being tested under a high strain rate or rapid loading. Impact values depend to a high degree on the testing method used. The most commonly applied laboratory measurement test procedure for impact energy is known as the Charpy test. The impact energy from the Charpy test correlates with the area under the total stress-strain curve of Figure 2.11 shown below.^[63]

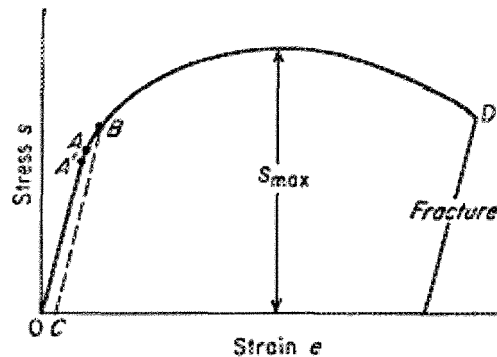


Figure 2.11 Typical tension stress-strain curve.^[63]

A computer-aided Instrumented Charpy Impact test was used to provide the load-time information in addition to data concerning the energy absorbed. The instrumented test makes it possible to divide the energy absorbed into (i) the energy required to initiate fracture, designated E_i , and known as the pre-maximum load energy, (ii) the energy required to propagate brittle fracture, or the post-maximum load energy, and (iii) the energy associated with shear lip formation, or the post-brittle fracture energy, as illustrated in Figure 2.12.^[64] In most cases, including that of Al-Si alloys, the latter two energies join together and cannot be readily distinguished, as depicted by the crack propagation impulse area marked II in Figure 2.13,^[65] considered to be the crack propagation energy and thus designated E_p . Thus, impact energy is the sum of the three energies as illustrated in Figure 2.12 or else it is the sum of the two energies, namely, energy for crack initiation and energy for crack propagation represented by the area under the load-time curve in Figure 2.13, or the total energy, E_T . Impact energy is also dependent to a high degree on the alloy microstructure, which is controlled mainly by the various alloying and melt-processing parameters. The correlation between impact energy and the following parameters: (i)

cooling rate, (ii) magnesium content, (iii) aging conditions, and (iv) microstructural characteristics is the main focus of the present study, where, in order to increase the accuracy of the measurement and to emphasize the effects of the microstructure, Charpy unnotched samples were employed. When a notch is present, the impact energy obtained is much lower than that obtained with an unnotched sample, and may be more dependent on the notch geometry than on the microstructure.^[66] Such observations have been reported by other researchers^[67,68] in their investigations of the impact properties of Al-Si cast alloys. Some of these studies will be reviewed briefly in the present work in the context of the alloys and microstructural parameters investigated.

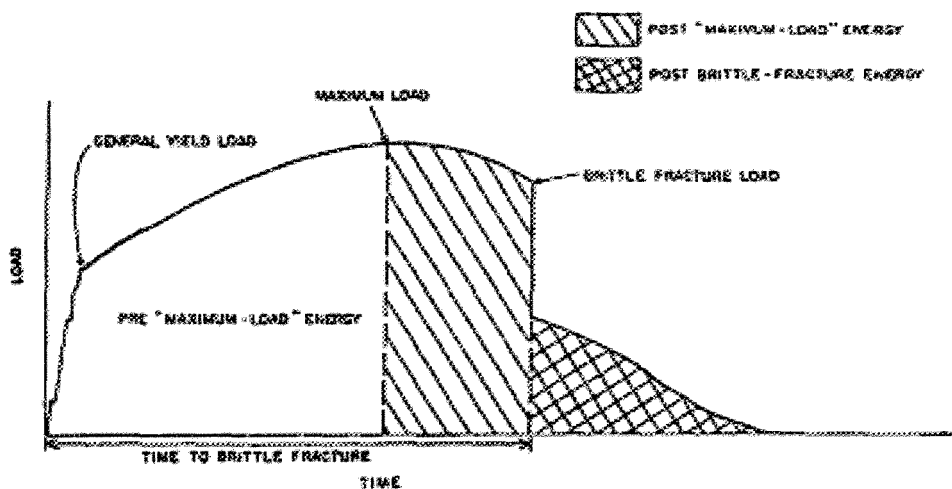


Figure 2.12 An idealized load-time trace for an impact Charpy V-notch specimen.^[64]

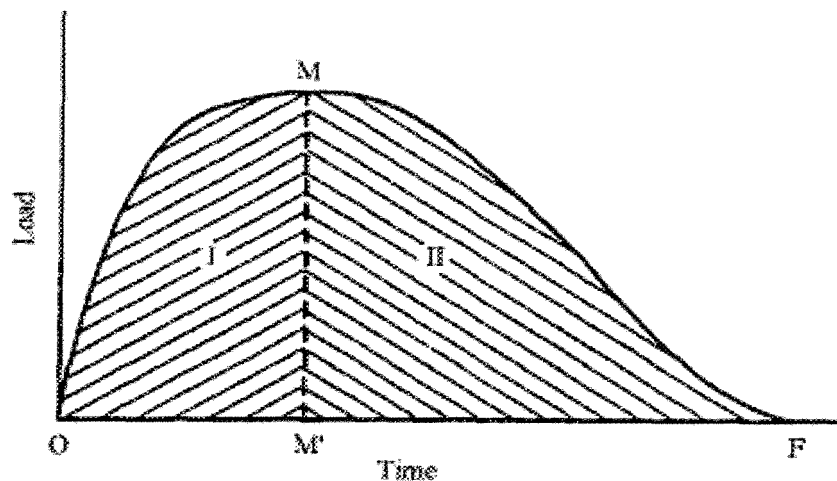


Figure 2.13 Schematic representation of relationship between load and time in a Charpy impact test. M: Maximum load; I: Crack initiation impulse; II: Crack propagation impulse; OM': Crack initiation time; M'F: Crack propagation time.^[65]

2.8.2.1 Effect of Sample Configuration

Impact values depend strongly on sample configuration, particularly when a notch is present, in which case the energy obtained will be much lower than that of an unnotched sample; these values will be more greatly dependent on notch geometry, than on the microstructure. This type of dependence will decrease the accuracy when evaluating the effects of alloying and melt processing parameters on the impact energy.

The impact energies of unnotched, U-notched and V-notched samples of 356 alloys were determined by Tsukuda *et al.*^[69] Maintaining all other parameters at the same values, the unnotched samples displayed much higher impact values than the notched samples. The U-notched samples possessed somewhat higher impact energies than the V-notched samples. The largest improvements were observed on going from the V-notched to the unnotched samples; most of them being over 200% with the highest at 247% and the lowest

at 146%. Between the U-notched and V-notched samples, the former showed improvements of ~60% over the latter with the highest at 65% and the lowest, nil.

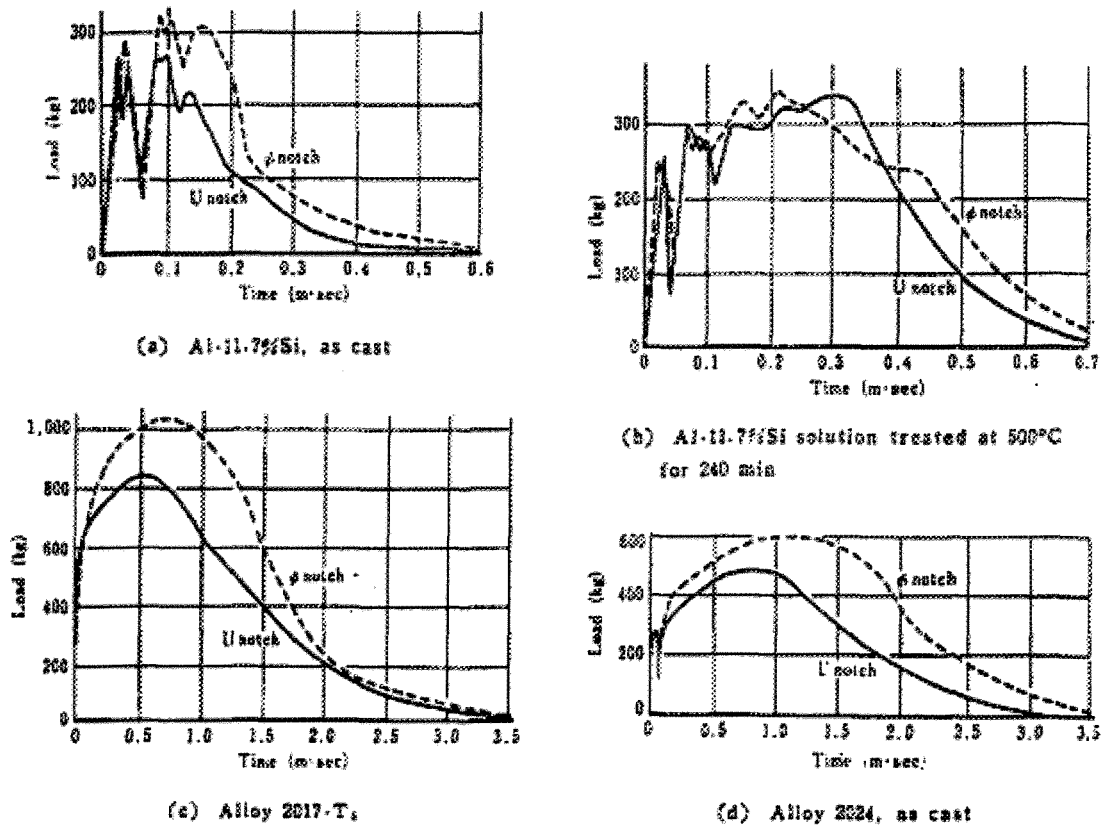


Figure 2.14 Load-time relationship for Φ -notch and U-notch specimens.^[65]

The difference between the load-time curves for Φ -notch and U-notch specimens of Al-Si alloys, as observed in the work of Komatsu *et al.*,^[65] is shown in Figure 2.14. The configuration of the Φ -notch specimens used in their study is shown in Figure 2.15, while the U-notch specimens were made according to JIS Z 2202 (No. 3) specifications. Higher energy values may be obtained from the Φ -notch specimen. Since the impact energy of Al-Si alloys is relatively low compared to that of steel samples, it is reasonable to employ

samples which can provide higher impact energy values and thus facilitate the analysis with respect to alloying and melt processing parameters.

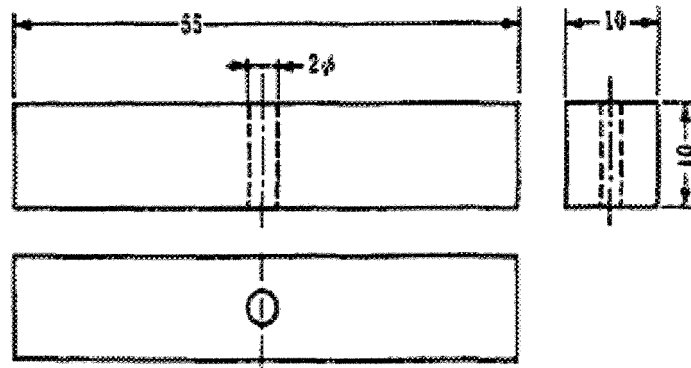


Figure 2.15 Dimensions of Charpy test specimens (mm).^[65]

A comparison between impact energies obtained from the Charpy V-notch Test and the Mesnager Impact Test was conducted by Richard.^[70] It should be noted that the Charpy V-notch Test sample is similar to the Charpy single beam specimen type A, ASTM E23,^[71] while the Mesnager Test sample is similar to the Charpy specimen type C, ASTM E23^[71] but with possibly different depth values. The Mesnager Test generally yielded higher values, and an impact energy correlation between the two sample types in aluminum alloys was obtained as follows:

$$E_{\text{Mesnager}} = 1.6 \times E_{\text{Charpy}} + 0.3$$

with E_{Mesnager} being expressed in J/cm^2 , and E_{Charpy} in J units of energy.

In North America, ASTM E23^[71] samples are most commonly employed for impact testing. The dimensions of such samples are the same as those of the unnotched samples used in the present work, except for the notch. With the notched Al-Si alloy samples used by Shivkumar *et al.*,^[72,73] extremely low impact energies were obtained in their work

compared to those obtained under the same conditions by Paray *et al.*^[66] who used unnotched samples instead (*cf.* 7.8 J with 15.12 J for unmodified 356 alloys, and 13.1 J with 22.82 J for modified 356 alloys). In view of the fact that unnotched samples were used in this study, higher impact energies were therefore expected to be obtained.

CHAPTER 3
EXPERIMENTAL PROCEDURES

CHAPTER 3

EXPERIMENTAL PROCEDURES

3.1 INTRODUCTION

This chapter will provide all the relevant details concerning the alloys and additives used in the current research, together with a description of the general melting and casting procedures applied; this will include a characterization of the microstructure and a discussion of the hardness and impact testing methods used to determine the mechanical properties of the alloys investigated. It is worthwhile mentioning here that the number of samples which were cast for the study was considerable, giving an idea of the quantity of molten metal which was processed in the preparation of the corresponding castings.

Three kinds of test samples were produced: (i) impact test specimens; (ii) hardness test bars; and (iii) samples for chemical analysis. The alloy codes for the various alloys which were prepared have been collectively listed in Table 3.2. Details of the experimental procedures adopted are provided in the following subsections.

3.2 ALLOY PREPARATION AND MELTING PROCEDURE

Both industrial-commercial and experimental 319 alloys were used in the present study. The industrial B319 alloy was received in the form of 12.5 Kg ingots, the chemical composition of which is shown in Table 3.1.

Table 3.1 Chemical composition of the industrial B319 alloy

Alloy	Element (wt%)							
	Si	Cu	Mg	Fe	Mn	Zn	Ni	Al
B319	6.75	3.082	0.2945	0.3003	0.2471	0.1126	0.0386	bal.

The magnesium level of the alloy was increased by adding pure Mg to the 319 alloy melt to obtain Mg levels of 0.3 wt% and 0.6 wt%; this was done in order to investigate the effect of Mg on the incipient melting of the alloy, as well as to compare the porosity levels obtained at the two different Mg levels. These alloys were respectively coded D7, or LD7, and D8, or LD8, as shown in Table 3.2.

Measured quantities of pure aluminum, silicon, copper, and magnesium were used to prepare the experimental 319 (Al-7%Si-3.5%Cu-Mg) alloy. The experimental base alloy was coded D1, or LD1, as shown in Table 3.2. Five other experimental alloys were prepared from the base D1, or LD1, alloy with Mg levels of 0.1, 0.2, 0.3, 0.4, and 0.6 wt%, respectively. Table 3.2 lists these experimental alloys and their respective codes.

Table 3.2 List of the alloys used in the present work and their respective codes

Alloy Type	Alloy Code	Nominal Composition
Experimental Alloy	D1 (or LD1)	Al-7%Si-3.5%Cu (Base Alloy)
	D2 (or LD2)	Base Alloy + 0.1 wt% Mg
	D3 (or LD3)	Base Alloy + 0.2 wt% Mg
	D4 (or LD4)	Base Alloy + 0.3 wt% Mg
	D5 (or LD5)	Base Alloy + 0.4 wt% Mg
	D6 (or LD6)	Base Alloy + 0.6 wt% Mg
Industrial Alloy	D7 (or LD7)	B319 Alloy + 0.3 wt% Mg
	D8 (or LD8)	B319 Alloy + 0.6 wt% Mg

The experimental alloys were prepared using an electrical resistance furnace having a large 40-Kg crucible capacity, as shown in Figure 3.1. About 35 Kg of each alloy was prepared. The melting temperature was maintained at $750^{\circ}\text{C} \pm 5^{\circ}\text{C}$. Samplings for chemical analysis were taken from each experimental alloy melt which had been prepared. The melts were poured into ingots which were then set aside for ulterior use. The actual chemical compositions of these experimental alloys and the two industrial alloys used are shown in Table 3.3.



Figure 3.1 Furnace used for preparing experimental alloys.

Table 3.3 Average chemical composition (wt%) of the experimental alloys and industrial alloys studied

Alloy Code	Element Concentration (wt %)							
	Si	Fe	Cu	Mn	Mg	Zn	Ni	Al
D1 (or LD1)	6.76	0.201	3.812	0.0059	0.0081	0.0042	0.0114	Bal.
D2 (or LD2)	6.59	0.1899	3.569	0.0065	0.1067	0.0044	0.0098	Bal.
D3 (or LD3)	6.39	0.1815	3.465	0.0069	0.2384	0.0050	0.0096	Bal.
D4 (or LD4)	6.62	0.1822	3.562	0.0023	0.3219	<0.0017	0.0100	Bal.
D5 (or LD5)	6.64	0.1847	3.606	0.0030	0.4256	<0.0017	0.0099	Bal.
D6 (or LD6)	6.66	0.1890	3.564	0.0034	0.636	<0.0017	0.0092	Bal.
D7 (or LD7)	7.43	0.3197	3.314	0.2874	0.3376	0.1255	0.0452	Bal.
D8 (or LD8)	7.47	0.3138	3.375	0.2847	0.643	0.1260	0.0449	Bal.

In the above table, D the code corresponds to the non-modified alloy which was cast using the star-like mold, and LD corresponds to the non-modified alloy cast using an L-shaped mold. In the case of the modified alloys, the codes D and LD are represented by DS and LDS, respectively.

3.3 MELTING AND CASTING PROCEDURES

The alloy ingots were melted in a 40-kg capacity SiC crucible using an electrical resistance furnace where the melting temperature was maintained at $750 \pm 5^\circ\text{C}$. At this temperature, measured Mg and Sr additions were made to the melt by means of a perforated graphite bell. Strontium was added in the form of Al-10% Sr master alloy to obtain 200 ppm Sr levels, whereas Mg was added in the form of the pure metal.

Prior to casting, the molten metal was degassed for 15 minutes using pure, dry argon; in this case the degassing speed/time was kept constant at 150 rpm/15 min. In addition to the required number of castings prepared from each melt, two samplings for

chemical analysis were also taken from each melt, one before the start of casting and one at the end of casting. The chemical analysis was carried out using arc spark spectroscopy at GM facilities in Milford, NH. The actual chemical composition of each of these alloys is shown in Table 3.3 representing average values taken over three spark measurements made for each chemical analysis sample. For each set of melt conditions, identical castings were prepared for metallographic observations, hardness measurements, and impact testing.

The various 319 alloys were used to prepare castings from which test bars were obtained for hardness and impact testing purposes. With this aim in mind, the molten metal was poured into a permanent mold which had been preheated to 450°C.

Because of its high cooling rate, the star-like mold was used to prepare the impact test bars and the hardness test samples as well as to take metallographic measurements. This particular mold is shown in Figure 3.2 with the casting still intact in the bottom half of the mold and the open upper half behind it. Each casting provides ten impact bars which are cut from the casting and then machined to the required ASTM specifications for conducting Charpy impact tests after that.

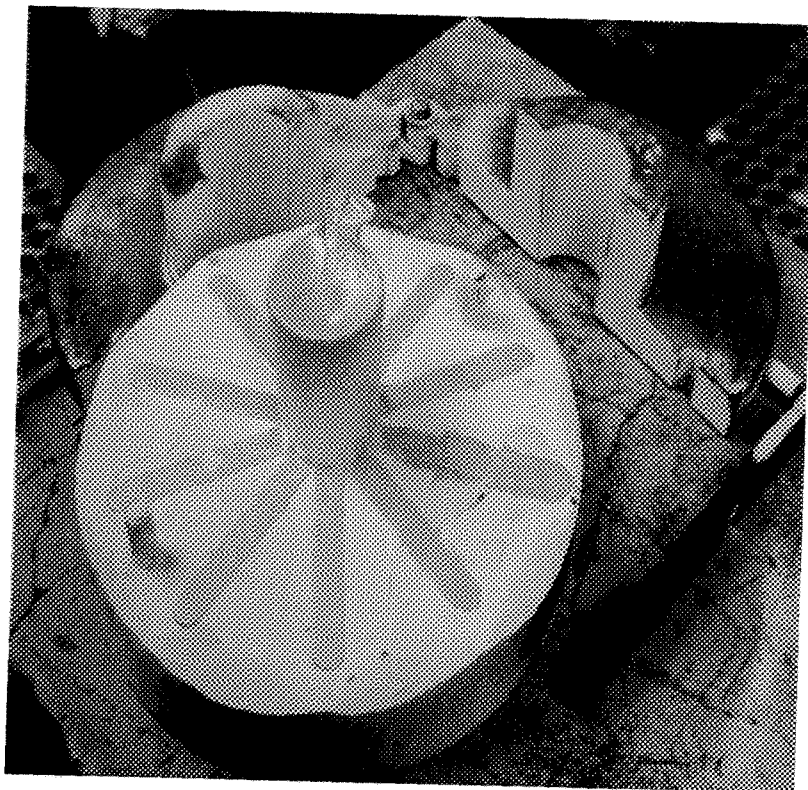


Figure 3.2 Star-like metallic mold used to prepare impact test bars.

The L-shaped mold, used specifically for its low cooling rate, was chosen to prepare the impact test bars and the hardness test samples as well as to make metallographic measurements; this mold may be seen illustrated in Figure 3.3. Each casting provides twelve impact bars which are cut from the casting and then machined to the required ASTM specifications for conducting Charpy impact tests subsequently.



Figure 3.3 L-shaped metallic mold used to prepare impact test bars.

3.4 SOLUTION HEAT TREATMENT AND AGING

The bars were prepared for each alloy composition and divided into sixteen sets; one set was kept in the as-cast condition; one set was solution heat-treated at 495°C for 8 hours, then quenched in warm water at 65°C and maintained in solution heat-treated conditions; seven sets were solution heat-treated at 495°C for 8 hours, then quenched in warm water at 65°C followed by artificial aging at 180°C for 2, 4, 6, 8, 12, 24, and 48 hours, respectively; the remaining seven sets were solution heat-treated at 495°C for 8 hours, then quenched in warm water at 65°C followed by artificial aging at 220°C for 2, 4, 6, 8, 12, 24, and 48 hours, respectively. The solution and aging heat-treatments were carried out in a forced-air Blue M Electric Furnace equipped with a programmable temperature controller, accurate to $\pm 2^\circ\text{C}$. The aging delay was less than 10 s. For each

individual heat treatment, five test bars were used. The above procedures were applied in the heat treatment of the hardness and impact test samples.

3.5 MECHANICAL TESTING

The mechanical properties of the alloys examined in this study were evaluated through their hardness and impact properties. A description of the castings prepared for these tests and the details relating to the test samples sectioned from the respective castings have already been provided in subsection 3.3, above.

3.5.1 Hardness Testing

Hardness test bars measuring 10 mm x 10 mm x 55mm were cut from the casting, as shown in Figures 3.4 and 3.5. All test samples were heat-treated in the same way as the impact samples, while the specimen surfaces were polished with fine sandpaper to remove any machining marks. The hardness measurements were carried out on the as-cast and heat-treated samples using a Brinell hardness tester, applying a steel ball of 10 mm diameter and a load of 500 kgf for 30 seconds. Figure 3.4 shows the Brinell hardness tester used for these measurements. An average of four readings obtained from two perpendicular surfaces was taken to represent the hardness value in each case.

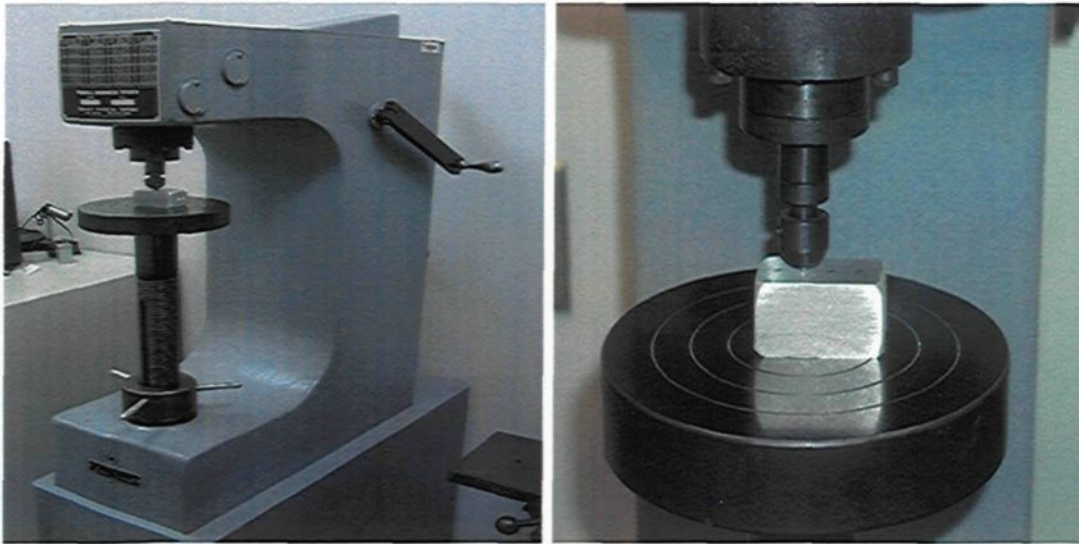


Figure 3.4 Brinell hardness tester used for hardness measurements.

3.5.2 Impact Testing

As mentioned earlier in subsection 3.3, each impact mold-casting provided ten impact test bars and each L-shaped mold provided twelve bars. The samples were sectioned from the casting, and machined according to the dimensions shown in the diagram in Figure 3.5. The specimen surfaces were polished with fine sandpaper to remove any machining marks; it should also be noted that the impact tests were performed on unnotched samples.

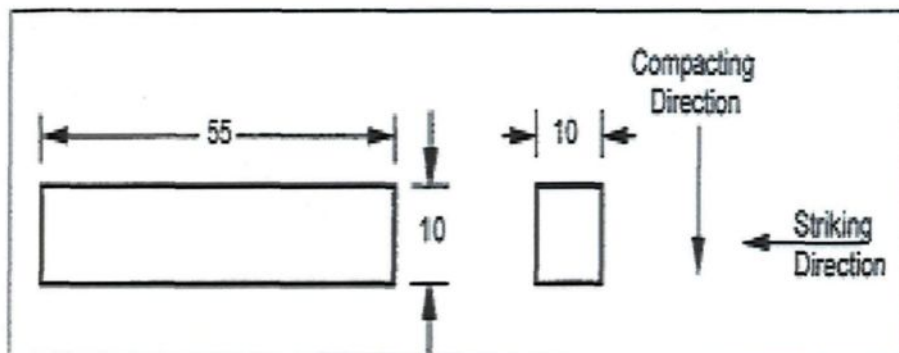


Figure 3.5 Charpy unnotched impact specimen (all dimensions in mm).

A computer-aided instrumented SATEC SI-1 Universal Impact Testing Machine (SATEC Systems Inc., Model SI-1D3), as shown in Figure 3.6, was used to carry out the impact tests. This machine is equipped with bolt-on weights in addition to the pendulum. The pendulum is capable of being latched in two separate modes, known as “high latch” and “low latch,” providing a total of four operating capacities, namely, a capacity of 25 ft-lbs (33.9 J) on low latch and 60 ft-lbs (81.35 J) on high latch without the bolt-on weights attached, and a capacity of 50 ft-lbs (67.8 J) on low latch and 120 ft-lbs (162.7 J) on high latch with the additional weights attached. A data acquisition system connected to the impact machine monitored the dynamic behavior of the test specimen and measured the load and energy values as a function of time.



Figure 3.6 A computer-aided instrumented SATEC SI-1 Universal Impact Testing Machine, with a Dynatup IPM/PC impact testing system for data acquisition.

The total absorbed energy (E_t) during impact testing was determined, together with a number of specific parameters such as crack initiation (E_i) and crack propagation (E_p) energies, total time, and the maximum load required to break the specimens. The load-deflection curves and energies absorbed were obtained using a Dynatup IPM/PC Impact Testing System. The average values of the energies obtained from the five samples tested for each alloy condition were taken as the representative values for that particular condition.

3.6 METALLOGRAPHY AND MICROSTRUCTURAL EXAMINATION

Samples for metallography were sectioned from the impact-tested bars of all the alloys studied about ~10 mm below the fracture surface. Two samples measuring 10 x 10 mm were sectioned off to study each alloy condition. One sample was used in the as-cast condition, while the second sample was solution heat-treated. The samples were then mounted in bakelite using a Struers Labopress-3 Mounting Press with a force of 30 N; the heating time was 9 min and the cooling time was 6 min. After that, the samples were polished using a Struers Tegrapol-35 Grinder-Polisher to obtain the desired fine finish (1 μm Mastermet). Details of the grinding and polishing procedures are provided in Table 3.4.

At each stage of the procedure, the coolant which was used also acted as a lubricant and ensured constant cleaning of the paper and the specimen simultaneously. Between the different stages, the samples were cleaned with water. Care was taken to see that the pressure exerted on the specimen was high enough to ensure proper cutting by the abrasive and a sufficient rate of abrasion, without the unwanted production of heat and premature

wear and tear on the abrasive.

Table 3.4 Grinding and polishing procedures for metallographic samples

Stage	Abrasive	Particle Size (μm)	Coolant	Pressure (N)	Time (sec)	Speed (rpm)
1	SiC (120)	125	Running water	30	60	150
2	SiC (240)	52	Running water	30	60	150
3	SiC (320)	35	Running water	30	60	150
4	SiC (400)	22	Running water	30	60	150
5	SiC (600)	14	Running water	30	30	150
6	SiC (800)	10	Running water	30	30	150
7	Diamond	9	Special oil	30	360	150
8	Diamond	6	Special oil	30	360	150
9	Diamond	3	Special oil	30	360	150
10	Mastermet	1	Running water	30	180	80

Note: Special Oil indicates lubricant fluid.

The microstructures of the polished sample surfaces were examined using an optical microscope linked to a Clemex image analysis system, as shown in Figure 3.7. The eutectic silicon particle characteristics, including area, length, aspect ratio, roundness, and density, were measured and quantified. For each sample, 50 fields at a magnification of 500X were examined, so as to cover the entire sample surface in a regular and systematic manner. In addition, porosity measurements were carried out, over 50 fields per sample, at a magnification of 100X. The porosity parameters measured were percentage porosity, pore area, and pore length. As a rule, the outer edges of a sample were avoided in taking these measurements so as to eliminate any distortions which might occur in the peripheral regions. Figure 3.7 shows the Optical Microscope - Clemex Image Analyzer system used for these measurements.



Figure 3.7 Optical Microscope - Clemex Image Analyzer system.

CHAPTER 4
MICROSTRUCTURE AND HARDNESS
OF 319-TYPE Al-Si-Cu-Mg ALLOYS

CHAPTER 4

MICROSTRUCTURE AND HARDNESS OF 319-TYPE

Al-Si-Cu-Mg ALLOYS

The microstructure of an alloy is influenced by its chemical composition, the melt treatment conditions, the solidification rate and the type of heat treatment applied. Copper and magnesium, for example, are added to Al-Si-Cu alloys for strengthening, whereas iron is an undesirable impurity element which not only forms harmful intermetallics, but, in turn, facilitates the formation of porosity due to the presence of these intermetallics. Strontium is commonly added to modify the shape of the eutectic silicon from acicular to fibrous (this is known as "eutectic modification"). However, it also favors the formation of porosity. The cooling rate used has a direct effect on the resulting grain size as well as the size of the microconstituents (which precipitate) and the amount of porosity formed. These variables, in turn, can affect the mechanical properties and the fracture behavior of an alloy.

The effects of the above-mentioned parameters on the hardness and impact toughness of Al-Si-Cu-Mg alloys will be respectively elaborated upon and discussed in this and the following chapter. The results are presented and discussed thereafter. Hardness refers to the resistance of a material to permanent penetration by another harder material with measurement being made after the applied force has been removed. The Brinell hardness test is a widely used and accepted method for determining a material's hardness

value.

4.1 EFFECT OF MODIFICATION

Eutectic silicon morphology (particle size and shape) plays a vital role in determining the mechanical properties of Al-Si alloy castings. Under normal cooling conditions, the eutectic Si particles, present as coarse, acicular needles, act as crack initiators which lower the mechanical properties. The addition of small amounts of Sr to the melt alters the acicular morphology of these Si particles to fibrous, which greatly improves the mechanical properties. Silicon particle characteristics can also be affected via thermal modification by subjecting the casting to a high temperature treatment for long periods. These two types of modification have been used together to produce the desired properties in a casting. The primary aim of modification is to alter the morphology and distribution of eutectic Si particles in order to improve the alloy mechanical properties. Moreover, modification neutralizes the detrimental effect of the plate-like iron intermetallics and, in turn, further improves the mechanical properties.

The changes in microstructure during heat treatment for unmodified and Sr-modified samples, initially consists of the Si particles breaking down into smaller fragments and spheroidizing gradually. Prolonged solution heat treatment leads to coarsening of these particles. The change in Si morphology occurs via separation and spheroidization; the Si particles separate into segments at corners or thin growth steps, but retain their flake morphology and, subsequently, these broken segments spheroidize so that the Si particle aspect ratio decreases. These results agree with theoretical predictions that

the initial breakdown of a eutectic structure during elevated temperature treatment arises from shape perturbations in the second phase constituent. The eutectic Si particles gradually decompose into a series of nearly spherical crystals, with the driving force for this process being a reduction in the total interfacial energy of the system (subsection 2.3).

The mechanical properties of Al-Si foundry alloys are influenced by the microstructure, which itself depends strongly on the solidification conditions and alloy composition. The presence of copper in the 319 alloy drastically changes the fracture behaviour of the alloy. When the Al_2Cu phase is present, the fracture seems to no longer be controlled by the Si particles. Although the eutectic Si has been modified by the presence of Sr in the alloy, the impact strength is not improved. In addition to the modification of the Si phase, there is a tendency to form blockier Al_2Cu particles in the presence of Sr, although finer, eutectic-like Al_2Cu can also form. In some cases, the Al_2Cu is segregated to certain regions of the sample. All of these factors, coupled with the brittle nature of the Al_2Cu phase, likely contribute to the very low impact strengths of 319 alloys which contain significant amounts of Al_2Cu .^[1,6,66] Paray *et al.*^[66] reported that modification improved the unnotched impact strength of both as-cast and heat-treated A356.0 and 413.0 alloys.

De la Sablonnière and Samuel^[31] found that the average Si particle size in the 319 alloy containing 0.5wt% Mg is generally larger than for an alloy with a low Mg content. For the 319 alloy containing a low level of Mg, the roundness of the Si particles increases with increasing solution temperature, reflecting a continuous process of spheroidization. Conversely, in the 319 alloy with 0.5wt% Mg, spheroidization proceeds up to a certain stage (12hrs/510°C + 12hrs/525°C), then decreases at higher solution temperatures; this

may be noted from the corresponding Si particles roundness values. Polygonal Si particles in the 319 alloy with 0.5wt% Mg may be observed when a two-step solution heat treatment (12hrs/510°C + 12hrs/540°C) is applied. The authors explain that in the first instance, the Si particles undergo the normal fragmentation-spheroidization-coarsening process with progressing solution treatment. In the second case, however, it appears that a number of Si particles undergo spheroidization, leading to coarser, primary-type Si particles for the same range of solution treatment conditions (subsection 2.3).

4.2 EFFECT OF MAGNESIUM

The effect of magnesium additions to Al-Si-Cu alloys has already been discussed in subsection 2.4. With respect to incipient melting, the addition of Mg can bring about the segregation of the Al₂Cu phase, so that it becomes more difficult to dissolve during solution heat treatment. An addition of up to 0.5wt% Mg leads to a significant increase in the volume fraction of the Cu-containing phase with a clear tendency toward segregation in localized areas, leading to the formation of a block-like, rather than a fine eutectic-like, Al₂Cu phase. It is important to avoid segregation of the copper phases in order to prevent incipient melting and ensure that the alloy properties and castings remain sound. Paray *et al.*^[66] reported that 0.4wt% Mg resulted in a rapid decrease in the impact strength of Al-Si foundry alloys for both the as-cast and T6 heat treatment conditions.

Silicon alone contributes very little to the strength of aluminum casting alloys, yet provides a very effective level of strengthening when combined with magnesium to form Mg₂Si. The Mg₂Si phase is soluble in the alloy to a limit of ~0.7wt% Mg, and provides the

precipitation strengthening basis for the heat-treatable alloys.^[74] De la Sablonnière and Samuel^[31] found that “burn spots”, resulting from the burning of the molten copper phase in 319 alloy test bars containing a high level of Mg, occur when solution heat treatment is carried out at $T > 520^{\circ}\text{C}$. These authors also demonstrated that $\sim 0.5\text{wt}\%$ Mg led to a significant decrease in the eutectic Si temperature. This temperature determines the maximum temperature that the 319 alloy can be exposed to during heat treatment, without any incipient melting (subsection 2.4).

4.3 COMBINED EFFECTS OF MAGNESIUM WITH STRONTIUM

Joenois and Gruzleski^[75] reported that $\sim 1\text{wt}\%$ Mg refined the Si phase in non-modified Al-Si alloys. However, when combined with Sr, Mg had a negative effect on Sr-modification, where it changed the microstructure from a well-modified to a partially modified one. This itself occurs as a result of the precipitation of the $\text{Mg}_2\text{SrAl}_4\text{Si}_3$ intermetallic phase, which forms prior to the eutectic reaction. It is likely that a higher amount of Sr is required to achieve a full modification of the Si structure when Mg is present.

Heusler and Schneider^[25] reported that in an Al-11%Si alloy containing 100 ppm Sr, a eutectic temperature depression of 4K was achieved. It was also indicated that an additional increase in the Sr content did not lower the eutectic temperature any further. In the presence of Mg, a depression of 4K was observed for 50 ppm Sr, and a maximum depression of 7-8K for 100-150 ppm Sr. Nevertheless, in the Mg-free sample modified with 100 ppm Sr, the Al-Si eutectic was observed to be better modified than in the Mg-

containing alloy modified with the same amount of Sr, indicating that the interaction between Sr and Mg leaves less Sr available for modification of the Al-Si eutectic in the Mg-containing alloy.^[25]

From the work of Roy *et al.*^[53] on the effect of Sr-Mg interaction in reducing the porosity volume fraction in Al-Si-Cu alloys, it was reported that the base alloy (having no Sr or Mg, with a melt hydrogen level of ~0.3ml/100g Al) exhibited ~2 vol.% porosity. Additions of 300 ppm Sr and 0.5wt% Mg provided a sounder casting (for the same hydrogen level), with a porosity level of ~0.8%. Samuel *et al.*^[76] reported that the addition of both Mg and Sr can lead to severe segregation of the Al₂Cu phase in 319.2 alloys, resulting in large amounts of the coarse block-like phase, compared to the finer eutectic-like form.

4.4 EFFECT OF COOLING RATE

The cooling rate has a direct effect on the size and distribution of microstructural phases in a casting, and in turn, the mechanical properties. A decrease in the cooling rate of the casting lowers the mechanical properties of the alloy. This is a reflection of two aspects of the cast structure: (1) the difficulty of obtaining a fine modified structure at very slow cooling rates, and (2) the increased tendency for castings to be less sound if they solidify slowly.^[1] Aluminum dendrites and eutectic silicon shape/size vary with cooling rate, becoming finer at rapid cooling rates. Iron intermetallics in the alloy vary greatly in size and composition with cooling rate as well as magnesium content.

The cooling rate affects the pore size as well as the microstructure (*i.e.* mainly the

dendrite arm spacing), which, in turn, controls the threshold cell size and, hence, the pore size. An increase in cooling rate decreases both the total pore volume fraction as well as the average pore size (equivalent average pore diameter) in both modified and non-modified Al-Si alloys. The area percent porosity, maximum pore length and maximum pore area increase with the local solidification time for a constant melt hydrogen content. For a given melt hydrogen content, the pore volume fraction and the pore size decrease as the cooling rate increases. This cooling rate dependence of the pore volume fraction increases markedly at lower cooling rates ($<1^{\circ}\text{C}/\text{sec}$). The cooling rate is the more important variable in controlling the size and distribution of the intermetallic phases and porosity.^[77]

4.5 EFFECT OF HEAT TREATMENT

The heat treatment of Al-Si-Cu alloys has already been discussed in subsection 2.6. The initial strength of the Al-Si alloy may be enhanced by the addition of alloying elements such as copper, magnesium and silicon. Since these elements, whether alone or in various combinations, show increasing solid solubility in aluminum with increasing temperatures, it is possible to subject them to thermal treatments which improve the alloy strength and ductility. These heat treatments consist of three stages: (1) solution heat treatment, (2) quenching and (3) a combination of natural and artificial aging. For Al-Si-Cu alloys, the improvement in properties is primarily due to the precipitation of Al_2Cu within the alloy matrix during aging. Changes in the morphology of silicon during solution treatment also contribute to an improvement in the alloy properties.

The purpose of solution heat treatment is to put the maximum amount of hardening

solutes, *e.g.* Cu and Mg, into solid solution in the aluminum matrix. The temperature of the solution heat treatment must, therefore, be as close as possible to the eutectic temperature, without overheating or partially melting the copper phases. The dissolution rate of intermetallic compounds formed during solidification is temperature sensitive and even a 10°C increase in temperature could have an appreciable effect on optimum solution times and, subsequently, on the mechanical properties (subsection 2.6).

Yang^[78] recommended a solution treatment temperature guideline for experimental and industrial 319 alloys to avoid or minimize the occurrence of incipient melting. Moreover, the solution heat treatment temperatures in each case were suggested to never exceed the following values: (1) 535°C for an experimental 319 alloy with 0wt% Mg, (2) 525°C for an experimental 319 alloy with 0.3wt% Mg, (3) 510°C for an experimental 319 alloy with 0.6wt% Mg, (4) 520°C for an industrial 319 alloy with 0.3wt% Mg, and (5) 520°C for an industrial 319 alloy with 0.6wt% Mg.

4.6 EFFECT OF INTERMETALLIC PHASES

The copper and iron intermetallic phases of Al-Si-Cu alloys have been discussed in subsection 2.5. The presence of copper in Al-Si-Cu alloys leads to the formation of the Al₂Cu copper intermetallic. If iron is also present in the alloy, then it partially goes into solid solution in the matrix and, in part, forms intermetallic compounds (including the plate-like β -Al₅FeSi and the script-like α -Al₁₅(Mn,Fe)₃Si₂ phases) during solidification. In the solidification process, β -Al₅FeSi platelets are very active sites for the nucleation of the Al₂Cu phase. The addition of Mg leads to the formation of the π -Al₈Mg₃FeSi₆ phase with

script morphology. Under cooling rates close to equilibrium conditions for multi-component 3xx alloys, and at $\sim 540^\circ\text{C}$, the Mg_2Si and $\pi\text{-Al}_8\text{Mg}_3\text{FeSi}_6$ phases begin to precipitate. When the temperature is lowered to between $490\text{-}530^\circ\text{C}$, the precipitation of the Al_2Cu and $\text{Q-Al}_5\text{Mg}_8\text{Cu}_2\text{Si}_6$ phases occurs.^[79]

It has generally been reported that a higher Mg content increases the yield stress, while decreasing the ductility and the fracture toughness. Aside from having an effect on the age-hardening potential, magnesium also lowers the eutectic temperature and renders the eutectic Si structure more heterogeneous. It also appears to interfere with the modification of the eutectic structure when using Sr additions, resulting in a coarser and less uniform eutectic structure. The Mg content also affects the type and total volume fraction of Fe-bearing phases, which are known to have a detrimental effect on the mechanical properties, especially in Be-free alloys. The strain-hardening rate at low strains increases with Mg content, increasing the rate of the load applied onto the Si particles, and it has been suggested that this may lower the ductility of high-Mg non-modified alloys.^[80,81,82]

It is evident that the intermetallics in the high-Mg alloys are larger than in the low-Mg alloys. Furthermore, it can be seen that the average size of the intermetallics is affected by the cooling rate in both the non-modified and Sr-modified alloys. The iron-rich intermetallic phases observed in the low-Mg alloy were almost exclusively small β -phase (Al_5FeSi) plates. However, large π -phase ($\text{Al}_8\text{Mg}_3\text{FeSi}_6$) particles were dominant in the high-Mg alloy, along with a small proportion of the β -phase. In addition to its effect on the size and composition of the Fe-rich intermetallics, the Mg level also affected the volume

fraction of these phases. In the low-content Mg alloy, the volume fraction of intermetallics (primarily β -phase plates) was $\sim 0.5\text{wt}\%$, whereas in the high-content Mg alloy, it was $\sim 1.4\text{wt}\%$ and the intermetallics (primarily π -phase particles). These values were independent of the DAS for both alloys. The π -phase particles were seen more frequently in the Sr-modified alloy. At small DAS values, the rapid solidification refines the π -phase particles.^[81]

In the as-cast microstructure, iron intermetallics were present in the form of acicular or platelet shaped $\beta\text{-Al}_5\text{FeSi}$ particles, as well as script-like $\pi\text{-Al}_8\text{Mg}_3\text{FeSi}_6$ particles. The relative amounts of these two phases were found to vary with the iron and magnesium content as well as cooling rate. The relative amounts of β - and π -iron phase were changed during heat treatment with a reduction in the amount of π -phase at low and intermediate magnesium contents. Some undissolved Mg_2Si was also present at higher Mg levels. The β -phase platelets are large in size, have a large aspect ratio and are brittle, and thus are very detrimental. The π -phase particles, although also large in size, have a much more compact morphology (*i.e.* lower aspect ratio) than the β -platelets and are less detrimental to properties. However, the π -phase occupies a larger volume fraction for equivalent amounts of iron. The π -phase affects ductility, as it assists in crack propagation, and also removes magnesium from solution, thus decreasing Mg-Si precipitation. These effects may contribute to the levelling off of mechanical properties at higher magnesium levels.^[80,83,84]

Increasing the solidification rate reduces the size of microstructural features, including eutectic silicon and intermetallics; this renders crack propagation through the material more difficult, thereby increasing energy.^[80,84] Changing the aging condition from

under-aged to peak-aged increases the size of the Mg-Si precipitates formed, which then increases the stress on the atomic lattice, making dislocation movement more difficult.^[80]

During solution heat treatment, studies on the Al-7%Si-Mg alloy system have shown the π -Al₈Mg₃FeSi₆ phase present in lower Mg-containing (<0.5wt%) alloys transforms to clusters of very fine β -phase plates (or another phase without Mg), while the Mg is released into the aluminum matrix. In high Mg-containing (>0.5wt%) alloys, the solubility restricts the maximum level of Mg in the matrix and thus some of it remains in a slightly spheroidised π -phase after solution treatment. The transformation carries out nearly to completion in alloys with 0.3 or 0.4wt% Mg, but becomes increasingly less likely at 0.7wt% Mg. It is observed that the phase transformation in the low-Mg alloys is accompanied by an overall reduction in the total volume fraction of the Fe-rich intermetallics.^[83,85]

It is also observed that the solution treatment time and temperature are important parameters. The π -phase may still be incompletely dissolved after 6 hours, even in alloys with a low (~0.3wt %) Mg content.^[84,85] In a 319 alloy with 0.3wt% Mg, the dissolution of iron intermetallics improved with increasing solution temperature, where the optimum solution temperature for this alloy is 515-520°C. Solution heat treatments above this temperature range resulted in a large amount of liquid phase forming as a result of interdendritic and grain boundary remelting.^[83] A complete dissolution of the iron intermetallics seems to be less likely as Fe has negligible solubility in the aluminum matrix and, thus, the Fe intermetallics only transform from one phase to another, though some fragmentation and spheroidization may occur.^[84,85]

Observations of the heat-treated alloys show that there are very few dispersed β -platelets present in alloys with the lowest (0.05 wt%) Fe content, regardless the Mg content. However, as the amount of Fe increases, the number of these β -platelets also increases. The π -phase particles, whenever present in the heat-treated microstructures, show evidence of rounding, fragmentation and dissolution. The increase of the π -phase in the A357 alloys has two effects: (1) π -phase particle cracking decreases ductility, and (2) π -phase formation reduces the Mg available for age hardening.^[82,83]

The iron-containing intermetallic phases present within the microstructures of Al-Si alloys can usually be distinguished under the microscope by their dominant morphology and colour. Both of the so-called α -phases form in a script-like morphology (Figure 4.1(b)), yet the $\text{Al}_{15}(\text{Fe,Mn})_3\text{Si}_2$ version of the α -phase can also be found in a more compact and blocky form, or sometimes as polyhedral crystals. The π -phase also forms with a script-like morphology (Figure 4.1(d)) and is often, but not always, closely connected to the β -phase (Figure 4.1(c)), which, in turn, forms with a distinctive platelet morphology (Figure 4.1(a) and (c)). Although the β -phase has a three-dimensional platelet form, these platelets appear as “needles” when observed in a two-dimensional optical micrograph. The differing shapes of these iron intermetallics are in part responsible for the impact of iron on the castability and mechanical properties. Another critical issue for iron intermetallics and their effects is the sequence in which the different phases form during solidification, and this is influenced by both the concentrations of the elements involved and the cooling rate.^[85]

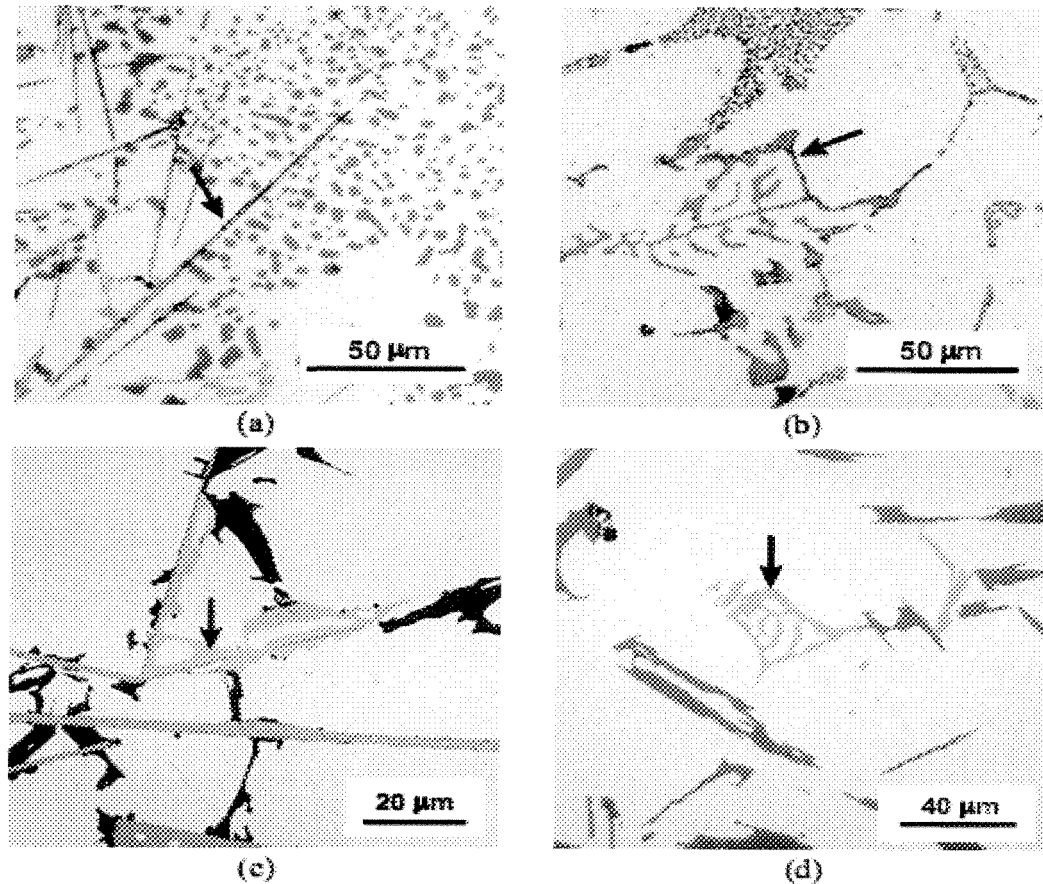


Figure 4.1 Optical micrographs showing various common iron-containing intermetallics (arrowed) and their typical morphologies in Al-5%Si-1%Cu-0.5%Mg-(Fe) alloys: (a) β -Al₅FeSi platelets, (b) script-like α -Al₈Fe₂Si, (c) π -Al₈Mg₃FeSi₆ phase growing from β and (d) script-like π -phase.^[85]

The presence of the π -Al₈Mg₃FeSi₆ and Mg₂Si phases in the as-cast microstructures primarily depends on the Mg content. The π -phase was the dominant phase in the as-cast condition, but the proportion of Mg₂Si increased as the Mg levels increased. Figure 4.2 illustrates a backscattered-electron SEM image obtained from an as-cast sample of slowly solidified high-Mg 603 alloy, in which it can be readily seen that the π -phase often grows in close association with β -phase particles.^[86]

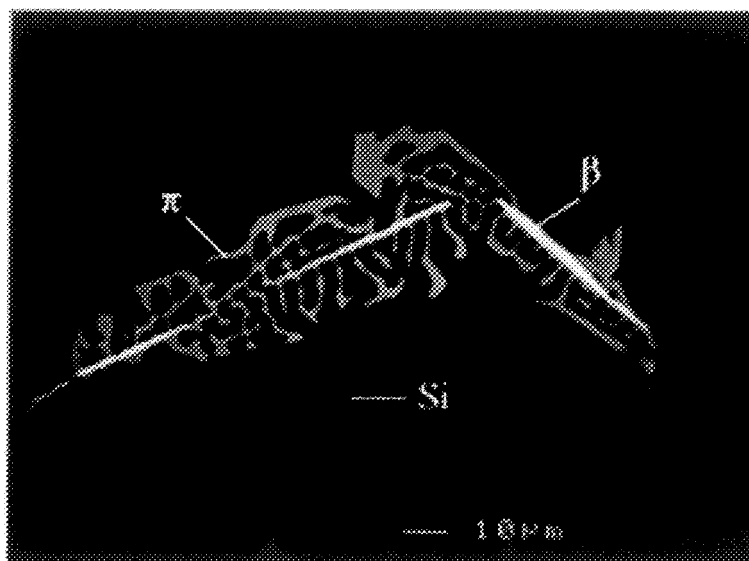


Figure 4.2 SEM backscattered-electron image of as-cast Sr-modified 603 alloy showing the close association sometimes observed between π - $\text{Al}_8\text{Mg}_3\text{FeSi}_6$ and β - Al_5FeSi .^[86]

4.7 RESULTS AND DISCUSSION

4.7.1 Microstructural Analysis

Samples for microstructural analysis were taken from the impact-tested bars ~10 mm below the fracture surface, where two samples measuring 10 mm x 10 mm were sectioned off to study each alloy condition, *i.e.* one sample was used in the as-cast condition, while the other was solution heat-treated. The silicon particle characteristics for both the experimental and industrial investigated base alloys in the as-cast and solution heat-treated conditions are summarized in Tables 4.1, 4.2, 4.3 and 4.4, respectively.

The Si particle measurements for the D1 experimental base alloy (without Mg) using the higher cooling rate star-like mold (24 μm DAS) are listed in Table 4.1. It can be seen that the Si particle area decreased from 29.60 to 5.22 μm^2 , the Si particle length

decreased from 17 to 5.16 μm , the aspect ratio decreased from 4.31 to 2.96, while the roundness ratio increased from 16.5 to 27% after Sr-modification.

Table 4.1 Silicon particle measurements for the D1 experimental alloy using the star-like mold (24 μm DAS)

Alloy (Condition)	Area (μm^2)		Length (μm)		Roundness Ratio(%)		Aspect Ratio	
	Av.	SD	Av.	SD	Av.	SD	Av.	SD
D1 (non-modified)	29.60	23.80	17.00	10.90	16.5	8.6	4.31	2.21
DS1 (Sr-modified)	5.22	4.78	5.16	3.09	27.0	9.6	2.96	0.99
D1 (non-mod. + SHT)	27.10	20.80	12.50	7.50	26.4	11.3	3.92	1.96
DS1 (Sr-mod. + SHT)	9.40	6.06	5.64	2.33	36.7	8.0	2.54	0.59

After solution heat treatment, the particle area decreased to 27.1 μm^2 , the particle length and aspect ratio decreased to 12.5 μm and 3.92, respectively. The roundness ratio increased to 26.4% for the non-modified experimental base alloy D1. Additionally, with respect to the solution heat-treated and Sr-modified base alloy DS1, the particle area and length increased from 5.22 to 9.4 μm^2 and 5.16 to 5.64 μm , respectively, while the aspect ratio decreased from 2.96 to 2.54, as a result of Si particles coarsening. These results confirm the Si particle morphology shown in Figure 4.3, and are in good agreement with those of Gruzleski and Closset,^[1,52] Hatch,^[42] Apelian,^[74] and Moustafa *et al.*^[87,88,89]

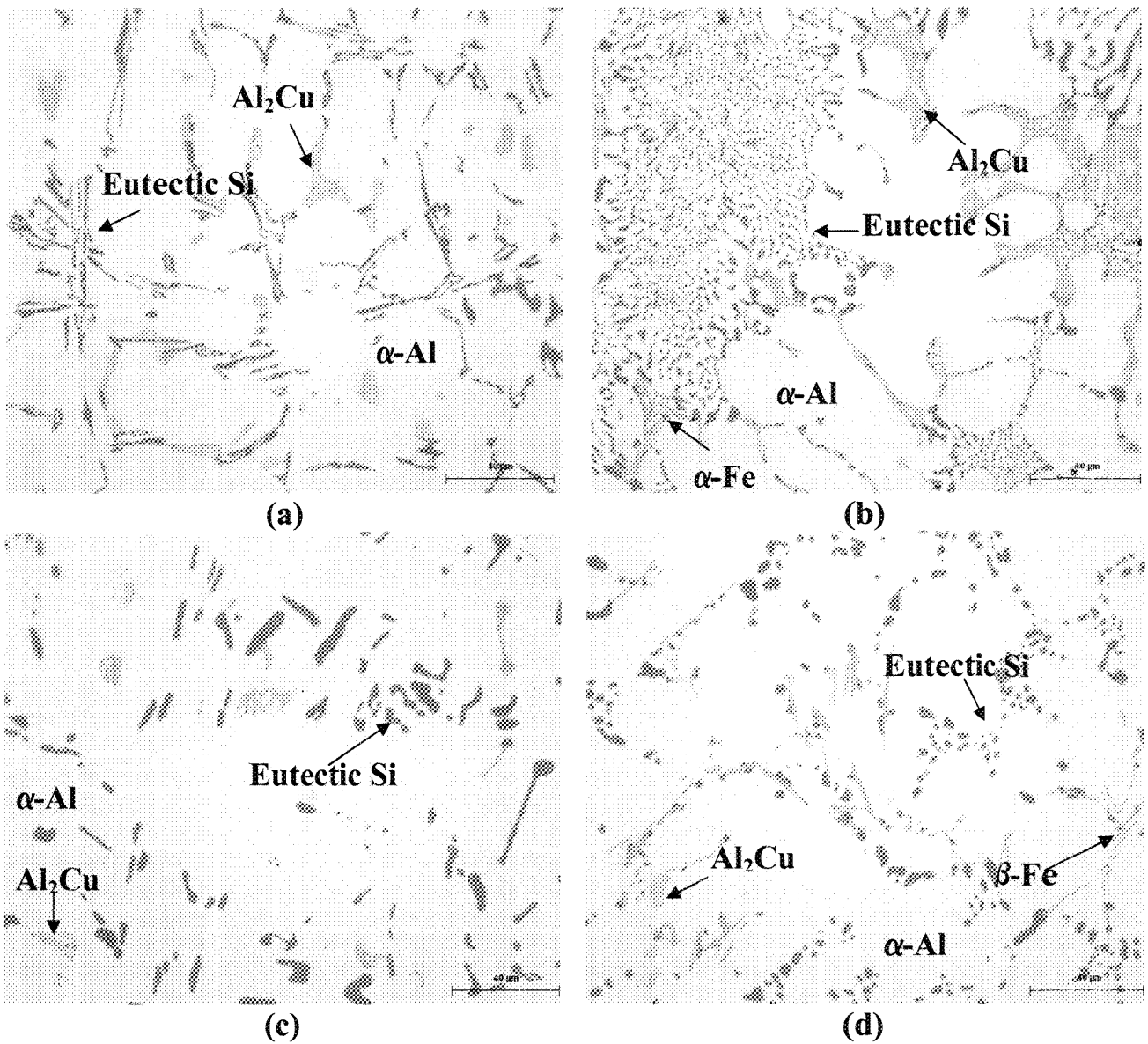


Figure 4.3 Optical microstructures observed in D1 experimental base alloy samples obtained from star-like mold castings: (a) as-cast D1 alloy, (b) Sr-modified DS1 alloy, (c) SHT D1 alloy and (d) SHT and Sr-modified DS1 alloy.

Table 4.2 summarizes the silicon particle characteristics of the same experimental base alloy (alloy LD1) using the lower cooling rate L-shaped mold (50 μm DAS). As a result of using this mold, the Si particle size increased as a direct effect of the slow solidification rate.

Table 4.2 Silicon particle measurements for the LD1 experimental alloy using the L-shaped mold (50 μm DAS)

Alloy (Condition)	Area (μm^2)		Length (μm)		Roundness Ratio(%)		Aspect Ratio	
	Av.	SD	Av.	SD	Av.	SD	Av.	SD
LD1 (non-modified)	72.00	68.70	25.00	16.00	17.2	8.8	4.14	2.12
LDS1 (Sr-modified)	4.51	3.60	4.58	2.45	29.5	9.6	2.89	0.93
LD1 (non-mod. + SHT)	61.50	49.60	19.70	12.50	23.6	10.5	3.85	1.78
LDS1 (Sr-mod. + SHT)	10.80	7.29	6.22	2.71	35.1	8.4	2.65	0.66

Table 4.3 summarizes the Si particle characteristics of the D7 industrial base alloy (0.3wt% Mg) using the higher cooling rate star-like mold. Compared to the Si particle characteristics observed for the D1 experimental base alloy, the Si particle characteristics in the D7 alloy were increased as a direct effect of chemical composition, namely the increased Mg content and the impurities present in the industrial alloy.

Table 4.3 Silicon particle measurements for the D7 industrial alloy using the star-like mold

Alloy (Condition)	Area (μm^2)		Length (μm)		Roundness Ratio(%)		Aspect Ratio	
	Av.	SD	Av.	SD	Av.	SD	Av.	SD
D7 (non-modified)	34.85	40.75	14.46	11.80	26.5	15.7	3.96	1.94
DS7 (Sr-modified)	4.87	4.19	4.84	2.48	27.2	8.5	2.65	0.64
D7 (non-mod. + SHT)	33.55	35.15	12.85	8.78	33.5	15.6	3.55	1.68
DS7 (Sr-mod. + SHT)	10.10	6.49	5.80	2.33	36.4	7.3	2.47	0.50

Table 4.4 summarizes the the Si particle characteristics of the LD7 industrial base alloy (0.3wt% Mg) using the lower cooling rate L-shaped mold. As a result of using this mold, the silicon particle size and characteristics increased as a direct effect of the slow cooling rate.

Table 4.4 Silicon particle measurements for the LD7 industrial alloy using the L-shaped mold

Alloy (Condition)	Area (μm^2)		Length (μm)		Roundness Ratio(%)		Aspect Ratio	
	Av.	SD	Av.	SD	Av.	SD	Av.	SD
LD7 (non-modified)	73.00	73.70	24.40	16.30	17.7	8.8	3.91	1.93
LDS7 (Sr-modified)	6.21	5.01	5.74	3.40	26.9	10.2	3.10	1.17
LD7 (non-mod. + SHT)	64.50	83.80	20.55	16.90	27.7	10.4	3.83	1.87
LDS7 (Sr-mod. + SHT)	11.60	8.13	6.31	2.77	35.5	8.3	2.61	0.68

The Si particle morphology obtained in samples of both as-cast and solution heat-treated D1 and DS1 alloys are shown in Figure 4.3. The microstructure shown in Figure 4.3(a) reveals the presence of coarse, acicular Si particles in the base alloy (no Mg). Figure 4.3(b) shows that strontium modification has transformed the Si particles into a fibrous form. The microstructures of Figure 4.3(c) and (d) demonstrate the effect of solution heat treatment on the Si particle morphology of the non-modified D1 alloy and Sr-modified DS1 alloy, respectively, through fragmentation, spheroidization and coarsening; these Si morphologies agree with the Si parameters listed in Table 4.1. In the as-cast microstructure, (Figure 4.3(a), the copper phase appears as block-like Al_2Cu and fine eutectic $\text{Al}-\text{Al}_2\text{Cu}$, nucleating on the coarse Si particles. The Sr-modified structure in Figure 4.3(b) shows the block-like Al_2Cu and Chinese script-like $\alpha\text{-Al}_{15}\text{Fe}_3\text{Si}_2$ phase. The microstructures of the solution heat-treated samples shown in Figure 4.3(c) and (d) show the presence of undissolved Al_2Cu and fragmented $\beta\text{-Al}_5\text{FeSi}$ platelets.

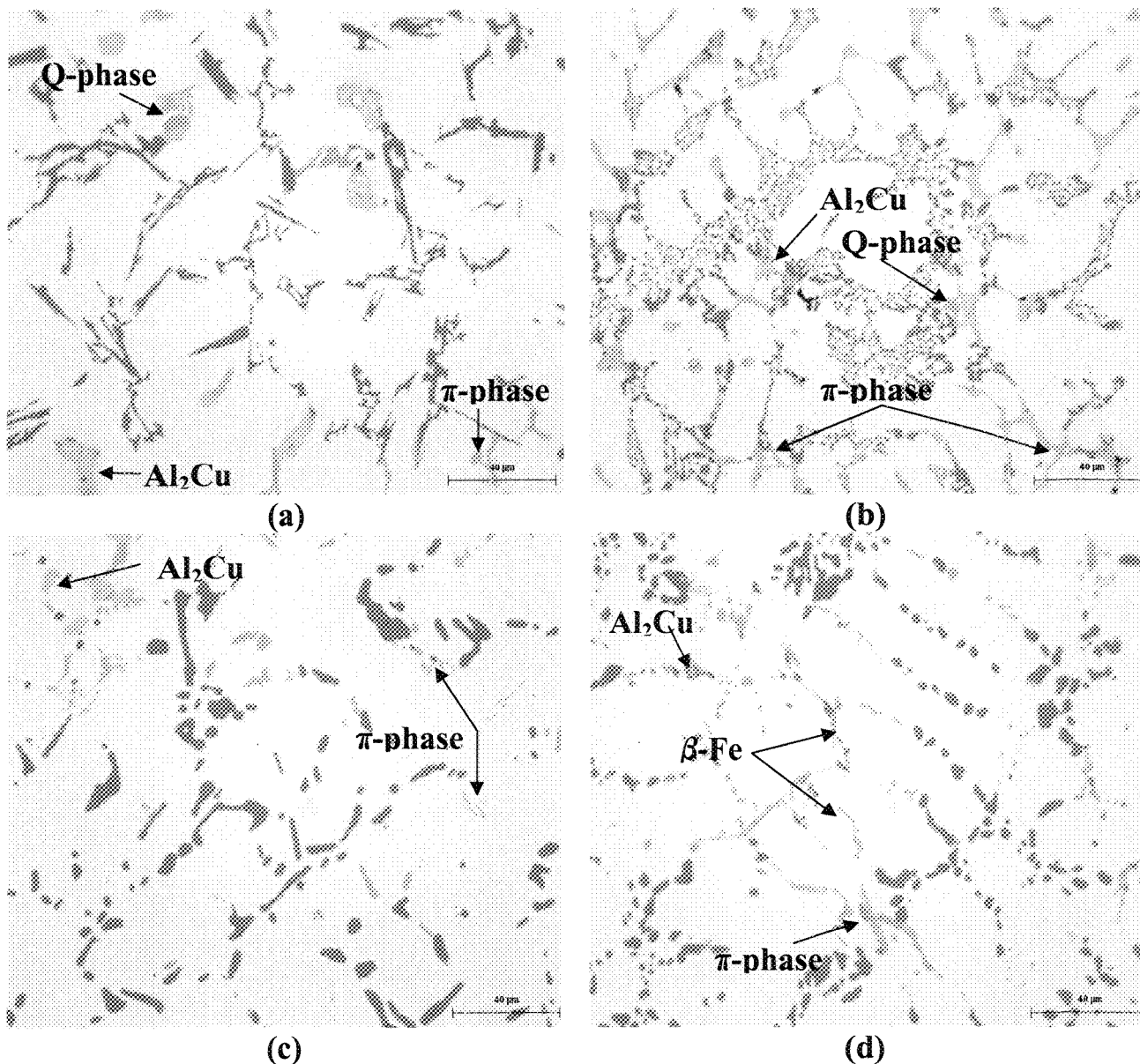


Figure 4.4 Optical microstructures observed in D6 experimental alloy samples obtained from star-like mold castings: (a) as-cast D6 alloy, (b) Sr-modified DS6 alloy, (c) SHT D6 alloy and (d) SHT and Sr-modified DS6 alloy.

When magnesium is added to the alloy, there is a tendency for segregation of the copper phase in localized areas, leading to the formation of the block-like, rather than the fine eutectic-like, Al_2Cu phase. Comparing the Si particle size and morphology of the D1 experimental base alloy (without Mg) in Figure 4.3(a) with that of the D6 experimental alloy (0.6wt% Mg) in Figure 4.4(a), it is seen that Mg does not affect the acicular nature of the Si particles.

Figure 4.4(b) illustrates how Mg hinders the modification effect of Sr, when added to the Sr-modified DS6 alloy. Moreover, Figure 4.4(b) reveals how some Si areas are fully modified, whereas others are only partially modified. These observations are in good agreement with Moustafa *et al.*^[87] and Paray *et al.*^[66] who reported that ~1 wt% Mg slightly refines the Si phase and has a negative effect on strontium modification, that is, it changes the microstructure from a well-modified to a partially modified one, due to the precipitation of $\text{Mg}_2\text{Sr}(\text{Si},\text{Al})$. The effects of modification and solution heat treatment on Si particles in the microstructures of Figure 4.4 for the D6 alloy are similar to those of Figure 4.3 for the D1 alloy.

The addition of Mg to the D6 alloy also causes segregation of the copper phase, leading to its precipitation in a block-like form. It is interesting to note that in the case of the D6 alloy, the $\text{Q-Al}_5\text{Mg}_8\text{Cu}_2\text{Si}_6$ phase also precipitates with a different morphology, *viz.*, a script-like, rather than an acicular and irregular, form as may be seen in the microstructure of Figure 4.4(b). During solidification, iron, along with other alloying elements, partly goes into solid solution, in the matrix, and partly forms intermetallic compounds, including the plate-like $\beta\text{-Al}_3\text{FeSi}$ phase, the Chinese script-like $\alpha\text{-Al}_{15}\text{Fe}_3\text{Si}_2$

phase as well as the script-like π - $\text{Al}_8\text{Mg}_3\text{FeSi}_6$ phase. This π -phase was seen to either dissolve (Figure 4.4(c)) or remain undissolved (Figure 4.4(d)).

The effects of modification, solution heat treatment and Mg content on Si particles and intermetallic compounds are variously demonstrated in the microstructures of Figures 4.5 through 4.11 for the D7 and D8 industrial alloys containing 0.3 and 0.6wt% Mg, respectively, and the LD6, LD7, and LD8 alloys for samples obtained from the L-shaped mold (i.e. at slow cooling rate). The microstructures shown in Figures 4.5, 4.6, 4.8, 4.9, and 4.11 are similar to those of Figure 4.3 for the D1 experimental alloy and Figure 4.4 for the D6 experimental alloy. The Si morphology in the microstructures of Figures 4.5, 4.7 and 4.9 agree with the Si parameters listed in Tables 4.3, 4.2 and 4.4, respectively. In addition to the copper and iron intermetallic compounds, the Mg_2Si phase is observed in the as-cast microstructures of both the experimental and industrial alloys containing 0.6wt% Mg, as shown in Figures 4.6, 4.8, and 4.11. In Figure 4.9, the presence of ultrafine Si particles within the Al- Al_2Cu eutectic structure is observed, these fine Si particles precipitate at the end of solidification. Magnified images of the encircled areas 1, 2, and 3 in Figure 4.9(d) are displayed in Figure 4.10 where these ultrafine Si particles may be clearly observed. Remnants of undissolved Al_2Cu after solution heat treatment may also be noted in Figure 4.9(c). Examples of ultrafine β -phase platelets observed in the microstructures of the solution heat-treated samples of LD1 and LD7 alloys are shown in Figures 4.7(c) and 4.9(d); the latter is presented in more detail in Figure 4.10.

The Si particle characteristics listed in Tables 4.1 through 4.4 confirm the Si particle morphologies shown in Figures 4.3 to 4.11 for all the experimental and industrial

alloys/conditions studied.

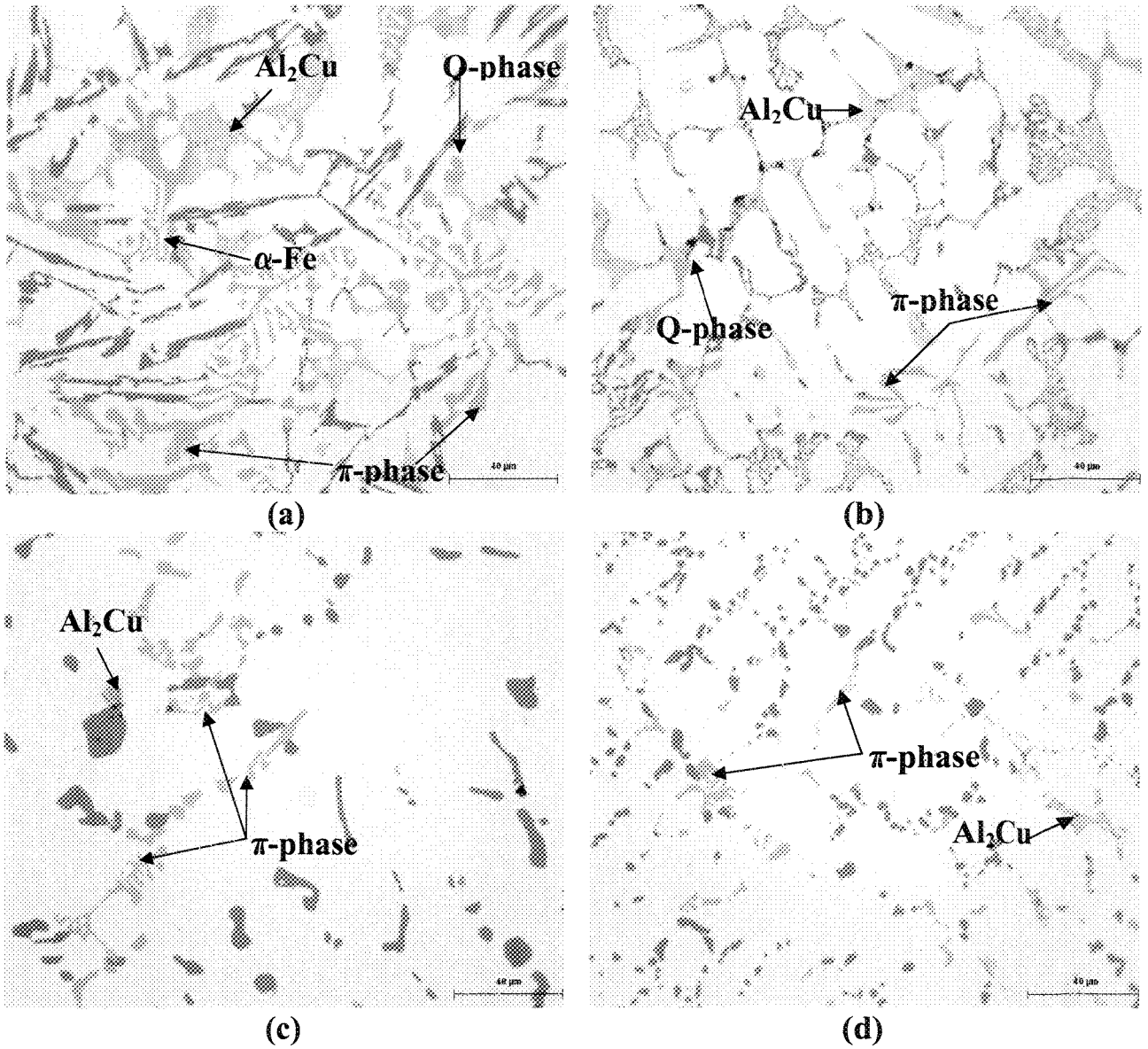


Figure 4.5 Optical microstructures observed in D7 industrial alloy samples obtained from star-like mold castings: (a) as-cast D7 alloy, (b) Sr-modified DS7 alloy, (c) SHT D7 alloy and (d) SHT and Sr-modified DS7 alloy.

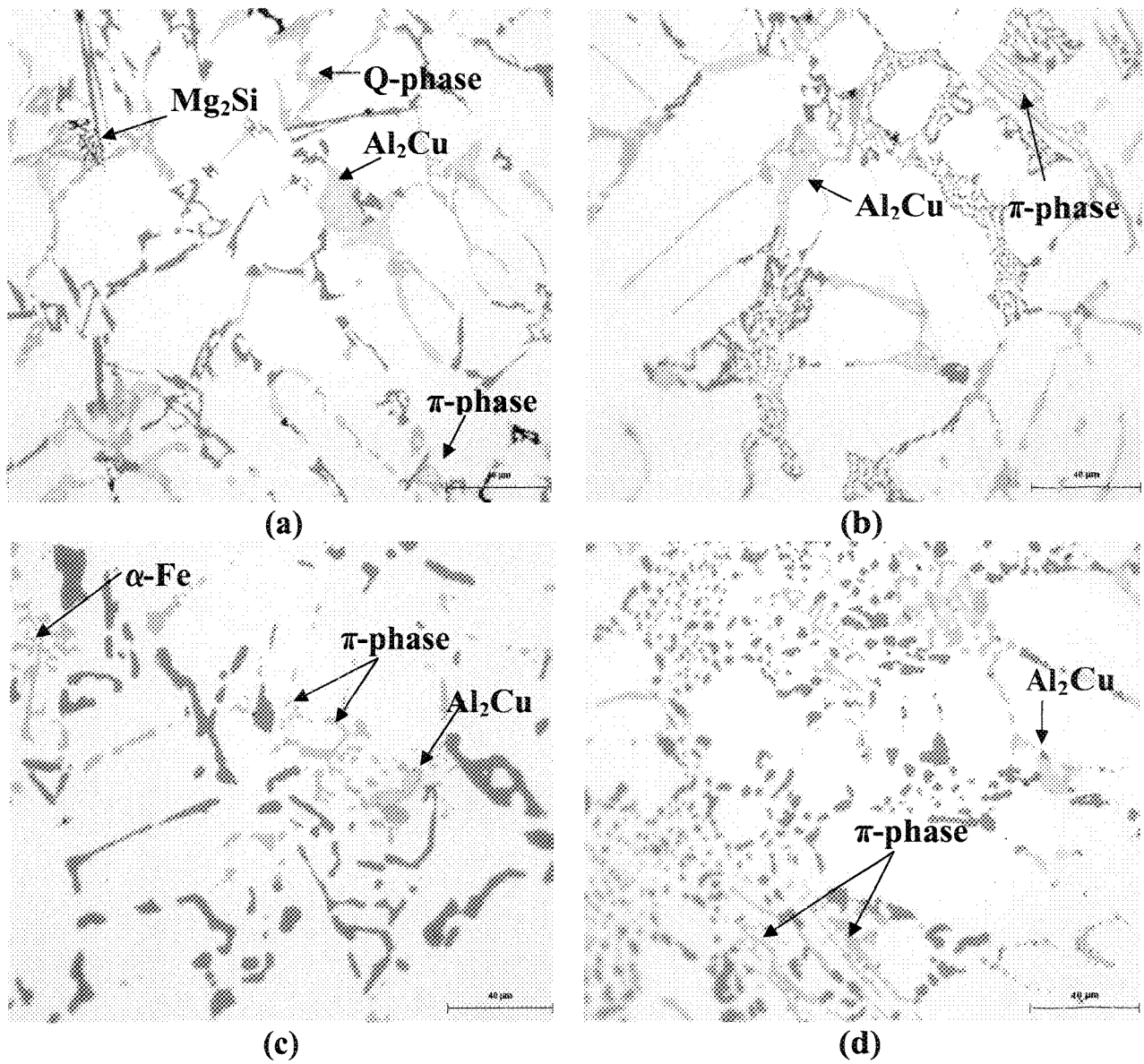


Figure 4.6 Optical microstructures observed in D8 industrial alloy samples obtained from star-like mold castings: (a) as-cast D8 alloy, (b) Sr-modified DS8 alloy, (c) SHT D8 alloy and (d) SHT and Sr-modified DS8 alloy.

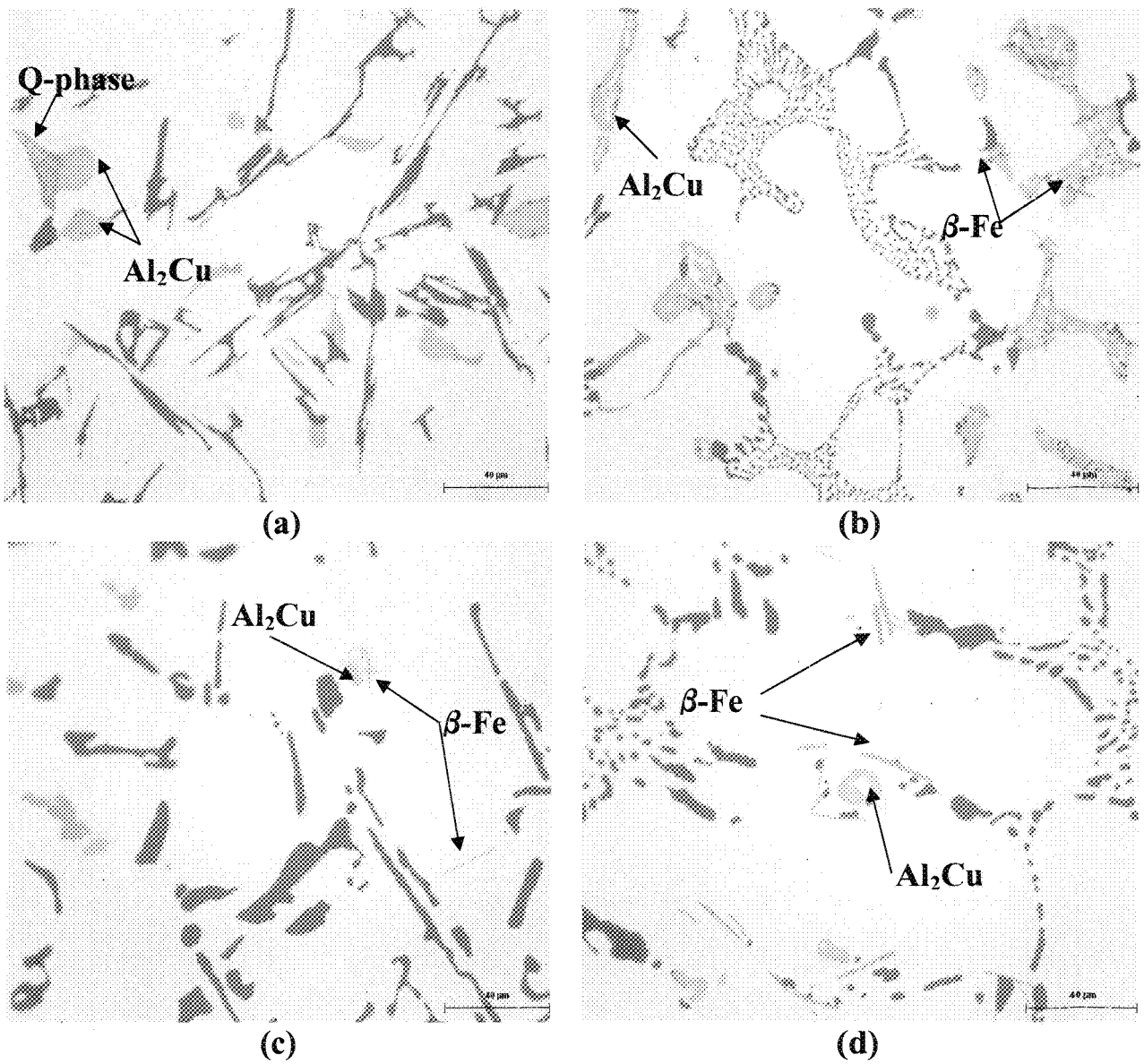


Figure 4.7 Optical microstructures observed in LD1 experimental base alloy samples obtained from L-shaped mold castings: (a) as-cast LD1 alloy, (b) Sr-modified LDS1 alloy, (c) SHT LD1 alloy and (d) SHT and Sr-modified LDS1 alloy.

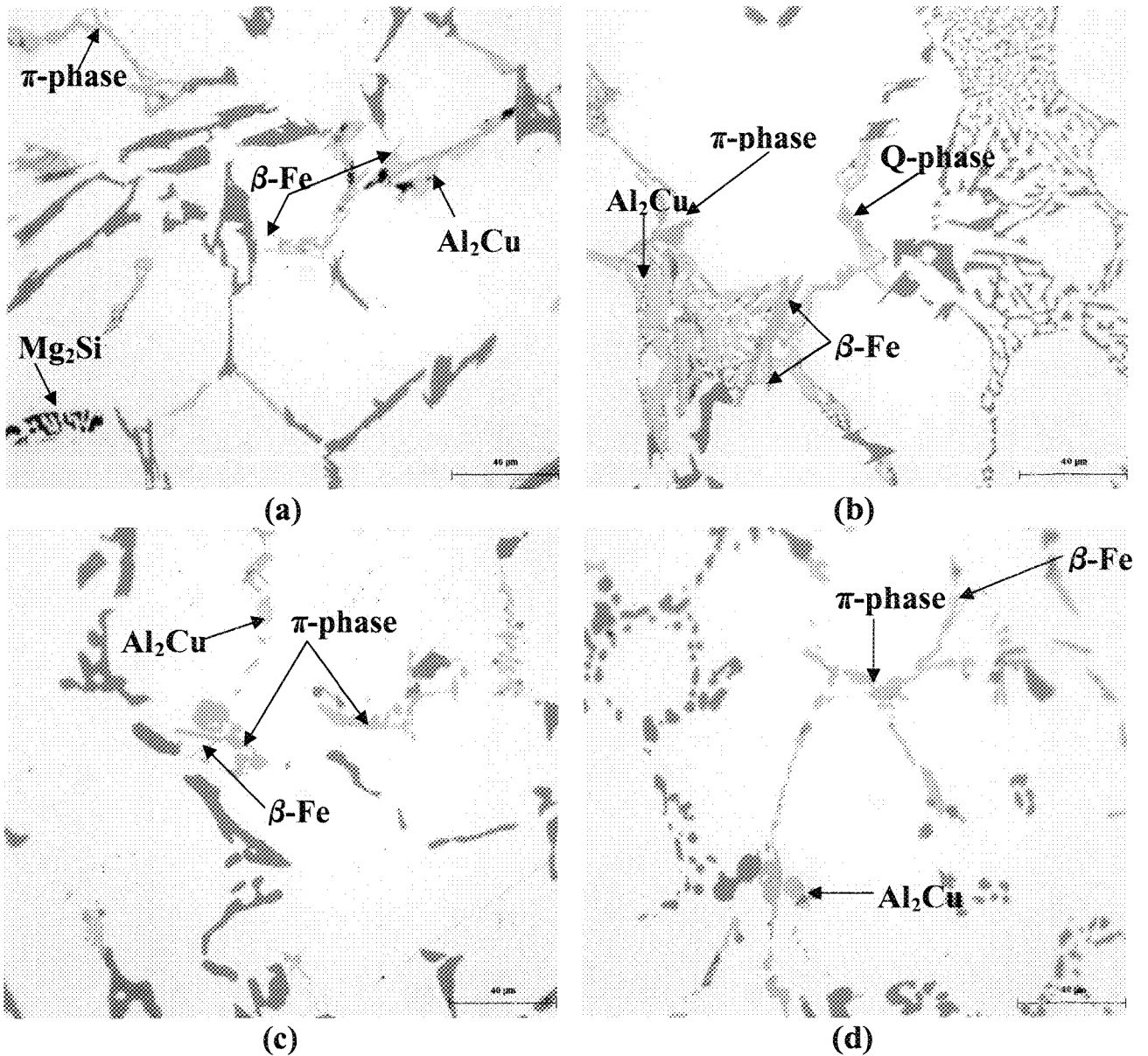


Figure 4.8 Optical microstructures observed in LD6 experimental alloy samples obtained from L-shaped mold castings: (a) as-cast LD6 alloy, (b) Sr-modified LDS6 alloy, (c) SHT LD6 alloy and (d) SHT and Sr-modified LDS6 alloy.

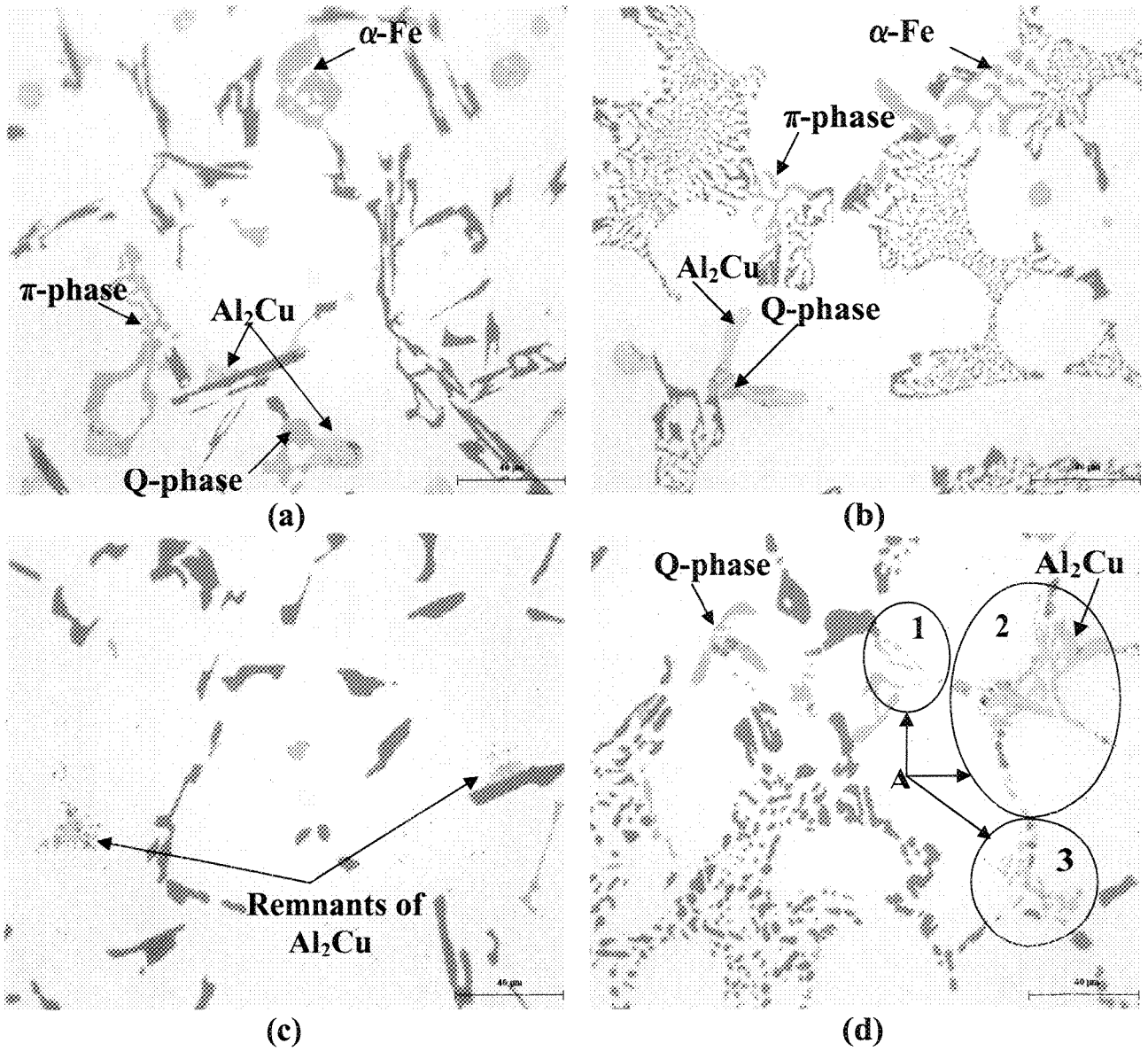


Figure 4.9 Optical microstructures observed in LD7 industrial alloy samples obtained from L-shaped mold castings: (a) as-cast alloy LD7, (b) Sr-modified alloy LDS7, (c) SHT alloy LD7 and (d) SHT and Sr-modified alloy LDS7.

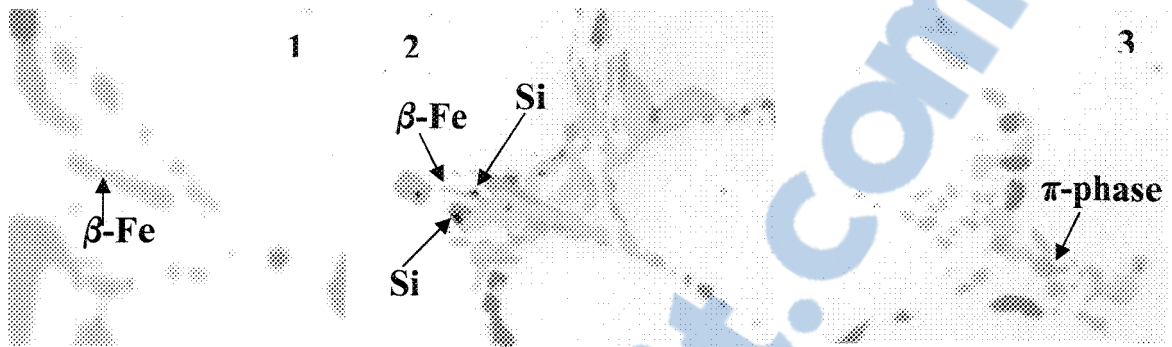


Figure 4.10 Magnified micrographs of the regions marked 1, 2, and 3 in Figure 4.9(d) of SHT Sr-modified LDS7 showing an ultrafine β - Al_3FeSi platelets in (1), ultrafine Si particles within the Al_2Cu eutectic phase in (2), and fine remnants of mostly dissolved π - $\text{Al}_8\text{Mg}_3\text{FeSi}_6$ phase.

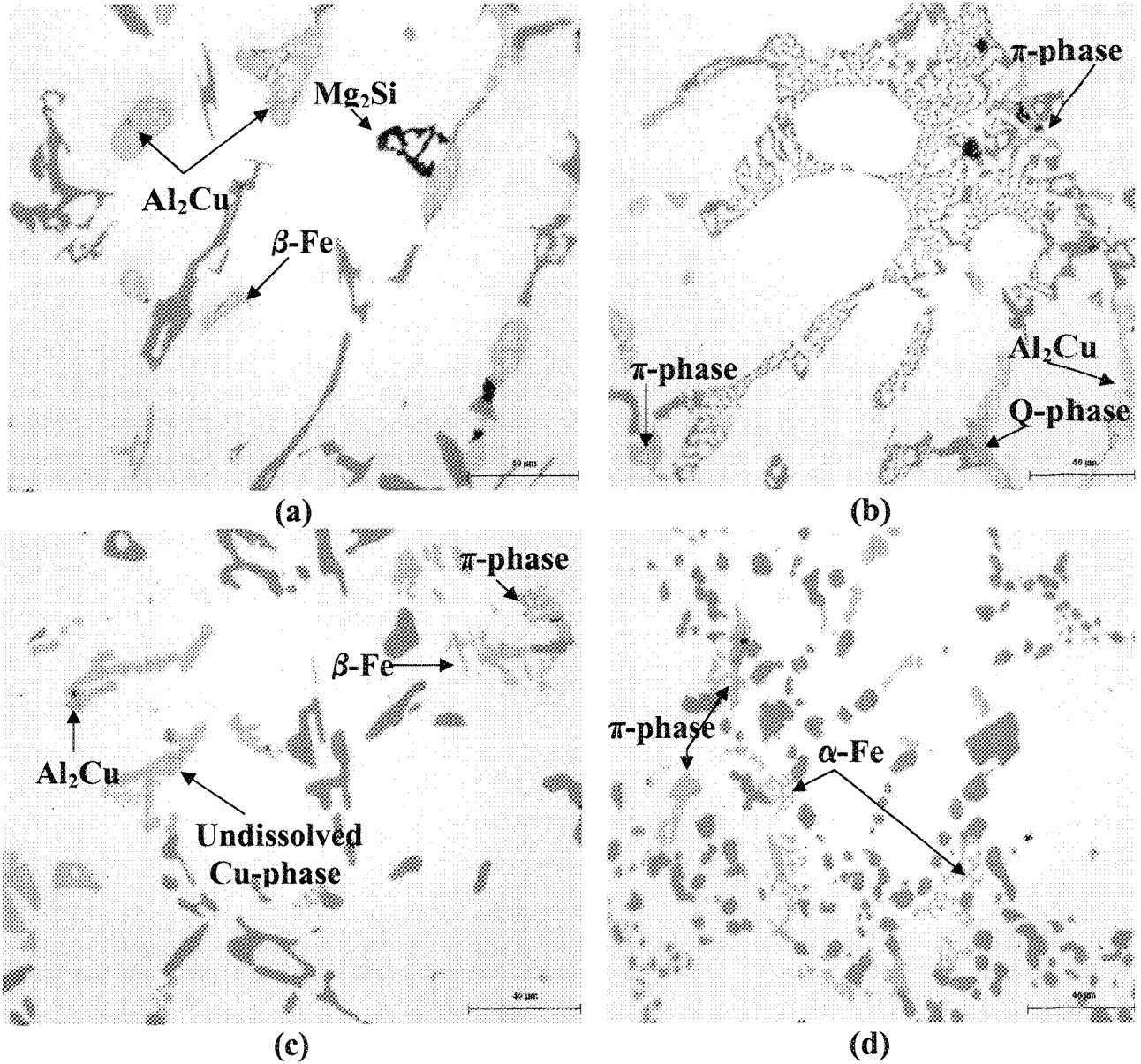


Figure 4.11 Optical microstructures observed in LD8 industrial alloy samples obtained from L-shaped mold castings: (a) as-cast LD8 alloy, (b) Sr-modified LDS8 alloy, (c) SHT LD8 alloy and (d) SHT and Sr-modified LDS8 alloy.

4.7.2 Porosity Characteristics

Porosity, resulting from a combination of shrinkage and dissolved gas, results in a degradation of certain important properties of aluminum castings and leads to reduced mechanical properties (namely, ductility, fracture toughness and fatigue life), poor surface appearance and some loss of pressure tightness. Conversely, the generation of porosity may contribute to improving hot-tearing resistance. With the use of mechanical degassing, it is possible to minimize gas porosity, while a well-designed gating/riser system can help to reduce the shrinkage porosity in the casting.

Roy *et al.*^[53,54] reported that the addition of Mg to the 319 alloy reduces the percentage porosity without a noticeable change in pore size and shape. These authors also observed that shrinkage pores nucleated at the interface of the blocky Al₂Cu particles in materials containing a very low level of hydrogen. The effect of Mg on microporosity formation in Al-Si-Cu casting alloys is not consistent, yet in most alloys, magnesium appears to decrease the porosity by ~0.01-0.3%.

Porosity measurements were carried out for the as-cast D1 base experimental alloy (without Mg) and the D7 base industrial alloy (0.3wt% Mg) in both the non-modified and Sr-modified conditions, using samples obtained from both the star-like and L-shaped molds.

Porosity parameters (area percentage porosity, pores area and pore length) for these alloys/samples are listed in Tables 4.5 and 4.6. These parameters were observed to increase for industrial alloys and for samples obtained at a low cooling rate (*i.e.* using the L-shaped mold), whereas they were seen to decrease in the modified alloy samples. These

observations are in good agreement with those reported by Roy *et al.*^[53,54]

Table 4.5 Porosity measurements for the as-cast alloys using the star-like mold

Alloy (Condition)	Area Perc. (%)		Area (μm^2)		Length (μm)	
	Av.	SD	Av.	SD	Av.	SD
D1 (non-mod. + exp.)	0.06	0.07	0.98	2.01	1.23	1.29
DS1 (Sr-mod. + exp.)	0.03	0.03	0.50	0.96	0.86	0.78
D7 (non-mod. + ind.)	0.08	0.09	3.59	10.31	2.08	3.13
DS7 (Sr-mod. + ind.)	0.06	0.08	2.47	8.44	1.87	2.39

Table 4.6 Porosity measurements for the as-cast alloys using the L-shaped mold

Alloy (Condition)	Area Perc. (%)		Area (μm^2)		Length (μm)	
	Av.	SD	Av.	SD	Av.	SD
LD1 (non-mod. + exp.)	0.06	0.05	1.30	3.93	1.21	1.62
LDS1 (Sr-mod. + exp.)	0.03	0.03	1.12	3.97	1.13	1.53
LD7 (non-mod. + ind.)	0.09	0.10	3.93	11.30	2.11	3.23
LDS7 (Sr-mod. + ind.)	0.07	0.07	2.62	9.30	1.91	2.49

4.7.3 Hardness

The hardness of Al-Si alloys depends mainly on the Mg and Cu content of the alloy as well as the aging conditions. An extensive study by Tash *et al.*^[90] was carried out to investigate the effect of metallurgical parameters in terms of alloying additions and intermetallic phases formed on the hardness of heat-treated cast 319 alloys. It was observed that the addition of Mg to Al-Si-Cu 319 alloys containing β -Fe and/or α -Fe intermetallics produced a remarkable increase in hardness at all aging temperatures in both the non-modified and Sr-modified conditions. Aging of these Mg-containing 319 alloys at 180°C for up to 8 hours produced a sharp rise in hardness during the first two hours of aging, followed by a broad peak or plateau spread between 2 and 8 hours.^[90,91] This may be

explained on the basis of the combined effect of Cu- and Mg-intermetallics in the 319 alloys, where hardening during aging occurs by the cooperative precipitation of Al_2Cu and Mg_2Si phase particles.^[30] The iron-intermetallic type/morphology influences the hardness of the heat-treated 319 alloys to some extent. In both the α -Fe and β -Fe intermetallic-containing 319 alloys, the Sr-modified alloys exhibited lower values of hardness, compared to the non-modified alloys.^[89]

It was found that the correlations obtained pertained to a range of aging time and temperature of 2-8 hours and 180-220°C, respectively, where a linear relation in the hardness profile (peak-to-overaged regions) was found. The hardness of the 319 alloys increased with magnesium and α -Fe-intermetallics volume fraction and decreased with strontium modification (Sr-ppm) and aging parameters (temperature and time). The contribution of Mg in increasing the hardness of heat-treated 319 alloys containing β -Fe intermetallics is more noticeable than in the 319 alloys containing α -Fe intermetallics.^[90]

Mohamed^[59] found that the 319 alloy hardness first increased with an increase in aging temperature up to 180°C, and thereafter decreased as the aging temperature was increased. The increase in hardness with the addition of Cu and Mg may be attributed to the formation of the hard and brittle (metastable) intermetallic Al_2Cu and Al_2CuMg phases, as well as to an increased bonding of the Si particles with the matrix, where the thermal energy is sufficient to precipitate such intermediate phases. The decrease in hardness at aging temperatures above 180°C may be due to the coarsening of the various microconstituents as well as to a decrease in cohesion with the matrix. The coarsening of hard intermetallic phases may reduce the barrier to dislocation movement and, hence, to

flow stress/hardness.

Table 4.7 summarizes the hardness of the as-cast experimental and industrial 319 alloys for non-modified and Sr-modified conditions, for samples obtained from both the star-like and L-shaped molds (coded D, DS and LD, LDS, respectively). It was found that the hardness increased with an increase in both the Mg content and cooling rate whereas it decreased with Sr-modification and the use of a low cooling rate for both the experimental and industrial alloys. These observations are in good agreement with those reported by Tash *et al.*^[90,91] and Moustafa *et al.*^[89]

Table 4.7 Hardness of the as-cast experimental and industrial 319 alloys

Alloy	Hardness (BHN)										
	Av.	SD									
D1	71.4	2.1	DS1	68.3	2.7	LD1	73.8	0.7	LDS1	72.5	1.3
D2	83.8	4.2	DS2	79.3	1.4	LD2	81.4	2.3	LDS2	84.2	1.9
D3	88.8	2.0	DS3	82.2	2.7	LD3	88.1	1.6	LDS3	80.2	7.6
D4	90.9	3.8	DS4	85.4	0.4	LD4	89.8	1.4	LDS4	85.1	0.5
D5	92.8	1.9	DS5	87.9	1.5	LD5	94.4	1.9	LDS5	90.5	1.4
D6	94.5	2.9	DS6	92.8	0.9	LD6	97.3	2.7	LDS6	92.3	1.3
D7	94.4	2.8	DS7	90.6	4.0	LD7	95.0	0.4	LDS7	73.6	7.7
D8	98.9	2.8	DS8	95.8	1.6	LD8	95.9	5.1	LDS8	94.1	1.5

D: non-modified/star-like mold; DS: modified/star-like mold; LD: non-modified/L-shaped mold; LDS: modified/L-shaped mold; D1-D6: experimental alloys; D7 and D8: industrial alloys; D1: base alloy (Mg-free); D2, D3, D4, D5, and D6: 0.1, 0.2, 0.3, 0.4, and 0.6 % Mg respectively; D7: 0.3 % Mg; D8: 0.6 % Mg; S: Sr-modification (200 ppm); Av.: average; and SD: standard deviation.

The effect of Mg addition on the hardness of T6 heat-treated non-modified and Sr-modified experimental 319 alloys was investigated as a function of aging time, as shown in Figures 4.12 and 4.13 for samples obtained from the star-like and L-shaped molds, respectively. Figure 4.12(a) depicts the Brinell hardness values for non-modified experimental alloys, including the highest recorded Brinell hardness value of all the alloys

tested (143.52 BHN for the non-modified experimental alloy D4 containing 0.3wt% Mg), while Figure 4.12(b) portrays the Brinell hardness values for the Sr-modified alloys. These two groups of curves were obtained using the higher cooling rate star-like mold. It was found that increasing the Mg content in the D1 Mg-free base alloy to 0.1wt% (*i.e.* D2 alloy), 0.2wt% (*i.e.* D3 alloy), 0.3wt% (*i.e.* D4 alloy), 0.4wt% (*i.e.* D5 alloy) and 0.6wt% (*i.e.* D6 alloy) increased the alloy hardness by ~32%, ~43%, ~46%, ~42% and ~42%, respectively.

It was also observed that an increase in the Mg content of up to 0.4wt% at different aging times resulted in a positive effect on hardness, indicating that the hardening is due to Mg₂Si precipitation in addition to the precipitation of Al₂Cu. The effect of Mg addition for the aged alloys is similar to that observed in the as-cast alloys. Aging of these Mg-containing 319 alloys at 180°C (T6 heat treatment conditions) for up to 48 hours produced a sharp rise in hardness during the first two hours of aging, followed by a broad peak or plateau spread between 2 and 12 hours as well as a noticeable period of over-aging after 12 hours. Modification with strontium (200 ppm) had a negative effect on hardness as shown in Figure 4.12(b). The effect of Mg-content for the Sr-modified alloys is similar to that for the non-modified alloys. These observations are in good agreement with those reported by Tash *et al.*^[90,91] and Moustafa *et al.*^[89]

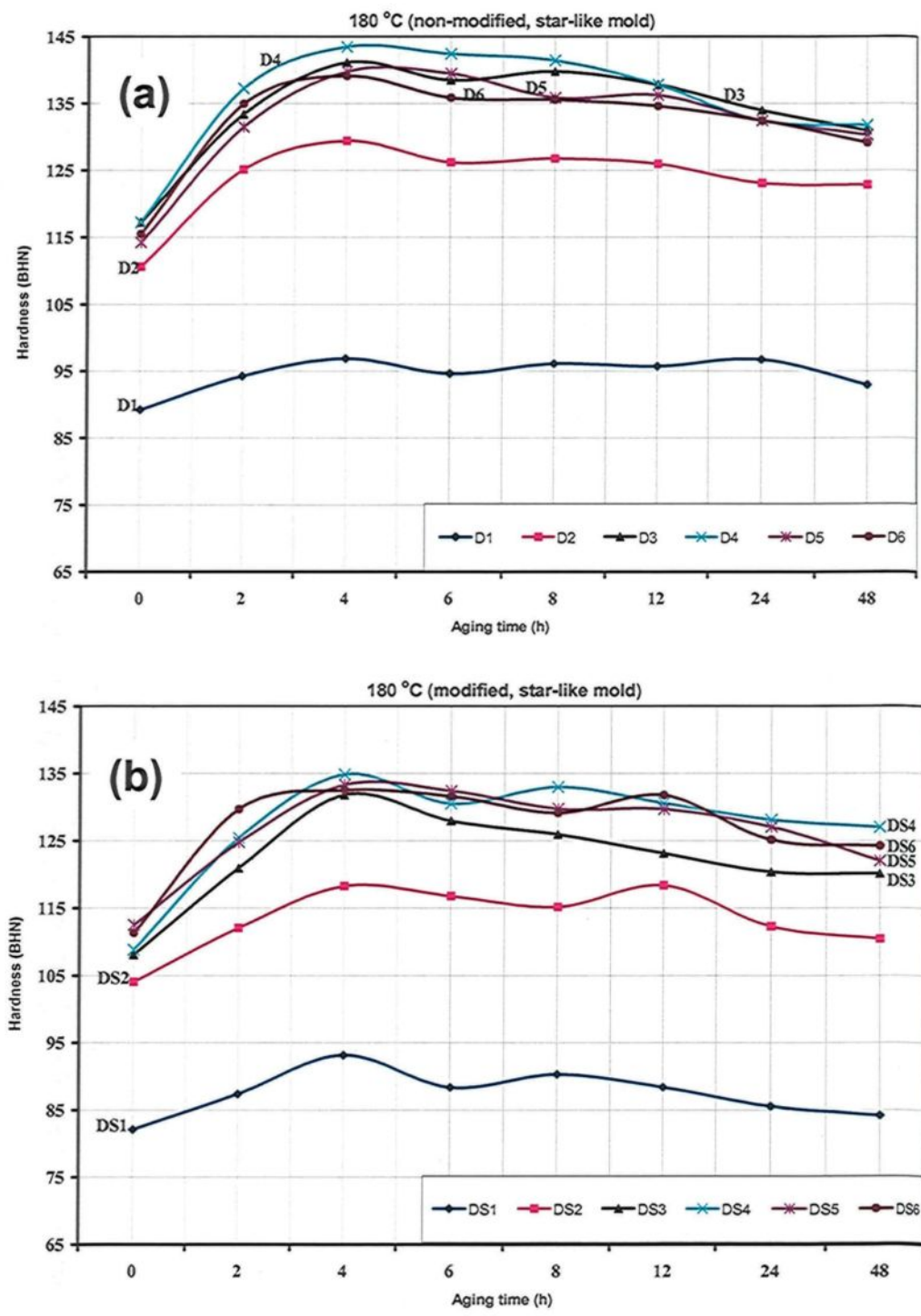


Figure 4.12 Hardness of T6-tempered experimental 319 alloys (aging temperature 180°C) as a function of aging time, using the star-like mold samples: (a) non-modified alloys, and (b) Sr-modified alloys.

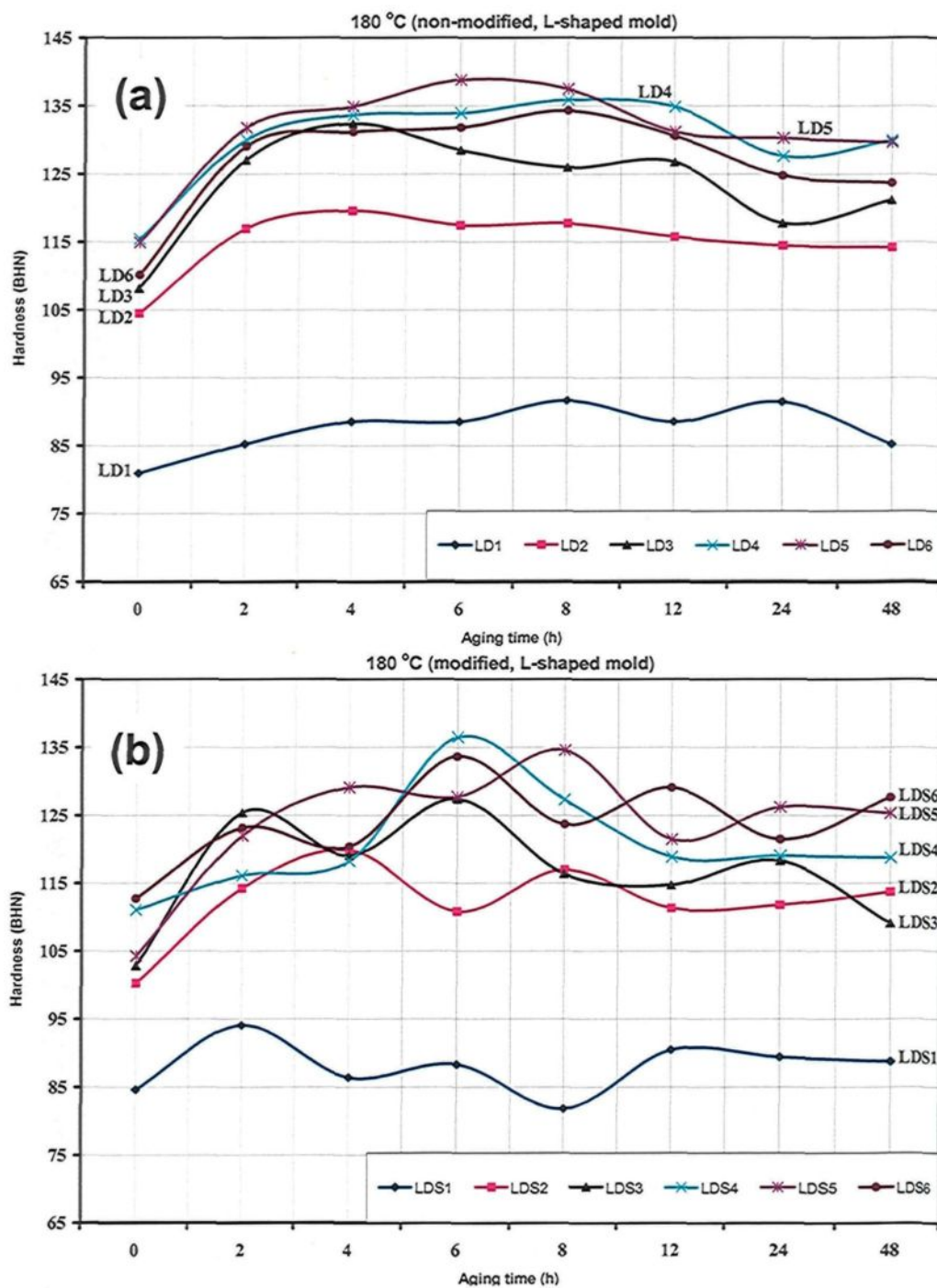


Figure 4.13 Hardness of T6-tempered experimental 319 alloys (aging temperature 180°C) as a function of aging time, using the L-shaped mold samples: (a) non-modified alloys, and (b) Sr-modified alloys.

The lower cooling rate L-shaped mold was used to investigate the effect of cooling rate on the hardness of the experimental 319 alloys, as shown in Figure 4.13. When compared to Figure 4.12, it can be seen that the slow cooling rate decreases the hardness in both the non-modified and Sr-modified T6 heat-treated alloys. Similar observations were made for the samples obtained from the higher cooling rate star-like mold.

The effect of Mg addition on the hardness of the non-modified and Sr-modified experimental 319 alloys as a function of aging time was investigated under T7 heat treatment conditions as well, and is shown in Figures 4.14 and 4.15 for samples obtained from the star-like mold and L-shaped mold, respectively. Similar observations were noted as in the case of the T6 heat-treated alloys. Aging of these Mg-containing experimental 319 alloys at 220°C (T7 heat treatment conditions) for up to 48 hours produced a sharp rise in hardness during the first two hours of aging, followed by an aging peak and a notable period of over-aging, after 2 hours of aging. These observations are in good agreement with the work of Tash *et al.*^[90,91]

The effect of Mg addition on the hardness of the non-modified and Sr-modified industrial 319 alloys as a function of aging time was investigated under both the T6 and T7 heat treatment conditions, for samples obtained from the star-like and L-shaped molds, respectively. The results are shown in Figures 4.16 and 4.17. It was observed that both the Mg-containing industrial 319 alloys and the Mg-containing experimental 319 alloys exhibited similar behavior with respect to the influence of Mg-content, Sr-modification, aging temperature (180°C vs 220°C), and cooling rate (star-like mold vs L-shaped mold).

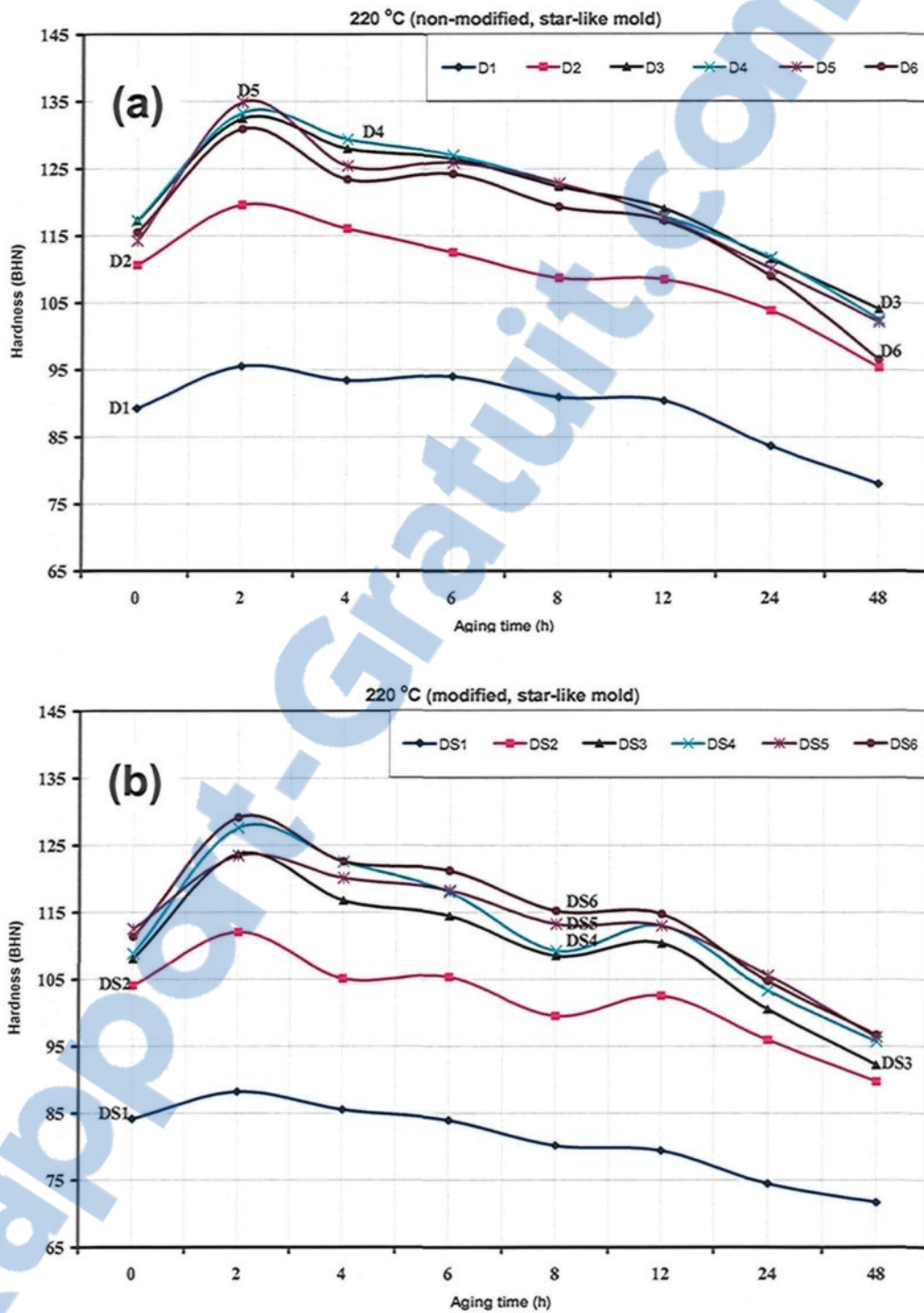


Figure 4.14 Hardness of T7-tempered experimental 319 alloys (aging temperature 220°C) as a function of aging time, using the star-like mold samples: (a) non-modified alloys, and (b) Sr-modified alloys.

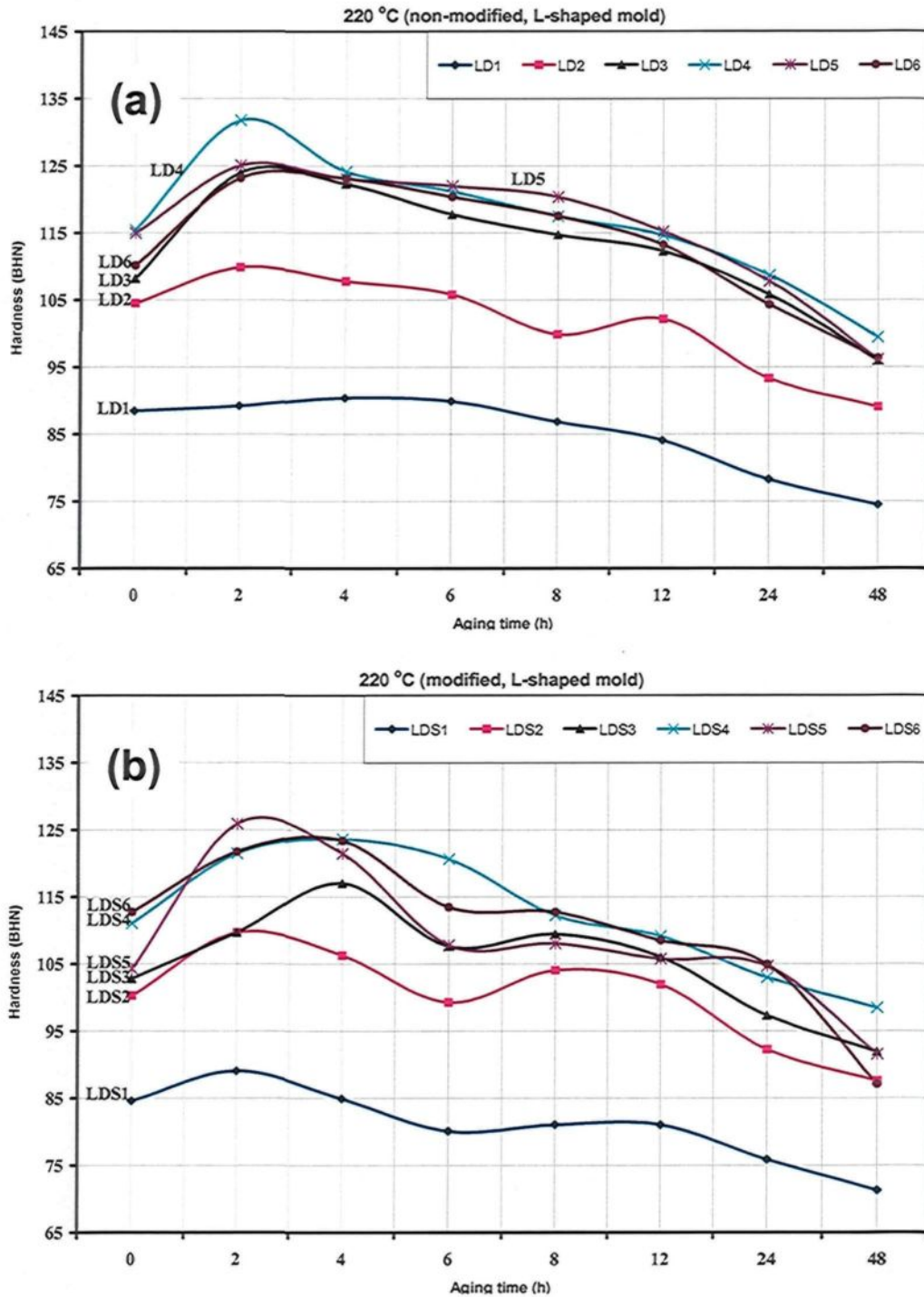


Figure 4.15 Hardness of T7-tempered experimental 319 alloys (aging temperature 220°C) as a function of aging time, using the L-shaped mold samples: (a) non-modified alloys, and (b) Sr-modified alloys.

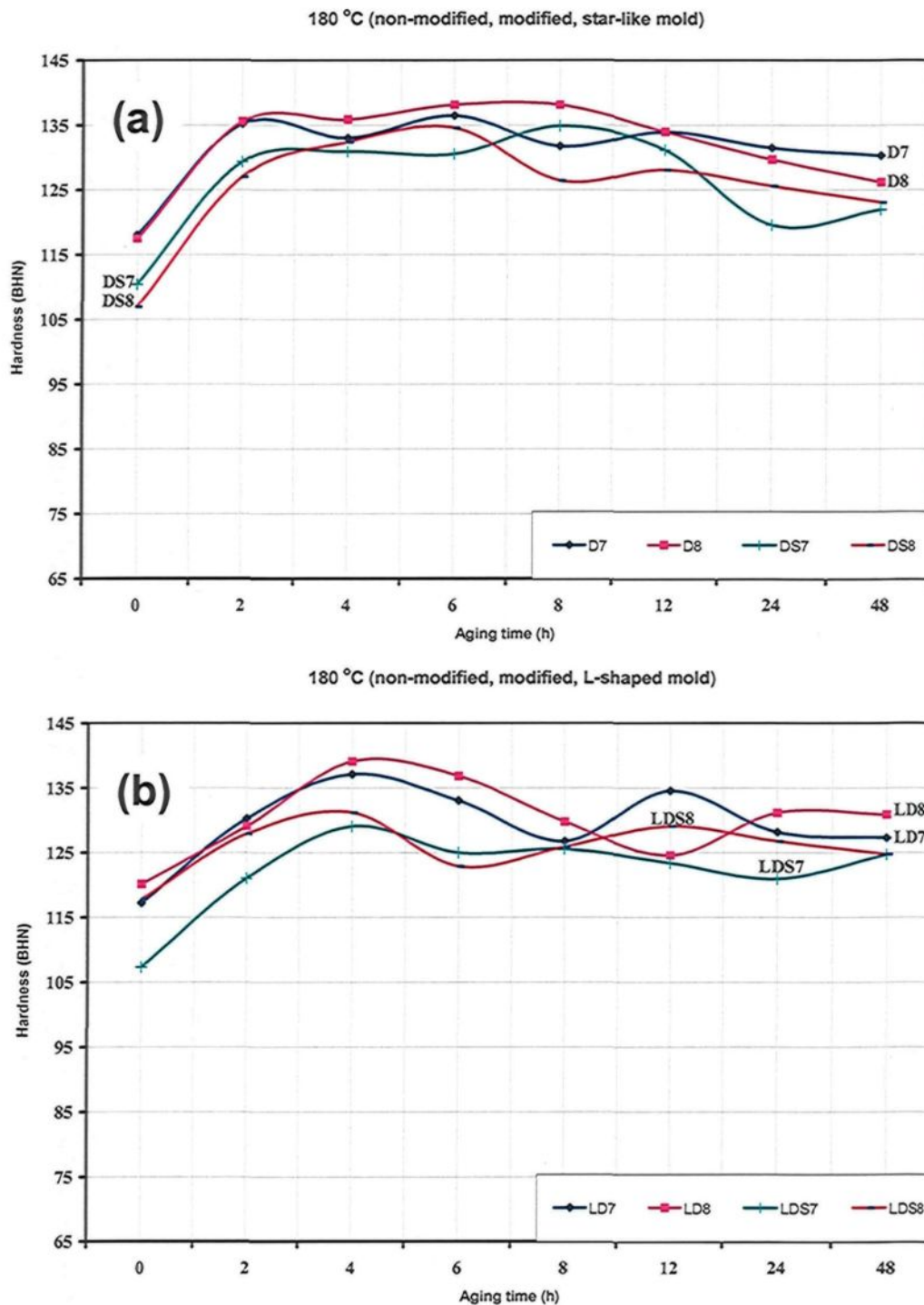


Figure 4.16 Hardness of T6-tempered industrial non-modified and Sr-modified 319 alloys (aging temperature 180°C) as a function of aging time for: (a) star-like mold samples, and (b) L-shaped mold samples.

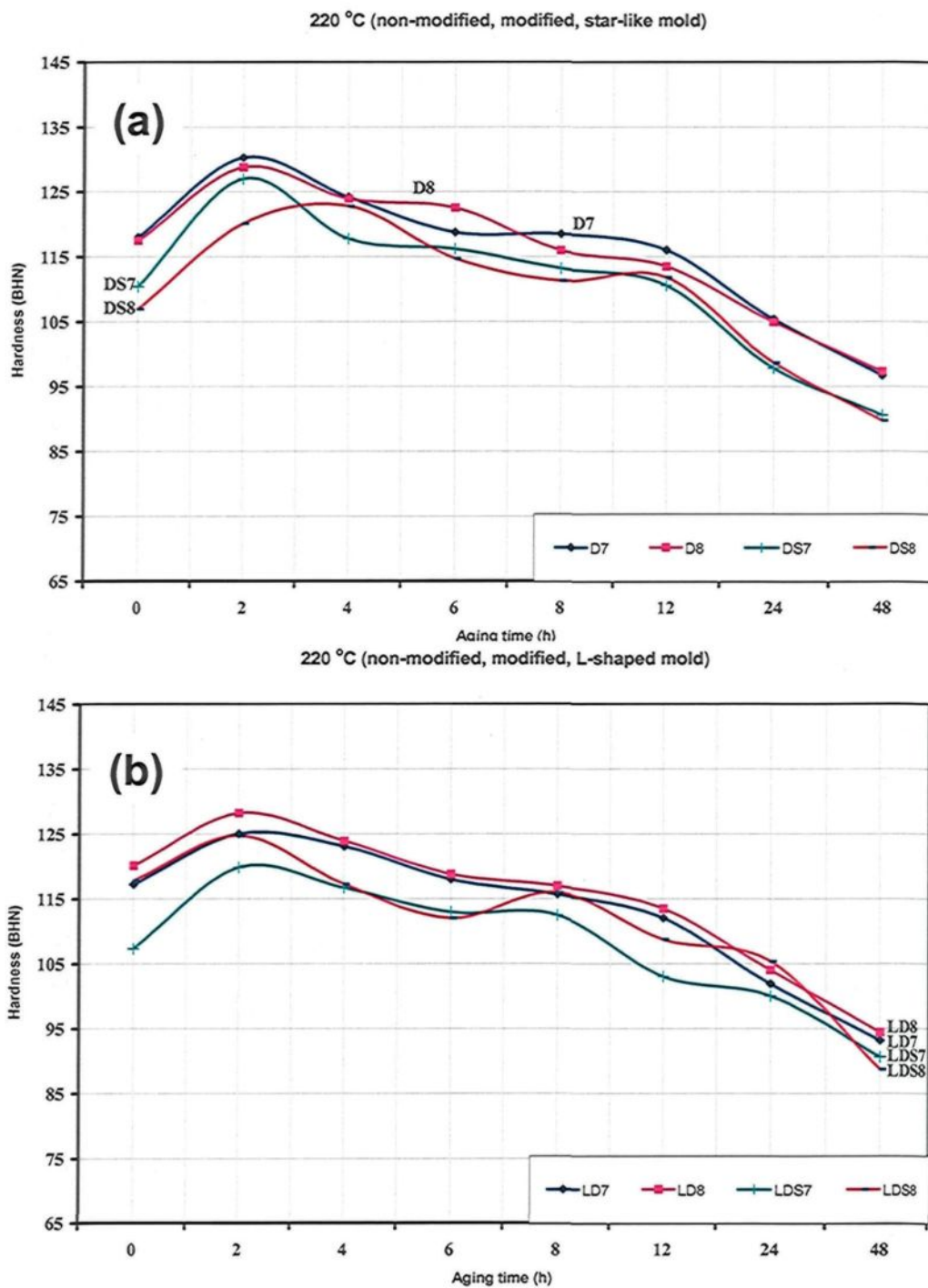


Figure 4.17 Hardness of T7-tempered industrial non-modified and Sr-modified 319 alloys (aging temperature 220°C) as a function of aging time for: (a) star-like mold samples, and (b) L-shaped mold samples.

The hardness curves shown in Figures 4.12 to 4.17, exhibit more than one peak or a wavy form with aging time, resulting from the presence of several hardening phases, including θ -Al₂Cu, β -Mg₂Si, and Q-Al₅Mg₈Si₆Cu₂ which contribute to the precipitation hardening of the alloys studied. These observations are in satisfactory agreement with the work of a number of researchers.^[58,92,93]

Similar observations for this wavy form were noted and explained for Al-Si-Cu-Mg 380 alloys by Morin,^[94] on the basis of two different types of structures which are likely be obtained during the aging treatment of 319 alloys. A schematic representation is shown in Figure 4.18. In structure (1), fine particles are present in the first region of the Guinier-Preston, or GP zone for phase 1. In structure (2), there is a fine coherent precipitate for phase 1 causing increased strength. In structure (3), there is an incoherent structure formed out of coarse particles, this structure (3) characterizes the equilibrium structure of such particles. Structure (4) is a mixture of fine coherent precipitates (phase 2) causing increased strength and coarse particles (phase 1). Structure (5) is an incoherent structure consisting of only coarse particles from both phases 1 and 2. The fine precipitates increase alloy strength whereas the coarse precipitates decrease it, reflecting the wavy form for alloy strength and hardness.

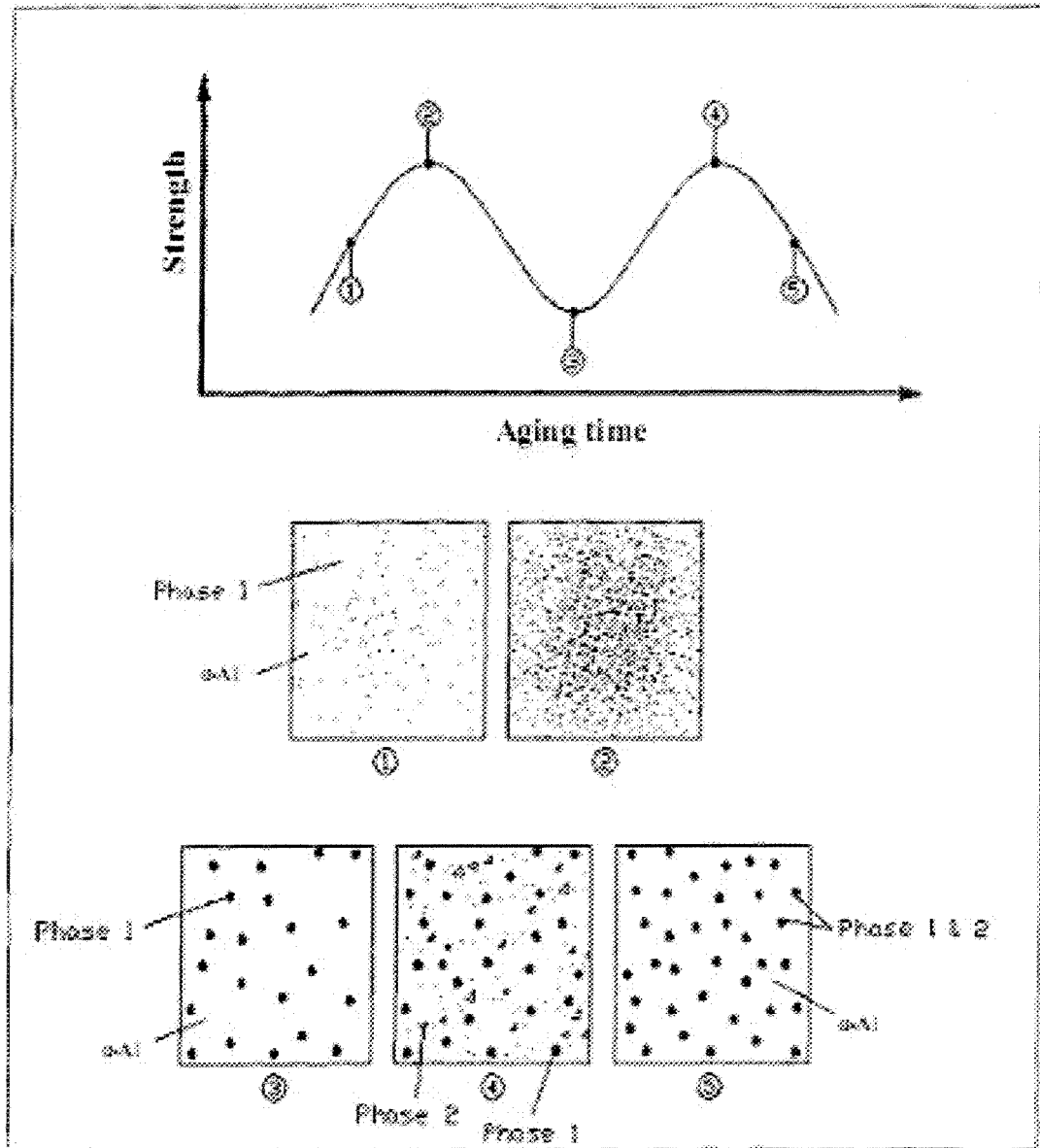


Figure 4.18 Schematic of the structures observed at the aging peak (coherent fine precipitates) and in the valley between two peaks (incoherent coarse precipitates): (1) first GP zone for phase 1; (2) coherent structure of phase 1; (3) incoherent structure of phase 1; (4) coherent structure of phase 2 and incoherent structure of phase 1; and (5) incoherent structure of both phases 1 and 2.^[94]

CHAPTER 5

IMPACT TOUGHNESS AND FRACTOGRAPHY

OF 319-TYPE Al-Si-Cu-Mg ALLOYS

CHAPTER 5

IMPACT TOUGHNESS AND FRACTOGRAPHY OF 319-TYPE Al-Si-Cu-Mg ALLOYS

Impact tests are known to be highly sensitive to additions made to the alloy sample of alloying and/or trace elements. Impact energy normally means the total energy absorbed by a specimen during fracture when it is tested under high strain rates or rapid loading conditions. Impact values depend to a strong degree on the testing methods used. The most commonly applied measurement procedure for obtaining impact energy is the Charpy test. The impact energy from this test correlates with the area under the total stress-strain curve shown in Figure 2.11, in Chapter 2.

A computer-aided Instrumented Charpy Impact test was used to produce the load-time information in addition to data concerning the energy absorbed. The instrumented test makes it possible to divide the energy absorbed into specific types: (i) the energy required to initiate fracture, designated E_i , and (ii) the crack propagation energy, designated E_p . The total impact energy, E_T , is the sum of the two preceding energies and is controlled mainly by various alloying and melt-processing parameters. The correlation between impact energy and cooling rate, Sr-modification, intermetallic compounds, porosity characteristics, Mg content, and aging conditions will be the main focus of this chapter. Charpy unnotched samples were used in the present work, so as to increase the accuracy of the measurement and to highlight the effects of the microstructure and the parameters listed earlier.

Fractography is defined as the study and documentation of fracture surfaces.^[95] The purpose of fractography is to analyze fracture features and attempt to relate the topography of the fracture surface to the causes and/or basic mechanisms of fracture.^[96] A knowledge of fracture behavior is of importance in upgrading material specifications, in improving product design, and in analyzing any failure to improve reliability.^[97]

In this chapter, the fracture behavior of Al-Si-Cu-Mg 319 alloys will also be considered so as to obtain a basic overview of this topic. Based on this, the fracture behavior of selected impact samples already tested for this study will be discussed. Attention will be focused on alloy sample conditions corresponding to Mg content and aging parameters for experimental 319 alloys.

5.1 EFFECTS OF SAMPLE CONFIGURATION

The effects of sample configuration have already been discussed in subsection 2.8. Impact values depend strongly on this factor, particularly when a notch is present, in which case the energy obtained will be much lower than that of an unnotched sample; these values will be more greatly dependent on notch geometry, than on the microstructure. This type of dependence will decrease the accuracy of results when evaluating the effects of alloying and melt processing parameters on impact energy. In this study, Charpy unnotched samples were used, in order to increase the precision of the measurements and to emphasize the effects of the microstructure. This microstructure depends on Mg content, Sr-modification, cooling rate, and aging conditions. An example of an unnotched ASTM E23^[71] sample is illustrated in Figure 3.5, Chapter 3, shown together with its respective dimensions.

5.2 EFFECTS OF MODIFICATION

The effects of Sr-modification on Al-Si-Cu alloys have already been discussed in subsection 4.1. Under normal cooling conditions, eutectic Si particles, present in the form of coarse acicular needles, act as crack initiators, thereby lowering the mechanical properties. The addition of small amounts of Sr to the melt alters the acicular morphology of these Si particles to a fibrous one, which brings about a great improvement in the mechanical properties. Silicon particle characteristics can also be affected through thermal modification by subjecting the casting to a high temperature treatment for extended periods. These two types of modification have been used together in tandem to produce the desired properties in the casting.

The presence of copper in the 319 alloy drastically affects the fracture behavior of the alloy. When the Al_2Cu phase is present, the fracture seems no longer to be controlled by the Si particles. Although the eutectic Si has been modified by the presence of Sr in the alloy, the impact strength is not improved. In addition to the modification of the Si phase, there is a tendency to form more block-like Al_2Cu in the presence of Sr, although dispersed Al_2Cu can also form. In some cases, the Al_2Cu segregates towards certain regions of the sample. In all likelihood, these factors, in conjunction with the brittle nature of Al_2Cu , contribute to the noticeably low impact strengths observed in 319 alloys which themselves contain significant amounts of Al_2Cu .^[1,6,66] Modification brings about significant improvements in the impact strength of both as-cast and heat-treated alloys. A certain notion of these beneficial effects may be obtained by consulting Figure 5.1. Here, the variation in unnotched impact strength for both as-cast and heat-treated Sr-modified 413.0

alloys is provided. It is clear that modification, particularly if combined with heat treatment, can lead to increases of several hundred percent.^[1] The alloy is imbued with impact strength through the ductile aluminum matrix which separates the brittle silicon phase. Any process which reduces the size of the brittle phase particles or increases their separation will improve impact properties. Paray *et al.*^[66] reported that modification improved the unnotched impact strength of both as-cast and heat-treated A356.0 and 413.0 alloys, whereas modified 319 and 332 alloys displayed relatively low impact strength.

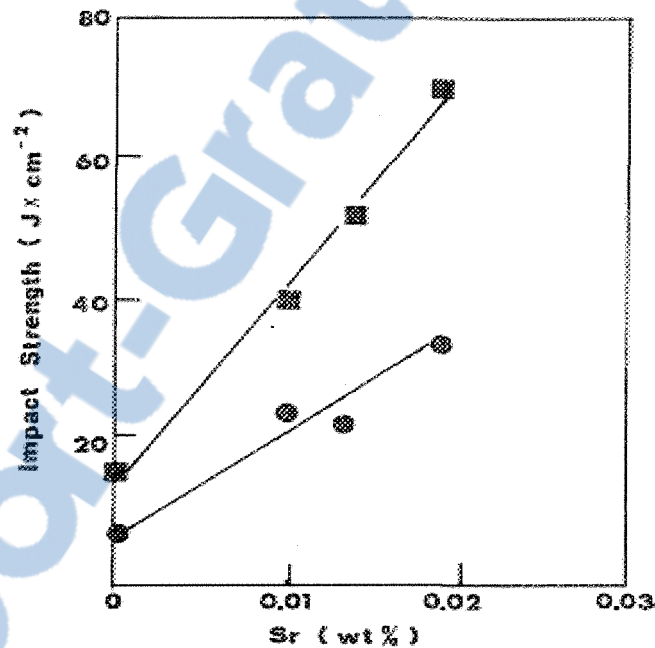


Figure 5.1 Impact strength of strontium-treated 413 alloy; as-cast ● and heat-treated ■ (13 hours/538°C and water quenched).^[1]

All indications so far point to impact properties being much more sensitive to modification than simple tensile properties. Once the initial modification is made, there is a good retention of mechanical properties.^[1] Modification with strontium for Al-Si alloys is used also for (i) improving machinability, (ii) reducing heat treatment times, (iii)

controlling porosity distribution, (iv) reducing hot tearing, (v) improving mold filling, and (vi) cutting down on scrap rates.^[98]

5.3 EFFECTS OF MAGNESIUM

The effects of adding magnesium to Al-Si-Cu alloys have already been discussed in subsection 4.2. With respect to incipient melting, the addition of Mg can bring about the segregation of the Al_2Cu phase, causing it to become more difficult to dissolve during solution heat treatment. An addition of up to 0.5wt% Mg leads to a significant increase in the volume fraction of the Cu-containing phase, showing a clear tendency to segregate towards localized areas, ultimately leading to the formation of the block-like Al_2Cu phase, rather than to one displaying a fine eutectic-like form. It is important to avoid segregation of the copper phases in order to prevent incipient melting and to ensure that the alloy properties and castings remain sound. Paray *et al.*^[66] reported that 0.4wt% Mg resulted in a rapid decrease in the impact strength of 319 alloys for both the as-cast and T6 heat treatment conditions.

Silicon alone contributes little to the strength of aluminum casting alloys, yet provides an observably effective level of strengthening when combined with magnesium to form Mg_2Si . The Mg_2Si phase is soluble in the alloy to a limit of ~0.7wt% Mg, and provides the precipitation-strengthening basis for the heat-treatable alloys.^[74]

5.4 COMBINED EFFECTS OF MAGNESIUM WITH STRONTIUM

The combined effects of adding magnesium with strontium to Al-Si-Cu alloys have already been discussed in subsection 4.3. Samuel *et al.*^[76] reported that the addition of both Mg and Sr can lead to severe segregation of the Al₂Cu phase in 319.2 alloys, resulting in the production of large amounts of the coarse block-like phase, compared to the finer eutectic-like form. These segregated block-like Cu-rich phase particles decrease the impact strength of the 319 alloys.^[66] Joenoes *et al.*^[75] reported that ~1 wt% Mg refined the Si phase in non-modified Al-Si alloys. When combined with Sr, however, Mg was observed to have a negative effect on Sr-modification, where it changed the microstructure from being a well-modified one to a partially modified one, thereby decreasing the impact strength for both Mg-containing and free-Mg alloys.

5.5 EFFECTS OF COOLING RATES

The effects of cooling rates have already been discussed in subsection 4.4. The cooling rate has a direct effect on the size and distribution of microstructural phases in a casting, and in turn, on the mechanical properties as well. It should be noted that a decrease in the cooling rate of the casting will lower the mechanical properties of the alloy.

Hotta *et al.*^[67] studied the impact energy of the AC4C (356) and AC2B (B319) alloys under different cooling rate conditions (*i.e.* different solidification times) in as-cast and T6 heat-treated samples. The results for the T6 heat-treated alloys are shown in Figure 5.2. It is clear that, with the decrease in solidification time (*i.e.* the increase in cooling rate), the impact energies increase correspondingly. Castings which have solidified in 700 to 800

sec possess impact energies less than half those of castings which have solidified in 20 sec. This result is attributed to the coarsening of the eutectic compounds as well as to an increase in the grain size and microporosity observed with the increase in solidification time.

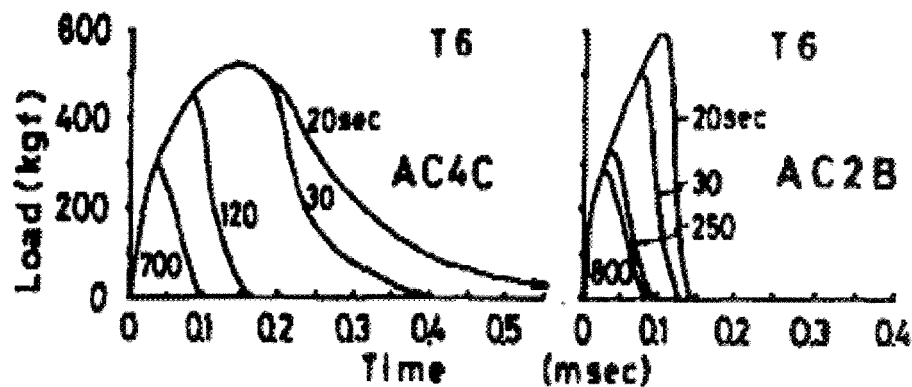


Figure 5.2 The effects of solidification time on the load-time relationship in the AC4C (356) and AC2B (B319) alloys (T6 treatment).^[67]

Hafiz and Kobayashi^[99] also compared the impact energies of eutectic Al-Si alloy samples obtained at different cooling rates, using two different mold types (steel and graphite) for casting. The impact energy values obtained at high cooling rates using a steel mold were superior to those obtained at low cooling rates using a graphite mold for the same Sr content, as can be seen from Figure 5.3. According to these authors, high cooling rates scale down the dimensions of the Si particles without any change in their shape or arrangement, which reduces the amount of primary Si in the matrix, leading to an increase in the amount of Al-dendrites.

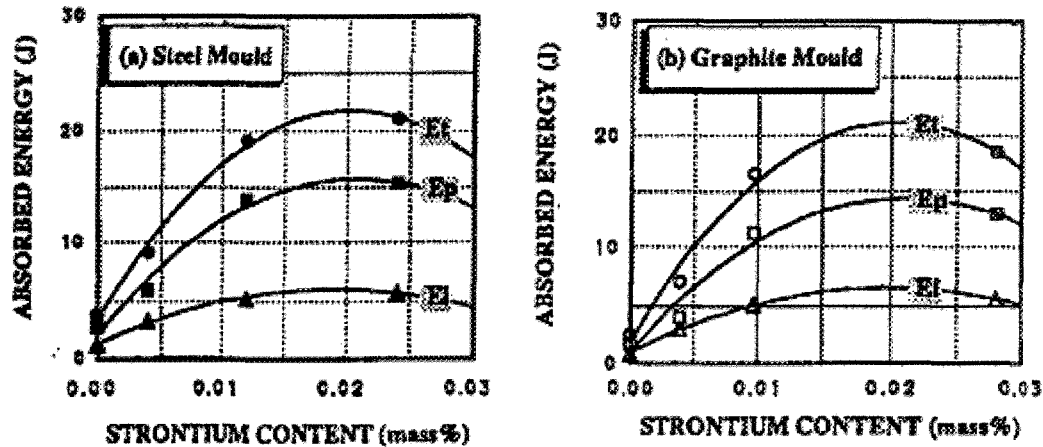


Figure 5.3 Impact toughness of eutectic Al-Si alloy as a function of Sr-content and solidification time.^[99]

Shivkumar *et al.*^[72,73] investigated the impact energy of 319 and 356 alloys using two different cooling rates for a sand mold and a water-cooled copper mold, where the alloys were T6 heat-treated using varying solution heat treatment times and different test temperatures. The results obtained for the samples which had been solution heat-treated for 8 h and impact-tested at room temperature using similar test conditions to those applied in the present work showed that the impact energies obtained at the higher cooling rate were higher in both 319 (*cf.* 0.88 J with 0.74 J for the non-modified, and 1.80 J with 1.36 J for the Sr-modified samples) and 356 (*cf.* 7.8 J with 1.4 J for the non-modified, and 13 J with 3 J for the Sr-modified alloy samples). Such differences result from the presence of much finer silicon particles obtained in the water-cooled copper mold casting compared to those in the sand mold casting. This refinement of silicon at high growth rates is often referred to as quench modification.

Similar observations were made by other researchers,^[66,70,100,101] where the different

cooling rates were variously achieved by using different molds with the same dimensions, or the same mold type having different dimensions, as in the case at present under study, or otherwise by using a mold which provided directional solidification.

Compared to tensile properties, the cooling rate has a more significant influence on impact properties, *i.e.* impact energy is more sensitive to microstructural changes than are the tensile properties. According to Richard,^[70] small variations in microstructure have a greater influence on impact energy than on elongation. The presence of micro-constituents, such as eutectic Si particles, in the form of platelets, and the effects they have on the sample notch, tend to degrade impact energy even more than elongation. Tsukuda *et al.*^[100] also reported that the impact energies of Al-Si alloys were more sensitive to the as-cast microstructure than were the tensile properties.

5.6 EFFECTS OF HEAT TREATMENT

The effects of heat treatment have already been discussed in subsection 4.5. The initial strength of the Al-Si alloy may be enhanced by the addition of alloying elements such as copper, magnesium, and silicon. Since these elements show increasing solid solubility in aluminum with increasing temperatures, it is possible to subject them to thermal treatments which will improve alloy strength and ductility. These heat treatments consist of three stages: (i) solution heat treatment, (ii) quenching, and (iii) a combination of natural and artificial aging processes. The improvement in the properties of Al-Si-Cu alloys is primarily due to the precipitation of Al_2Cu within the alloy matrix during aging. Changes in the morphology of silicon during solution treatment also contribute to an improvement in

the alloy properties. Yang^[78] recommended a solution-treatment temperature guideline for experimental and industrial 319 alloys to avoid or minimize the occurrence of incipient melting, as mentioned in subsection 4.5.

According to Paray *et al.*^[66] the impact energies for 319 alloys under T6-tempered conditions are relatively low. The presence of copper in Al-Si alloys drastically changes the fracture behavior of these alloys. When the Al₂Cu phase is present, the fracture seems not to be controlled by the Si particles any longer. Although the eutectic Si has been modified by Sr, the impact strength is not improved. In addition to the modification of the Si phase, there is a tendency to form more block-like Al₂Cu in the presence of Sr, although dispersed Al₂Cu also forms. In some cases, the Al₂Cu is segregated towards certain regions of the sample;^[66,74] it should be noted that the block-like Al₂Cu does not dissolve during heat treatment. All these factors taken in conjunction with the brittle nature of Al₂Cu are likely to have contributed to the noticeably low impact strength of 319 alloys which contain significant amounts of Al₂Cu. The shapes of the load-time curves for 319 alloys indicate clearly that these alloys are brittle.

5.7 EFFECTS OF INTERMETALLIC PHASES

The topics of the copper and iron intermetallic phases of Al-Si-Cu alloys have already been discussed in subsection 4.6. The presence of copper in Al-Si-Cu alloys leads to the formation of an Al₂Cu intermetallic compound. If iron is also present in the alloy during solidification, then it goes partially into solid solution in the matrix and, in part, forms intermetallic compounds including the plate-like β -Al₃FeSi and the Chinese script-

like α -Al₁₅(Mn,Fe)₃Si₂ phases. Throughout the solidification process, β -Al₅FeSi platelets are significantly active sites for the nucleation of the Al₂Cu phase. The addition of Mg leads to the formation of the π -Al₈Mg₃FeSi₆ phase displaying script-like morphology. For multi-component 3xx alloys, with cooling rates at close-to-equilibrium conditions, and at ~540°C, the Mg₂Si and π -Al₈Mg₃FeSi₆ phases begin to precipitate. When the temperature is lowered to between 490°C and 530°C, the precipitation of the Al₂Cu and Q-Al₅Mg₈Cu₂Si₆ phases occurs.^[79]

The work of Komastu *et al.*^[65] shows that iron has a detrimental effect on the impact strength of Al-Si alloys as a result of the formation of Al-Si-Fe compounds. With the increase in iron content, both the size and the amount of needlelike Al-Si-Fe compounds increase. The morphology and distribution of these undesirable constituents are not in any way changed by solution heat treatment at 500 °C, resulting in low impact energy values. Similar observations of these detrimental compounds were made by other researchers.^[102,103]

Studies carried out by Shivkumar *et al.*^[72,73] on 319 and A356 alloys did not differ greatly with regard to the dendrite arm spacings (DASs) obtained in both of these alloys when using the same mold. However, the A356 alloys had higher impact energy values than the 319 alloys under the same as-cast and T6 conditions. According to these authors, A356 is generally considered to be a relatively pure alloy with strict limits on impurity concentrations such as Fe, whereas in 319 alloys the iron level can be much higher than it is in A356. The impact energy or toughness of 319 alloys is thus limited by the Fe-containing intermetallic phases.

Similar studies were carried out by Paray *et al.*^[66] on Al-Si foundry alloys, where the iron content of their 356 and 319 alloys was 0.11% and 0.42%, respectively. These iron contents are similar to those in the present work. This would explain the relatively low impact energy values of the 319 alloys, compared to the 356 alloys. When comparing the differences in fracture behavior it becomes clear that in the 356 alloy, fracture behavior is governed by the amount, size, and morphology of the brittle eutectic Si particles, whereas in the 319 alloy, it is controlled by the brittle block-like Al_2Cu phase. According to this study,^[66] Al-Si foundry alloys containing Cu have poor impact properties; the presence of the copper contributes significantly to lowering impact properties; and the fracture behavior is influenced by undissolved Cu-phases and no longer by the Si particles.

5.8 IMPACT TEST RESULTS AND DISCUSSION

5.8.1 Impact Toughness

The impact properties of both experimental and industrial 319 alloys were assessed using Charpy instrumented impact testing; all the samples were heat-treated in keeping with Aluminum Association recommendations. Four groups were tested, one in the as-cast condition, and the others after solution heat treatment, T6 heat treatment, and T7 heat treatment. For each sample, the load, deflection, and energy data were recorded automatically at time intervals of 0.01 msec. From these samples, the load-time and energy-time curves, total energy (E_T), and the energy values for crack initiation (E_i) and crack propagation (E_p) were obtained for each sample.

As the total energy (E_T) is normally taken to represent the impact energy, this

parameter will be used mainly to discuss alloy impact properties in relation to (a) the different alloying and melt processing parameters, including Mg content, Sr-modification, and cooling rate, as well as intermetallic size and porosity; and (b) the heat treatment conditions, including the solutionizing conditions of time and temperature followed by the appropriate aging conditions.

Table 5.1 summarizes the total energy values of the as-cast experimental and industrial 319 alloys in both non-modified and Sr-modified conditions, for samples obtained from the star-like and L-shaped molds. Table 5.2 provides the crack initiation energies of the as-cast alloys investigated. According to the energy values which are listed in these two tables, the impact toughness increases with an increase in cooling rate and decreases with an increase in the Mg content and with Sr-modification for both the experimental and industrial alloys. The greater part of the total absorbed energy is used for crack initiation, *i.e.* the crack initiation energy is greater than the crack propagation energy, indicating the high ductility of the 319 alloys. These observations are in good agreement with those reported by Gruzleski and co-workers^[1,6,66] and Ma.^[104]

Table 5.1 Total absorbed energy of the as-cast experimental and industrial 319 alloys

Alloy	E_t (J)										
	Av.	SD									
D1	11.95	3.10	DS1	10.44	2.24	LD1	10.53	1.87	LDS1	9.49	2.52
D2	11.74	1.36	DS2	8.39	1.80	LD2	9.41	2.08	LDS2	7.19	2.05
D3	8.97	1.49	DS3	6.47	1.67	LD3	7.63	2.03	LDS3	5.18	1.39
D4	8.39	1.17	DS4	5.96	1.67	LD4	5.74	0.39	LDS4	3.81	0.57
D5	7.94	1.48	DS5	5.61	1.85	LD5	4.91	1.88	LDS5	3.27	0.78
D6	6.09	0.79	DS6	5.26	0.94	LD6	3.49	0.82	LDS6	3.19	1.31
D7	7.11	0.69	DS7	6.19	0.97	LD7	3.82	1.68	LDS7	3.51	1.63
D8	5.42	0.91	DS8	3.75	0.49	LD8	3.42	1.10	LDS8	3.37	0.40

Table 5.2 Crack initiation energy of the as-cast experimental and industrial 319 alloys

Alloy	E _i (J)										
	Av.	SD									
D1	8.28	2.87	DS1	6.81	1.69	LD1	7.08	1.69	LDS1	6.01	1.58
D2	7.71	1.07	DS2	4.76	1.10	LD2	5.66	1.14	LDS2	4.41	1.38
D3	6.29	1.57	DS3	3.75	1.09	LD3	4.47	1.80	LDS3	3.06	0.81
D4	4.86	0.75	DS4	3.26	1.17	LD4	3.19	0.27	LDS4	1.98	0.31
D5	4.58	1.04	DS5	2.99	1.08	LD5	3.15	1.22	LDS5	1.78	0.48
D6	3.33	0.51	DS6	2.72	0.56	LD6	2.13	0.41	LDS6	1.66	0.74
D7	4.09	0.43	DS7	3.21	1.63	LD7	2.29	1.01	LDS7	2.26	1.04
D8	2.92	0.6	DS8	1.89	0.25	LD8	1.83	0.59	LDS8	1.65	0.22

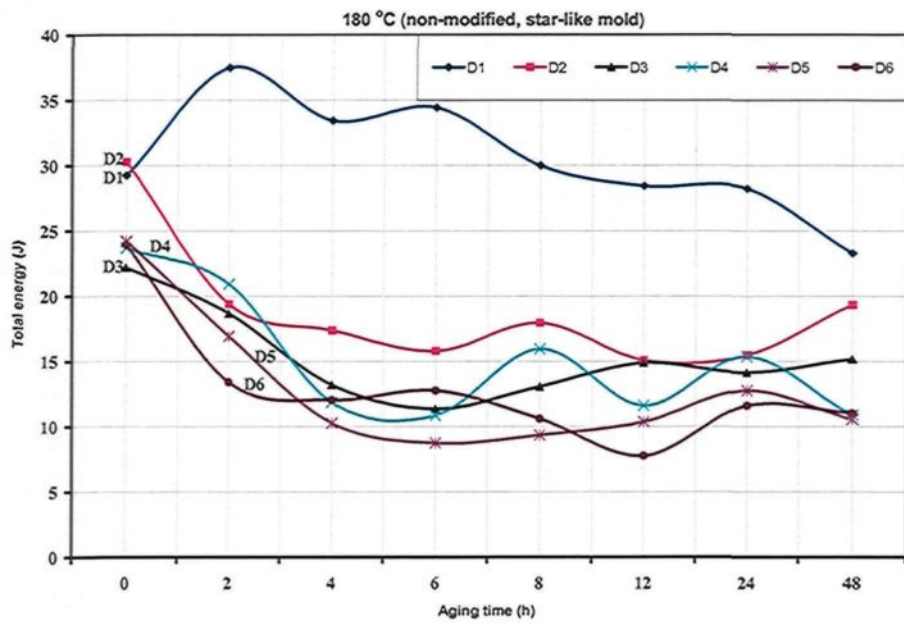
D: non-modified/star-like mold; DS: modified/star-like mold; LD: non-modified/L-shaped mold; LDS: modified/L-shaped mold; D1-D6: experimental alloys; D7, D8: industrial alloys; D1: base alloy (Mg-free); D2, D3, D4, D5 and D6: 0.1, 0.2, 0.3, 0.4 and 0.6 % Mg, respectively; D7: 0.3 % Mg; D8: 0.6 % Mg; S: Sr-modification (200 ppm); E_t: total energy; E_i: initiation energy; Av.: average; and SD: standard deviation.

Figures 5.4 and 5.5 display the effects of Mg addition on the impact energy values of non-modified and Sr-modified experimental 319 alloys as a function of aging time in the T6 heat-treated condition, for the samples obtained from star-like and L-shaped molds, respectively. Figure 5.4(a) shows the total impact toughness values for non-modified experimental alloys, including the highest recorded energy value of all the alloys tested, namely 37.5 J, for the non-modified experimental Mg-free alloy D1, while Figure 5.4(b) shows the energy values for the Sr-modified alloys. These two groups of curves were obtained using the higher cooling rate star-like mold. It was found that alloy toughness, or the total impact energy, decreased by ~39%, ~41%, ~42%, ~43% and ~43%, respectively, upon increasing the Mg content in the D1 Mg-free base alloy to 0.1wt% (*i.e.* D2 alloy), to 0.2wt% (*i.e.* D3 alloy), to 0.3wt% (*i.e.* D4 alloy), to 0.4wt% (*i.e.* D5 alloy), and finally to 0.6wt% (*i.e.* D6 alloy).

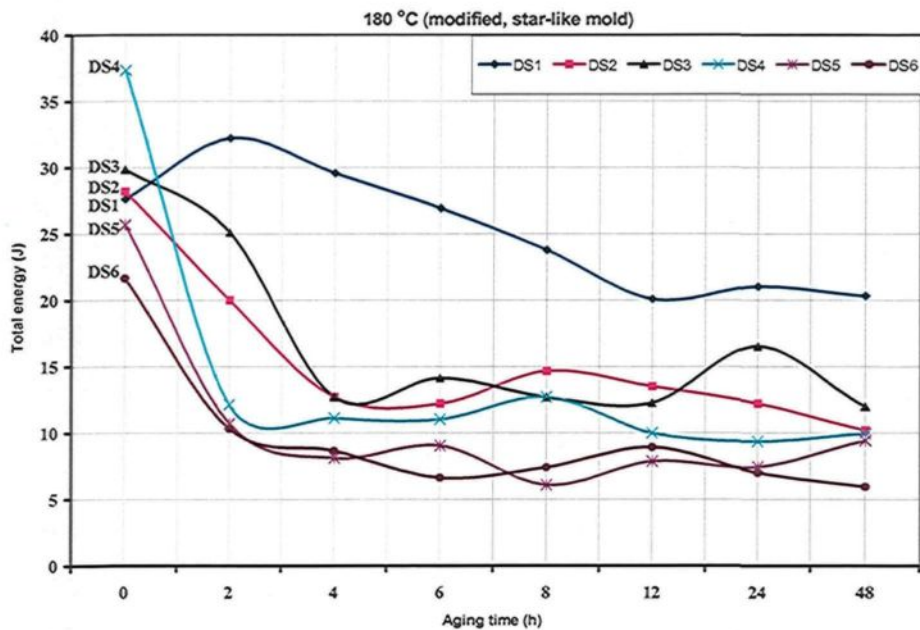
It was also observed that an increase in the Mg content of up to 0.4wt% for different

aging times has a negative effect on toughness, indicating that Mg has a modifying effect on the Si particles, with or without the presence of Sr. Magnesium addition also leads to the precipitation and segregation of Al_2Cu which segregates towards areas away from the Si particles. The effects of Mg addition on the aged alloys are similar to those observed for the as-cast alloys. Increasing the Mg level causes a number of intermetallics to form such as Mg_2Si and the harmful $\text{Q-Al}_5\text{Mg}_8\text{Cu}_2\text{Si}_6$ and $\pi\text{-Al}_8\text{Mg}_3\text{FeSi}_6$ phases. Both the insoluble Q-phases and the partially soluble π -phase have a negative effect on impact toughness and fracture behavior. The aging of these Mg-containing 319 alloys under T6 heat treatment conditions of 180°C for up to 48 hours produced a sharp decrease in impact toughness during the first two hours of aging, followed by a broad valley or plateau spread between 2 and 24 hours as well as a noticeable period of over-aging beyond 24 hours. Modification using 200 ppm strontium had a negative effect on impact toughness values, as shown in Figure 5.4(b). The effects of Mg-content on the Sr-modified alloys are similar to those obtained for the non-modified alloys. These observations are in satisfactory agreement with those reported by Gruzleski and co-workers^[1,6,66] and Ma.^[104]

A lower cooling rate L-shaped mold was also used to investigate the effects of cooling rate on the impact toughness of the experimental 319 alloy containing different amounts of Mg, as shown in Figure 5.5. When compared to Figure 5.4, it will be seen that the slow cooling rate decreases the impact toughness in both the non-modified and Sr-modified alloys in the T6 heat-treated conditions. With increasing Mg content and/or Sr-modification, similar observations, *i.e.* regarding the negative effects of Mg and Sr-modification, were made for the low cooling rate samples cast in the L-shaped mold.

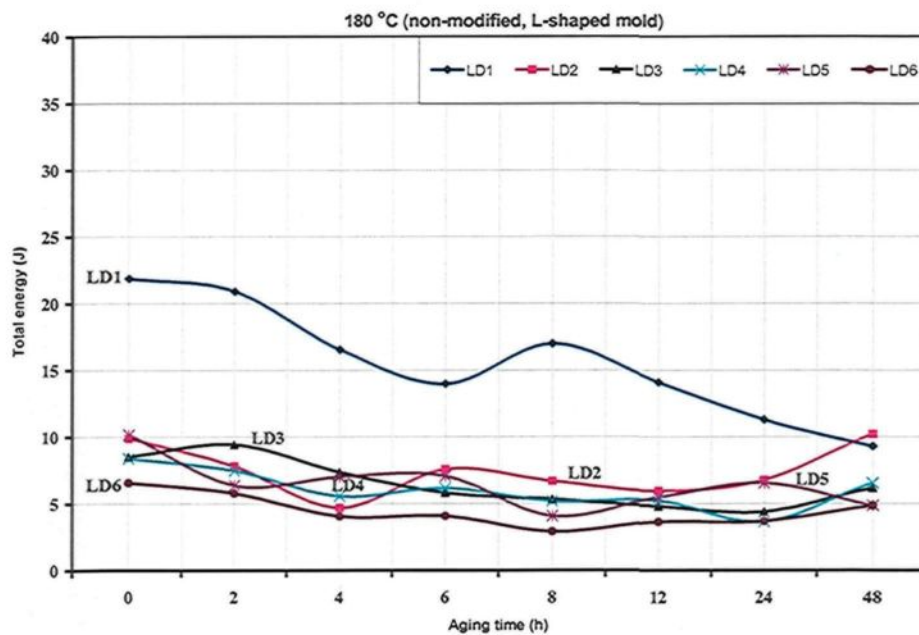


(a)

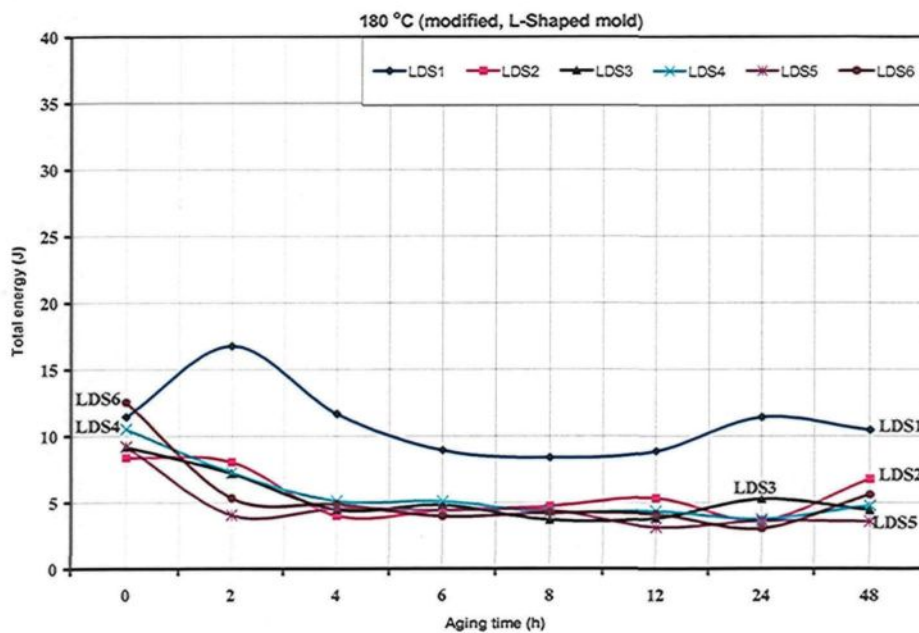


(b)

Figure 5.4 Total absorbed energy of experimental alloys in the T6-tempered condition (aging temperature 180°C): (a) non-modified alloys, and (b) Sr-modified alloys (samples obtained from the star-like mold).



(a)



(b)

Figure 5.5 Total absorbed energy of experimental alloys in the T6-tempered condition (aging temperature 180°C): (a) non-modified alloys, and (b) Sr-modified alloys (samples obtained from the L-shaped mold).

The negative effects of Sr-modification on the impact toughness of experimental 319 alloys involve the segregation of the brittle block-like Al_2Cu towards areas away from the modified Si particles. This block-like Al_2Cu as well as the $\text{Q-Al}_5\text{Mg}_8\text{Cu}_2\text{Si}_6$ phase are insoluble. Figure 5.6 shows these undissolved Cu-rich phases which control the impact toughness and the fracture behavior of the alloys investigated. This observation is in good agreement with that reported by Paray and co-workers.^[6,66]

Figure 5.6 shows the undissolved Cu-rich phases for both the non-modified (a, b) and Sr-modified (c, d) solution heat-treated base alloy. Microstructures (c) and (d), using the higher cooling rate star-like mold (DAS 24 μm), and the lower cooling rate L-shaped mold (DAS 50 μm), respectively, show the effects of Sr-modification which causes the segregation of the brittle undissolved block-like Al_2Cu towards areas away from modified Si particles. Microstructures (a) and (b), obtained using the two respective molds, display undissolved Cu-rich phases spread across the matrix; these samples displayed impact toughness values which were higher than those for (c) and (d), indicating the negative influence of Sr addition.

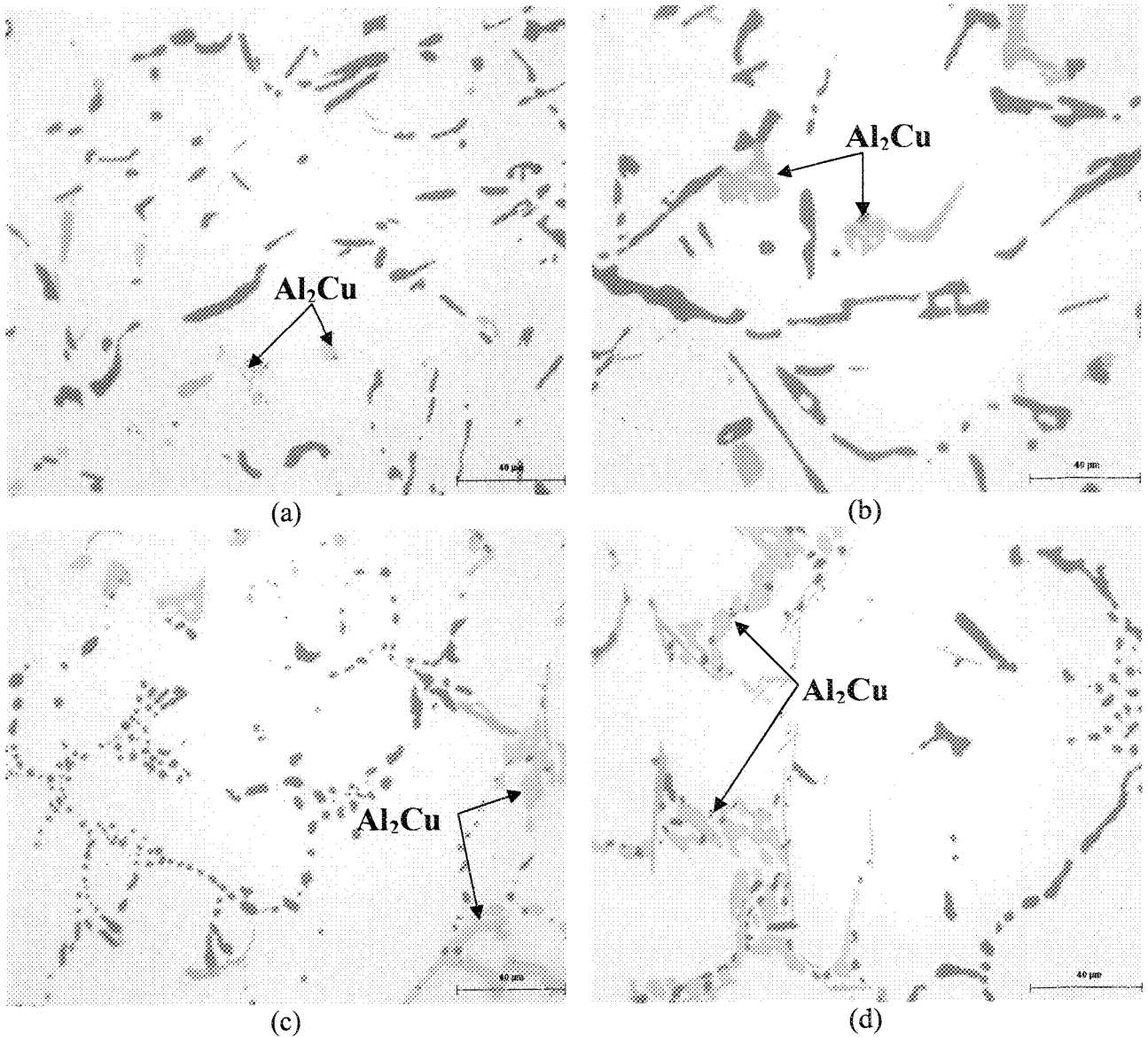


Figure 5.6 Undissolved Al_2Cu in solution heat-treated alloys: (a) alloy D1, (b) alloy LD1, (c) Sr-modified alloy DS1, and (d) Sr-modified alloy LDS1.

Table 5.3 summarizes the volume fraction of Al_2Cu (%) for both the as-cast and solution heat-treated experimental 319 alloy in non-modified and Sr-modified conditions, observed from the star-like and L-shaped mold samples. The volume fraction of Al_2Cu (%) for the Sr-modified alloy is higher than it is for the non-modified alloy in both the as-cast

and solution heat-treated conditions. These volume fraction values confirm: (i) the negative effects of modification on Cu-containing 319 alloys (~3.5% Cu); (ii) the decrease in impact energy values of Sr-modified 319 alloys in both the as-cast and solution heat-treated conditions; (iii) the toughness data summarized in Tables 5.1 and 5.2 and those plotted in Figures 5.4 and 5.5, as well as in Figures 5.7 to 5.16. These observations are all in satisfactory agreement with those reported by Ma^[104] and Tavitas-Medrano.^[105]

Table 5.3 Volume fraction of Al₂Cu (%) for the base alloy

Alloy	Volume Fraction of Al ₂ Cu (%)			
	As-Cast		SHT	
	Av.	SD	Av.	SD
D1	5.74	0.69	0.49	0.09
DS1	4.87	0.95	1.82	0.58
LD1	4.19	0.38	0.93	0.18
LDS1	4.27	0.45	2.15	0.63

The effects of Mg addition on the impact toughness of non-modified and Sr-modified experimental 319 alloys as a function of aging time was investigated under T7 heat treatment conditions and is shown in Figures 5.7 and 5.8 for samples derived from the star-like and L-shaped mold, respectively. The effects of the addition of Mg on 319 alloys are similar to those observed in both the as-cast and T6-treated alloys. Increasing Mg levels causes the formation of a number of intermetallics such as Mg₂Si as well as the harmful Q-Al₅Mg₈Cu₂Si₆ and π -Al₈Mg₃FeSi₆ phases. The latter two phases, whether the insoluble Q-phase or the partially soluble π -phase, have a negative effect on the impact toughness and fracture behaviour. Under T7 heat treatment conditions, increasing the Mg content

increases the impact energy levels to a greater extent with each increase in Mg addition, compared to those observed in the T6 heat-treated conditions. The aging of these Mg-containing experimental 319 alloys at 220°C, *i.e.* under T7 heat treatment conditions, for up to 48 hours, produced a sharp decrease in hardness during the first two hours of aging, followed by a broad plateau spread between 2 and 24 hours, as well as a noticeable period of over-aging after 24 hours. Experimental 319 alloys under T7 heat treatment conditions display higher impact toughness than T6-treated alloys as a result of the over-aging effect occurring with the T7 treatment. These observations are in satisfactory agreement with those of Tavitas-Medrano.^[105]

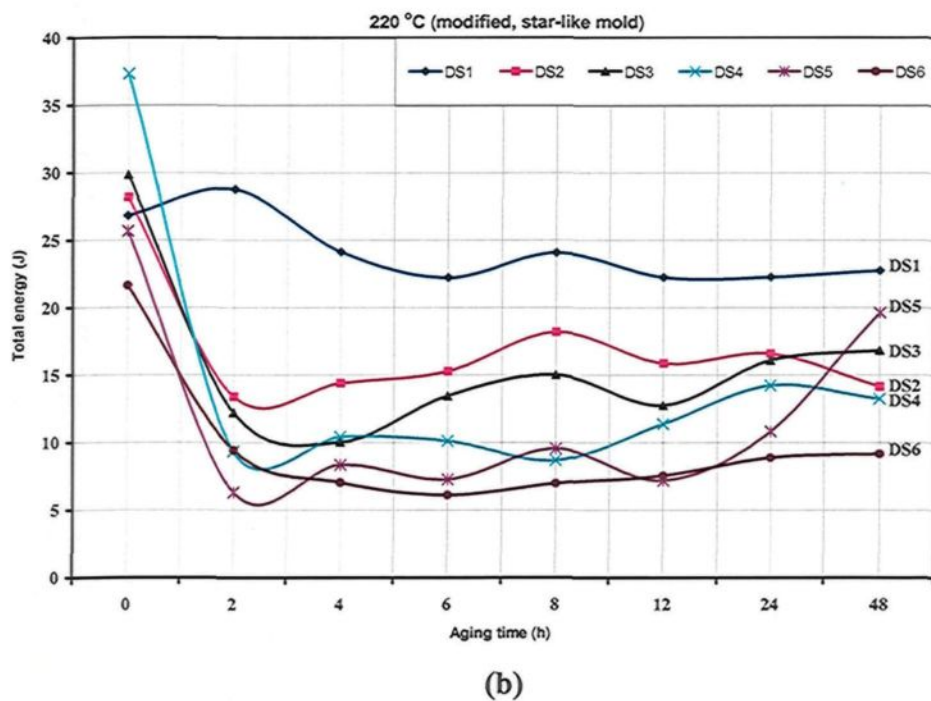
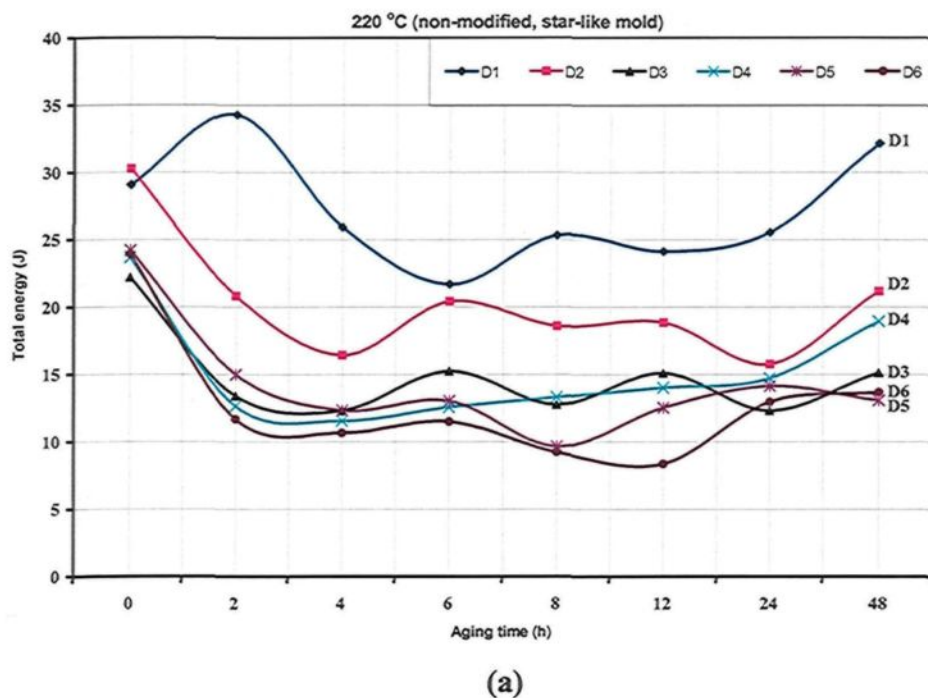
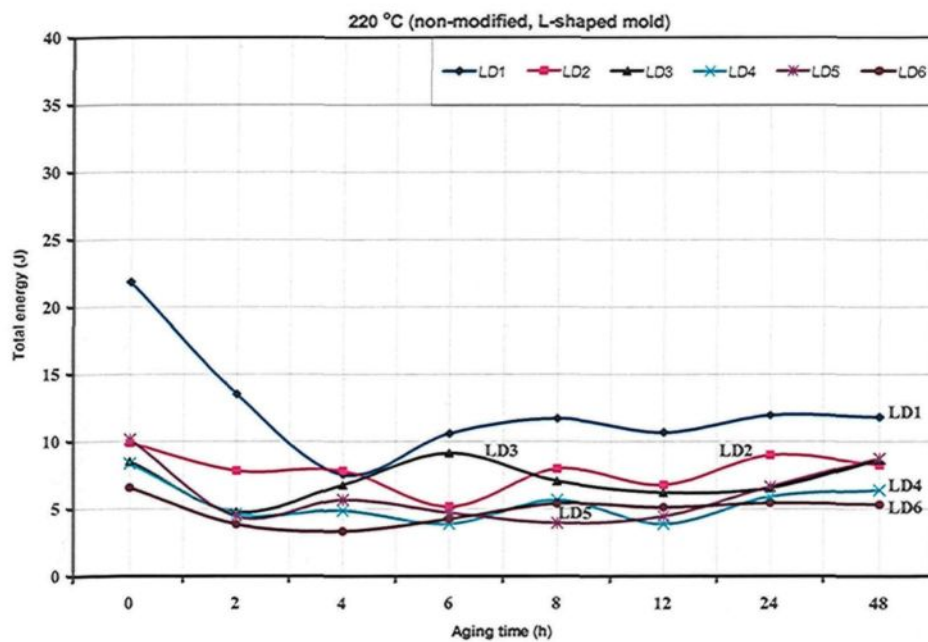
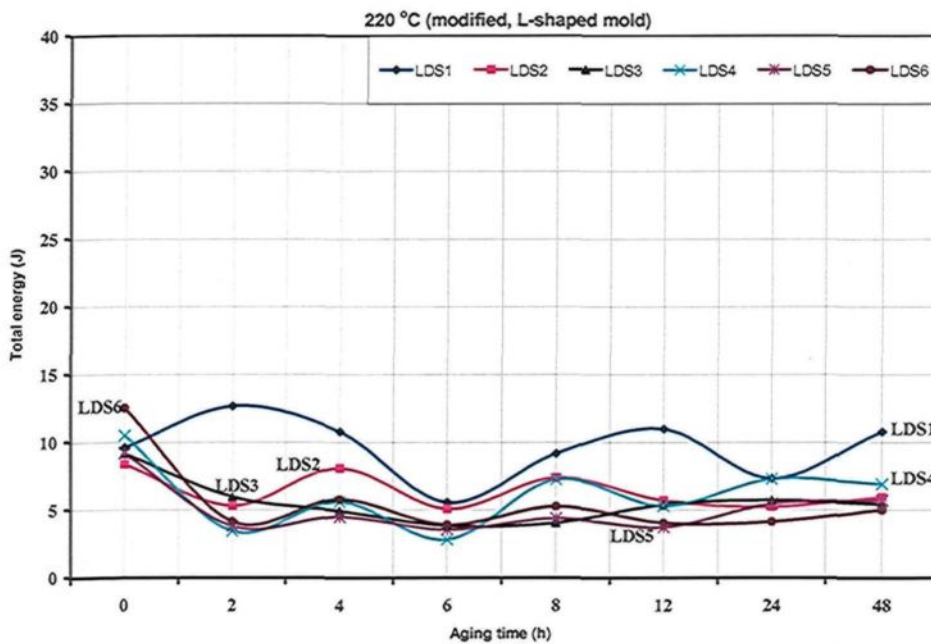


Figure 5.7 Total absorbed energy of experimental alloys in the T7-tempered condition (aging temperature 220°C): (a) non-modified alloys, and (b) Sr-modified alloys (samples obtained from the star-like mold).



(a)



(b)

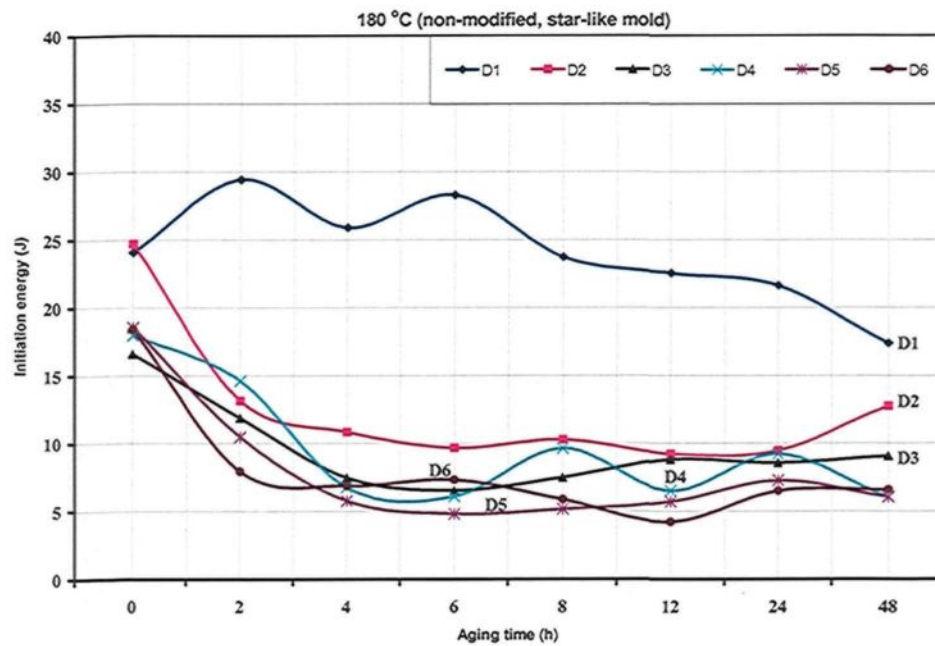
Figure 5.8 Total absorbed energy of experimental alloys in the T7-tempered condition (aging temperature 220°C): (a) non-modified alloys, and (b) Sr-modified alloys (samples obtained from the L-shaped mold).

The effects of Mg addition on the crack initiation energy of T6 heat-treated non-modified and Sr-modified experimental 319 alloys was investigated as a function of aging time, as shown in Figures 5.9 and 5.10 for samples obtained from the star-like and L-shaped molds, respectively. Figure 5.9(a) shows the initiation energy values for non-modified experimental alloys, including the highest recorded initiation energy value of all the alloys tested, which is 29.4 J for the non-modified Mg-free experimental alloy D1; Figure 5.9(b), on the other hand, portrays the energy values for the Sr-modified alloys. These two groups of curves were obtained using the higher cooling rate star-like mold. Similar observations have been made with regard to Mg addition, Sr-modification, and T6 heat treatment conditions for the total absorbed energy. A greater part of this energy is used for crack initiation, *i.e.* the crack initiation energy is greater than the crack propagation energy, reflecting the high ductility of the 319 alloys investigated. This ductility may be enhanced by alloy homogeneity and such strengthening intermetallic phases as Mg_2Si , Al_2CuMg , and $Q-Al_5Mg_8Cu_2Si_6$. Also, alloy homogeneity is likely to be increased in the presence of eutectic Al_2Cu .

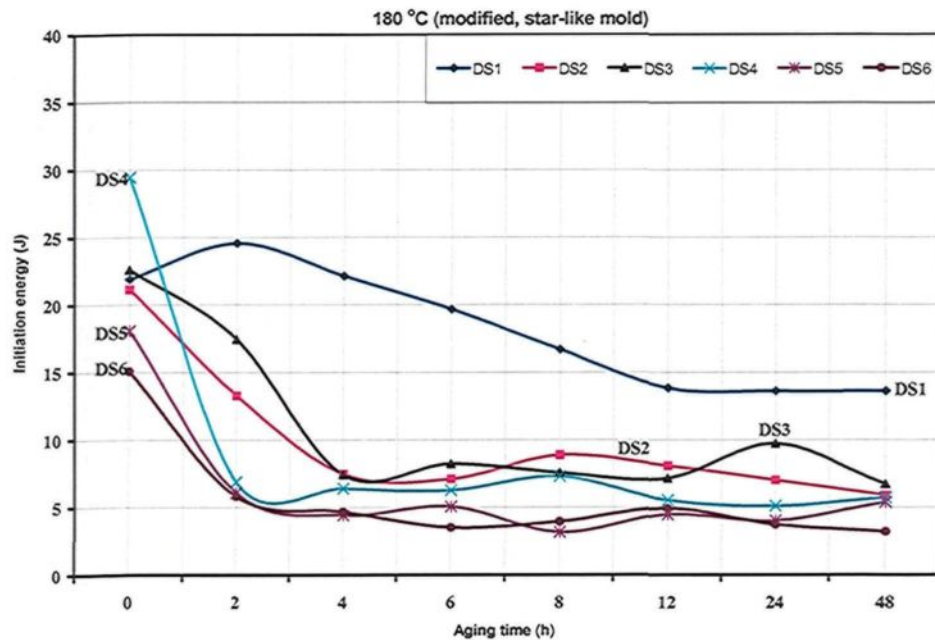
The lower cooling rate L-shaped mold was used to investigate the effects of cooling rate on the crack initiation in experimental 319 alloys at different levels of Mg addition, as shown in Figure 5.10. When compared to Figure 5.9, it will be observed that the slow cooling rate decreases crack initiation energy in both non-modified and Sr-modified alloys, under T6 heat treatment conditions. Similar observations were made for the alloys investigated using the higher cooling rate star-like mold. These results and observations regarding crack initiation energy confirm those obtained for total impact toughness energy

and are in satisfactory agreement with the work of other researchers.^[6,66,104,105]

The effects of Mg addition on the crack initiation energy of both the non-modified and Sr-modified experimental 319 alloys as a function of aging time were investigated for T7 heat treatment conditions, and are shown in Figures 5.11 and 5.12 for the star-like and L-shaped mold samples, respectively. Similar observations were made for the T7-tempered alloys as those noted for the alloys subjected to T6 heat treatment conditions.

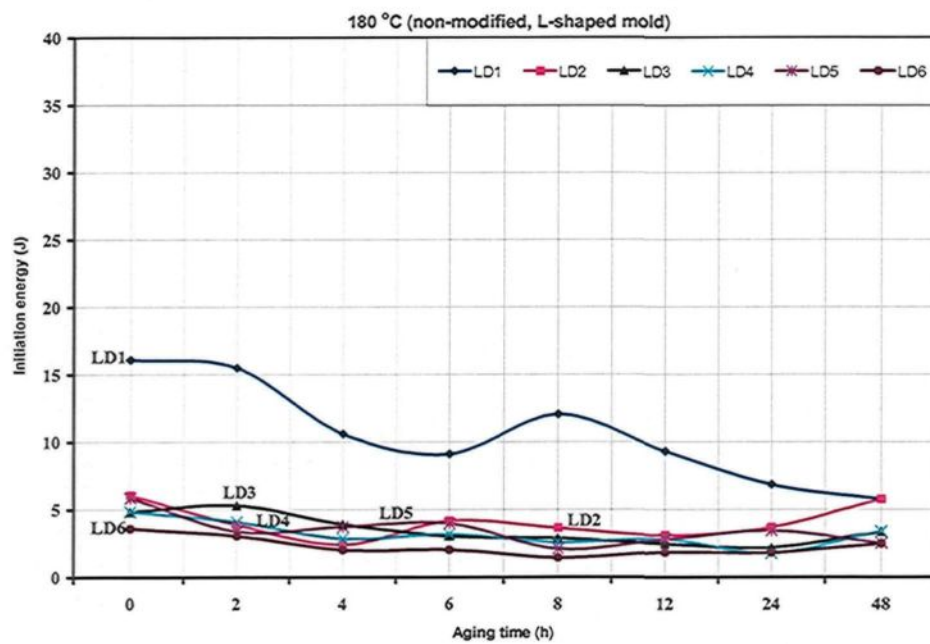


(a)

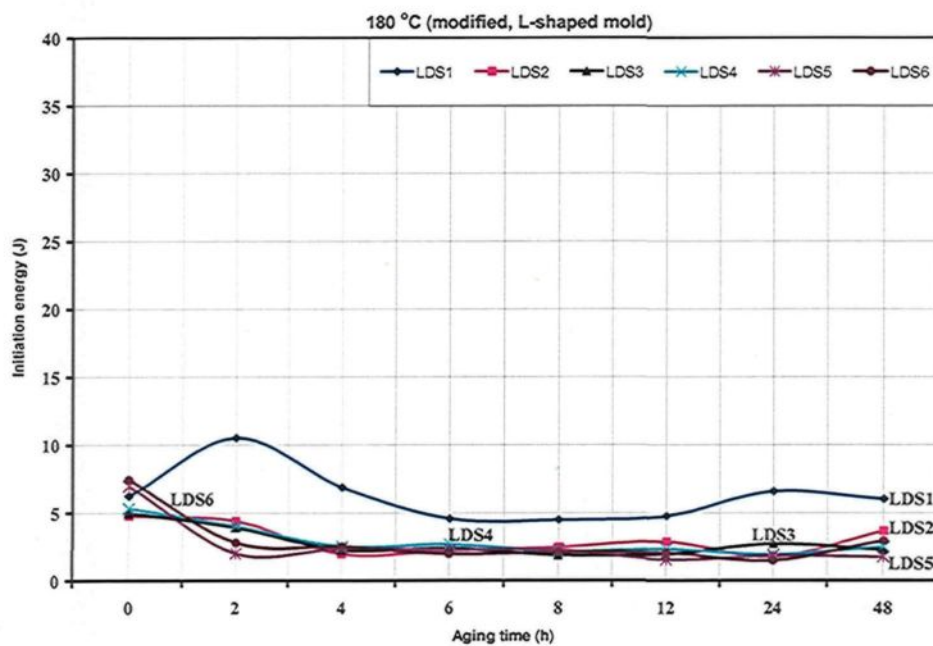


(b)

Figure 5.9 Crack initiation energy of experimental alloys in the T6-tempered condition (aging temperature 180°C): (a) non-modified alloys, and (b) Sr-modified alloys (samples obtained from the star-like mold).

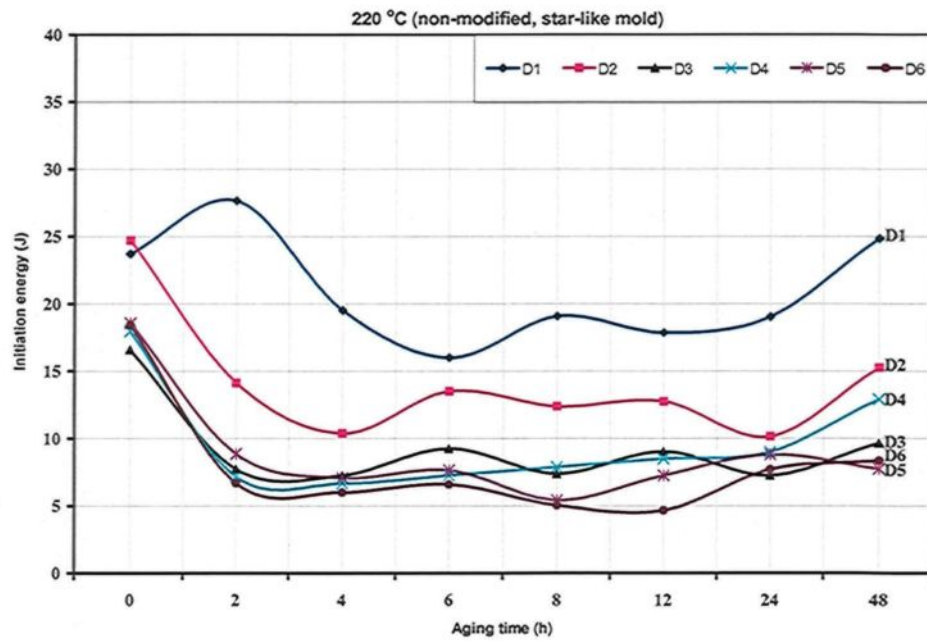


(a)

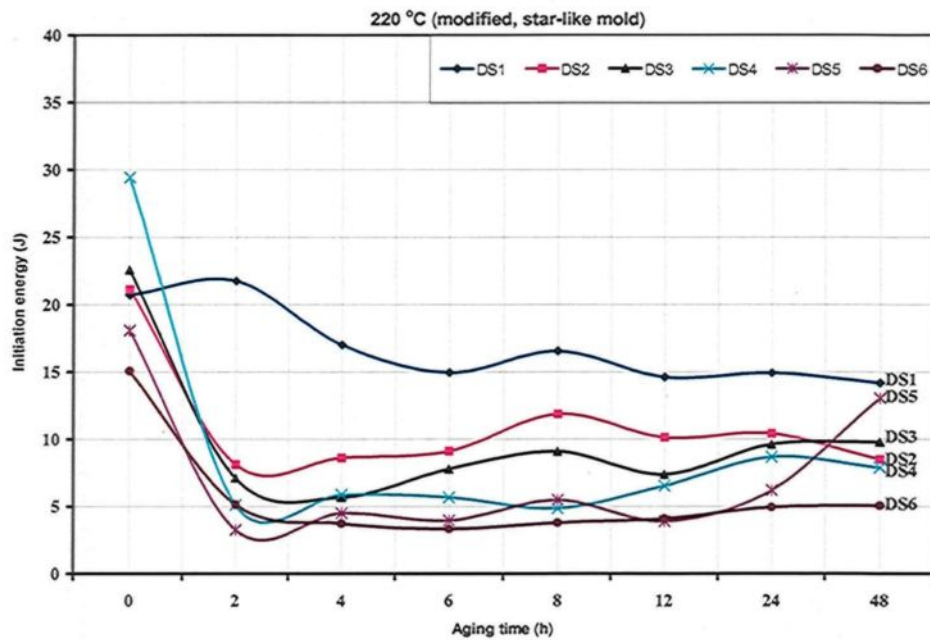


(b)

Figure 5.10 Crack initiation energy of experimental alloys in the T6-tempered condition (aging temperature 180°C): (a) non-modified alloys and (b) Sr-modified alloys (samples obtained from the L-shaped mold).

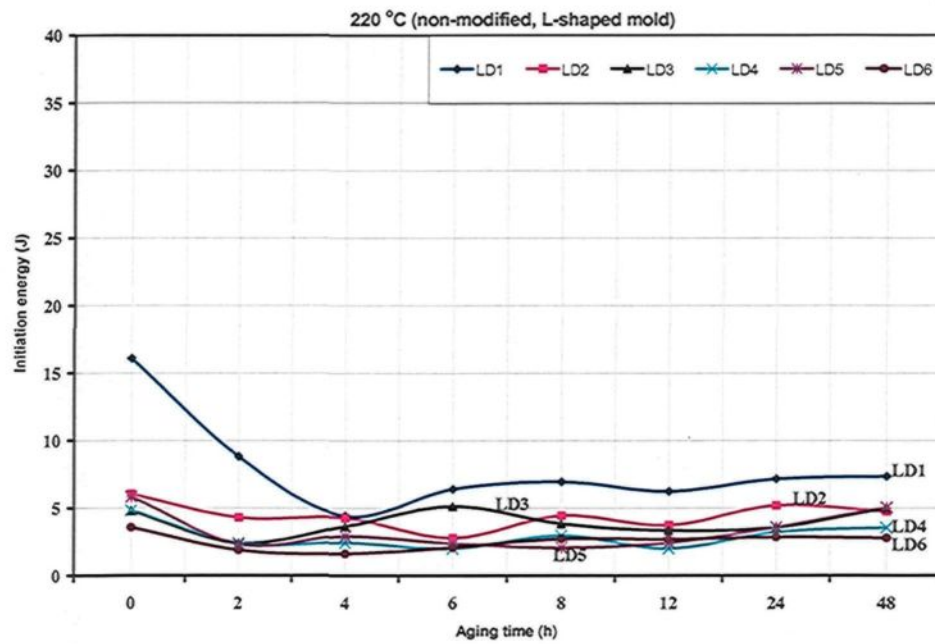


(a)

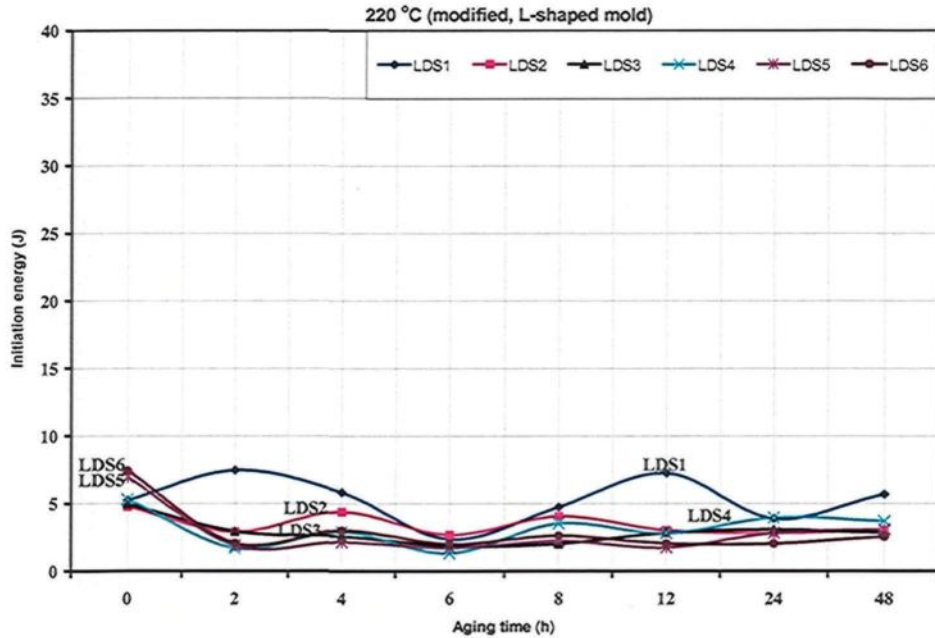


(b)

Figure 5.11 Crack initiation energy of experimental alloys in the T7-tempered condition (aging temperature 220°C): (a) non-modified alloys and (b) Sr-modified alloys (samples obtained from the star-like mold).



(a)

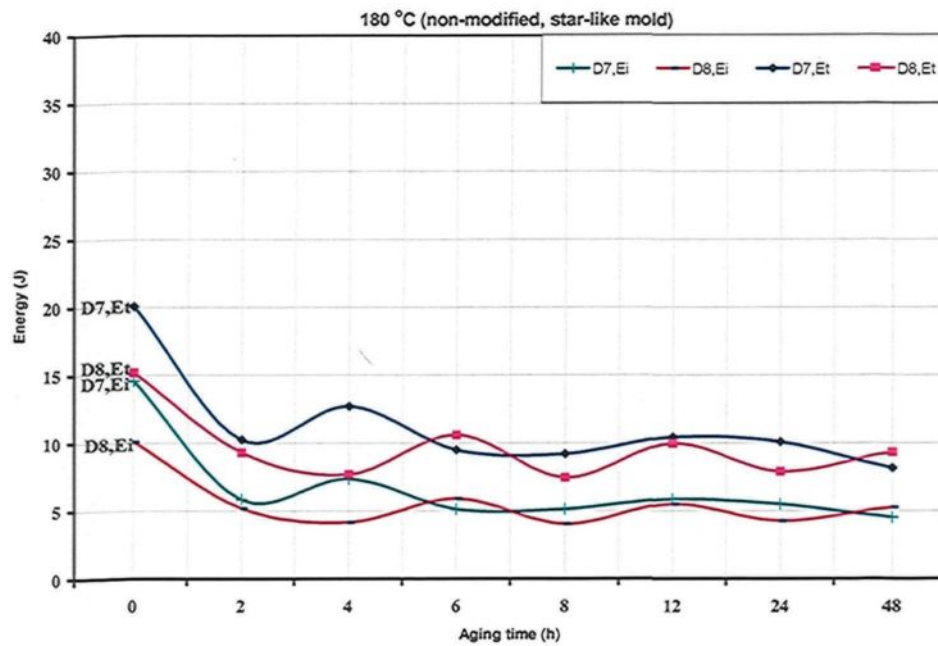


(b)

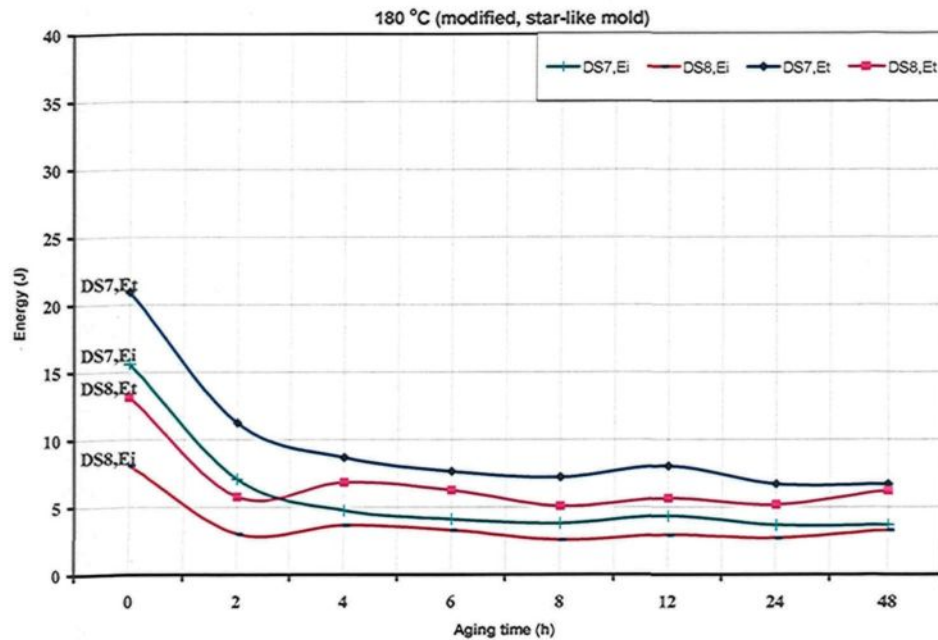
Figure 5.12 Crack initiation energy of experimental alloys in the T7-tempered condition (aging temperature 220°C): (a) non-modified alloys, and (b) Sr-modified alloys (samples obtained from the L-shaped mold).

The effects of Mg addition on the impact toughness of non-modified and Sr-modified industrial 319 alloys as a function of aging time were investigated under T6 heat treatment conditions, and are shown in Figures 5.13 and 5.14 for alloy samples obtained from the star-like and L-shaped molds, respectively. While similar trends were noted with regard to experimental alloys as described in preceding paragraphs (Figures 5.4, 5.5, 5.9, and 5.10), the industrial 319 alloys, however, clearly display lower impact toughness and crack initiation energies than the experimental alloys as a result of the presence of trace elements.

The effects of Mg addition on the impact toughness of non-modified and Sr-modified industrial 319 alloys as a function of aging time were also investigated under T7 heat treatment conditions, and are shown in Figures 5.15 and 5.16 for alloy samples obtained from the star-like and L-shaped molds, respectively. In comparison to the T6 heat treatment conditions, industrial 319 alloys which have undergone T7 heat treatment display higher impact toughness and crack initiation energy values than the T6-treated industrial alloys as a result of over-aging effects associated with the T7 heat treatment conditions. These observations regarding the industrial alloys confirmed the observations noted for the experimental alloys having the same Mg contents and aging conditions. The results and observations regarding the impact toughness for both the experimental and industrial 319 alloys investigated are thus confirmed and in satisfactory agreement with the studies carried out by other researchers on Al-Si-Cu-Mg alloys.^[1,66,67,68,72,73,104,105]

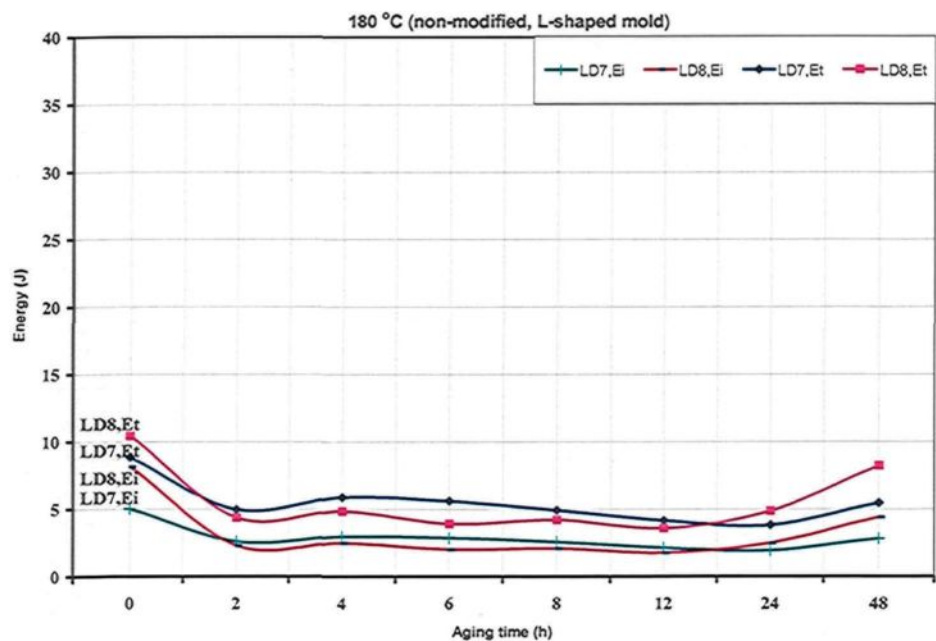


(a)

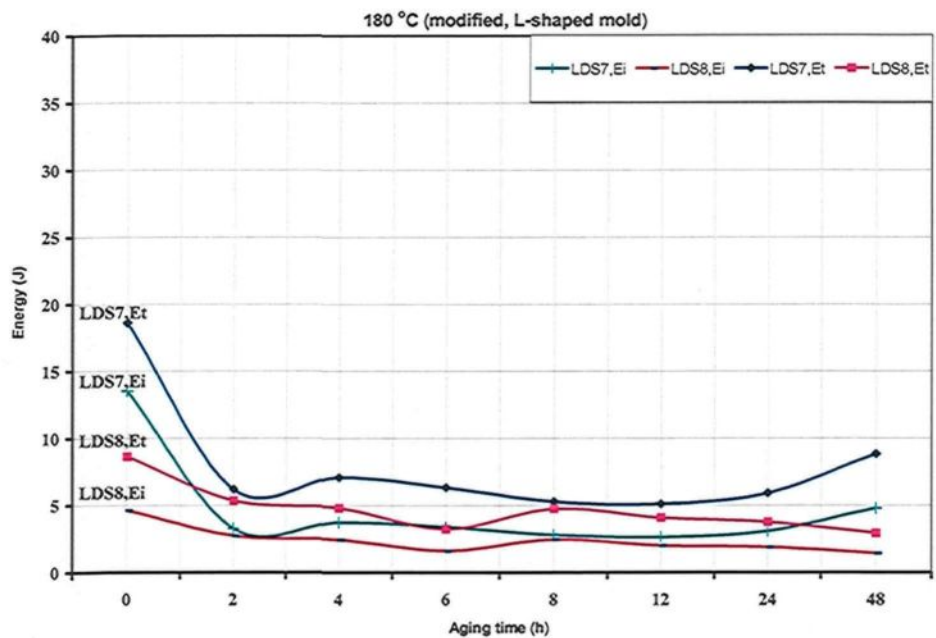


(b)

Figure 5.13 Impact toughness energy (total absorbed energy, E_t , and crack initiation energy, E_i) in industrial alloys after T6-temper treatment (180°C): (a) non-modified alloys, and (b) Sr-modified alloys (star-like mold samples).

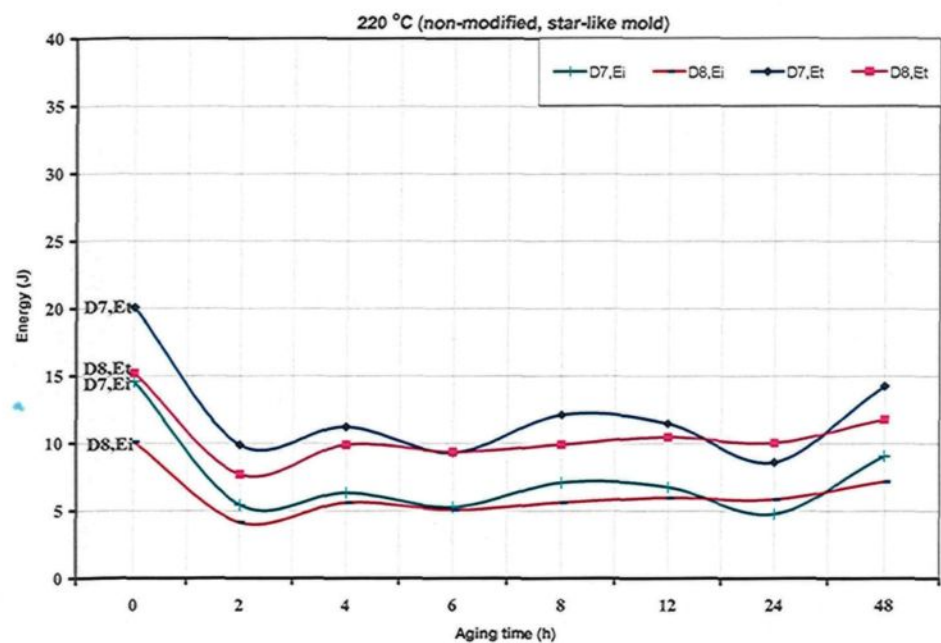


(a)

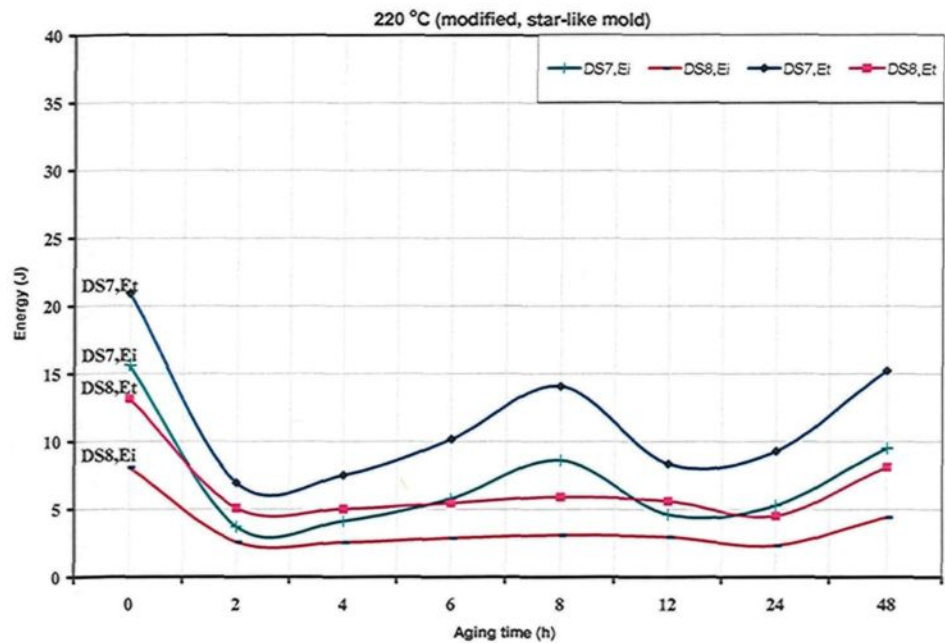


(b)

Figure 5.14 Impact toughness energy (total absorbed energy, E_t , and crack initiation energy, E_i) in industrial alloys after a T6-temper treatment (180°C): (a) non-modified alloys, and (b) Sr-modified alloys (L-shaped mold samples).

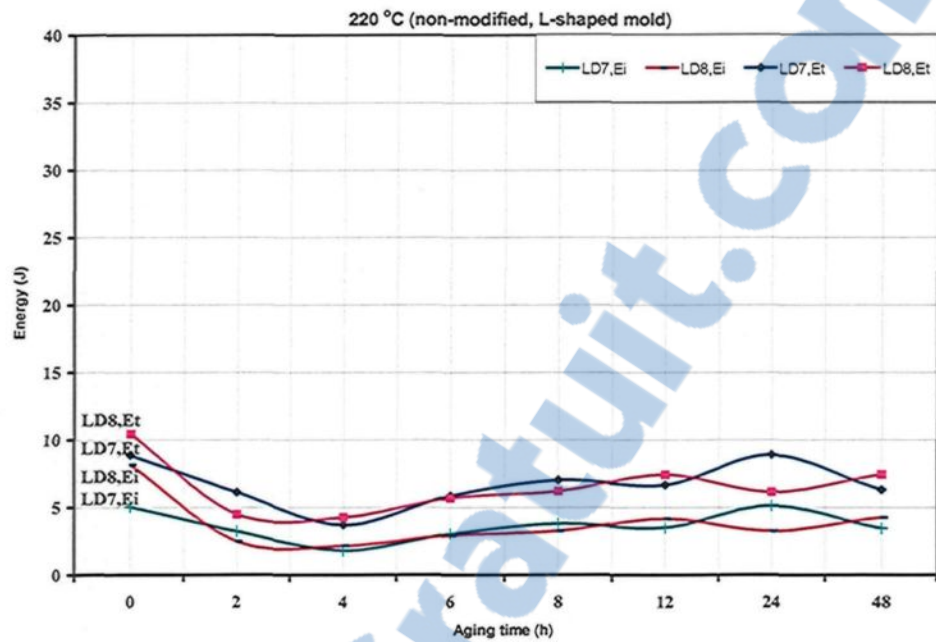


(a)

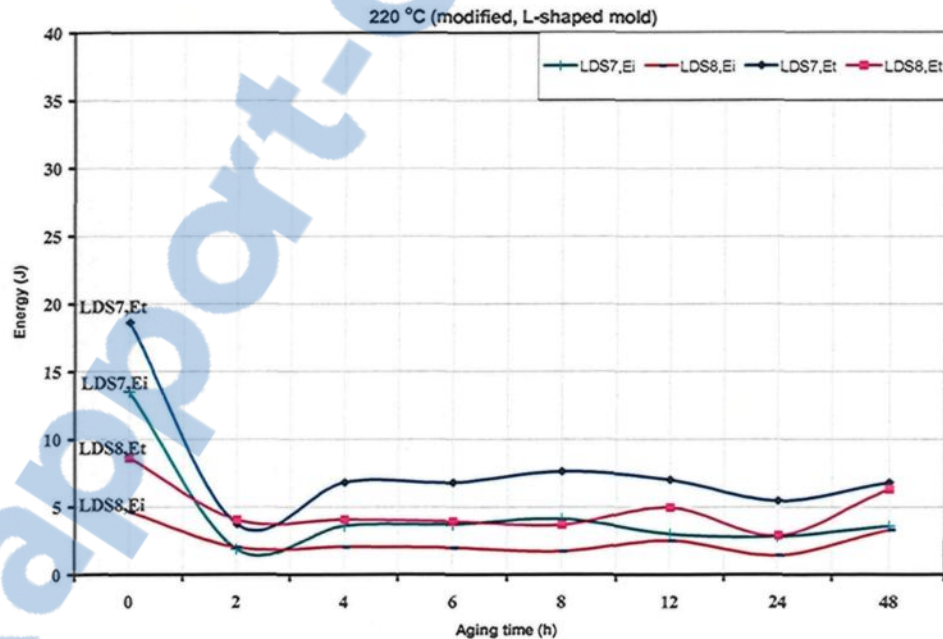


(b)

Figure 5.15 Impact toughness energy (total absorbed energy, E_t , and crack initiation energy, E_i) in industrial alloys after a T7-temper treatment (220°C): (a) non-modified alloys, and (b) Sr-modified alloys (star-like mold samples).



(a)



(b)

Figure 5.16 Impact toughness energy (total absorbed energy, E_t , and crack initiation energy, E_i) in industrial alloys after a T7-temper treatment (220°C): (a) non-modified alloys, and (b) Sr-modified alloys (L-shaped mold samples).

5.9 PRECIPITATION PROCESSES

The 319-type Al-Si-Cu-Mg alloys have become the object of extensive investigation considering their practical importance to the transport industry. All the experimental variables, such as solidification conditions, chemical composition, and heat treatment, are known to have an influence on the precipitation behavior; precipitation-hardening, however, is the most significant of these because of the presence of excess alloying elements from the supersaturated solid solution which form fine hardening precipitates during the aging process, which consequently act as obstacles to dislocation movement, and thereby increase the alloy strength.

According to the studies carried out by Tavitas-Medrano^[105] and Andrade-González^[106] for 319 alloys in the same conditions as those prevailing in the present work, the structural changes during the age-hardening process are, in reality, not so easy to distinguish. These structural changes result in curves displaying a multi-peak wave form for both strength and hardness values when plotted as a function of the aging conditions. With an increase in either aging temperature or time, different decomposition and precipitation processes occur, in some cases sequentially, and in others, simultaneously. These precipitation processes may be illustrated in detail after examining the 319 alloys in the current study. In these alloys, five stages of structural changes can be determined during the heat-treating operations and have been summarized in Table 5.4.^[106]

The first stage represents the structure prior to solution heat treatment. The precipitates may originate either in the cast structure or in any previous thermal treatment. In the second stage, the Cu atoms which had precipitated previously are taken into solution

at 500°C. The solution heat treatment also removes any previous cold work or precipitation hardening. The material is then quenched, bringing it from the solutionizing temperature to room temperature, thereby developing helical dislocations within the material.

Table 5.4 Age-hardening behavior of Al-Si-Cu-Mg alloys^[106]

Stage	Heat Treatment	Phases
I	None	Mostly precipitated as equilibrium Al ₂ Cu phases
II	Solution treatment and rapid cooling	All Cu in solution Most Mg phases in solution
III	Natural aging at room temperature	Segregation into GP I zones (coherent)
IV	Age hardening at 180°C	Dissolution of GP I zones Segregation into GP II zones (coherent) Precipitation of S' phase (Al ₂ CuMg)
	Further age hardening at 180°C	Increased diffusion into GP II zones and precipitation as θ phase (partially coherent) Precipitation of S' phase (Al ₂ CuMg) Precipitation of S'' phase Precipitation of β'' phase or β' phase (Mg ₂ Si) of a very minor species Precipitation of traces of Si
V	Overaging resulting from too long a treatment time	Precipitation of θ phase, the equilibrium phase (incoherent)

During natural aging, the dissociation of the supersaturated solid solution begins with the coherent precipitation of the Cu-rich GP zones which are only a few atoms thick. These precipitates stress the aluminum lattice and, because of their great number, form a

dense network which impedes dislocation movement during deformation. The extremely small zones originating at room temperature are called GP I zones and do not grow any further during subsequent artificial aging, but actually re-dissolve in a short time at temperatures between 150°C to 200°C, leading to a temporary reduction in hardness. This regression refers to the arrangement of the strengthening atoms after artificial aging, which is different from the one occurring after natural aging. Artificial aging at elevated temperatures causes new enrichment of the Cu atoms in the GP II zones soon after the end of the reversion.

As the artificial aging continues at approximately 180°C - 220°C, the formation of the metastable phase, θ , takes place; this corresponds to the equilibrium phase, Al_2Cu , in composition, although it has a different crystal lattice. Maximum hardness may be obtained during the appearance of the GP II zones and also at times for a mixture of GP II, θ' and a mixture of $\text{S}' + \theta' + \beta''$ and precipitating Si. The β'' phase or β' phase, Mg_2Si , is found only as a very minor species.

Although a number of authors^[58,92,93] have reported that they observed the Q' phase, these precipitates have electron diffraction patterns which are very close to those of the β'' (or β') phase. Also, copper and excess silicon refine β'' precipitates, while Mg facilitates the formation of the θ' phase instead of θ'' .^[92,93]

As soon as only θ' particles are present, the stage of overaging has been attained, characterized by a reduction in hardness and strength. When aged for longer times, the equilibrium phase, Al_2Cu , forms a relatively coarse precipitate which is visible under the optical microscope.

The change of phase composition is known to affect the aging response and mechanical properties of the alloy. Impurities and small additions can affect the hardening behavior of Al-Si-Cu-Mg alloys to a considerable extent, mainly due to the binding of main alloying elements in the form of insoluble particles, thereby decreasing Cu and Mg content in the supersaturated solid solution.

5.10 FRACTOGRAPHY RESULTS AND DISCUSSION

5.10.1 Secondary Electron Beam Imaging (SEM Fractography)

Figure 5.17(a) shows the fracture surface of the D1 alloy sample obtained from the star-like mold near the side where crack initiation occurred and which consists mainly of long Si particles with cracks within their interiors. Decreasing the cooling rate results in the fracture characteristics shown in Figure 5.17(b), corresponding to LD1 alloy sample obtained from the L-shaped mold, which are similar to those shown in Figure 5.17(a). The only observable difference is the larger size of the cracked silicon particles. The high magnification micrograph of the LD1 alloy sample shown in Figure 5.17(c) reveals segments of fractured Al_2Cu phase particles.

Modification of the D1 alloy with Sr results in the DS1 alloy sample exhibiting a dimple structure, signifying the ductile nature of this alloy, as displayed in Figure 5.18(a). The arrows in this figure point to the presence of several secondary cracks. Figure 5.18(b) reveals the presence of a massive fractured phase particle (arrowed) near the center of the micrograph. The associated EDS spectrum, Figure 5.18(c), shows strong reflections of Al and Cu elements revealing that the massive particle observed in Figure 5.18(b) is Al_2Cu .

The LDS1 alloy shows similar fracture features, as will be clear from Figure 5.19.

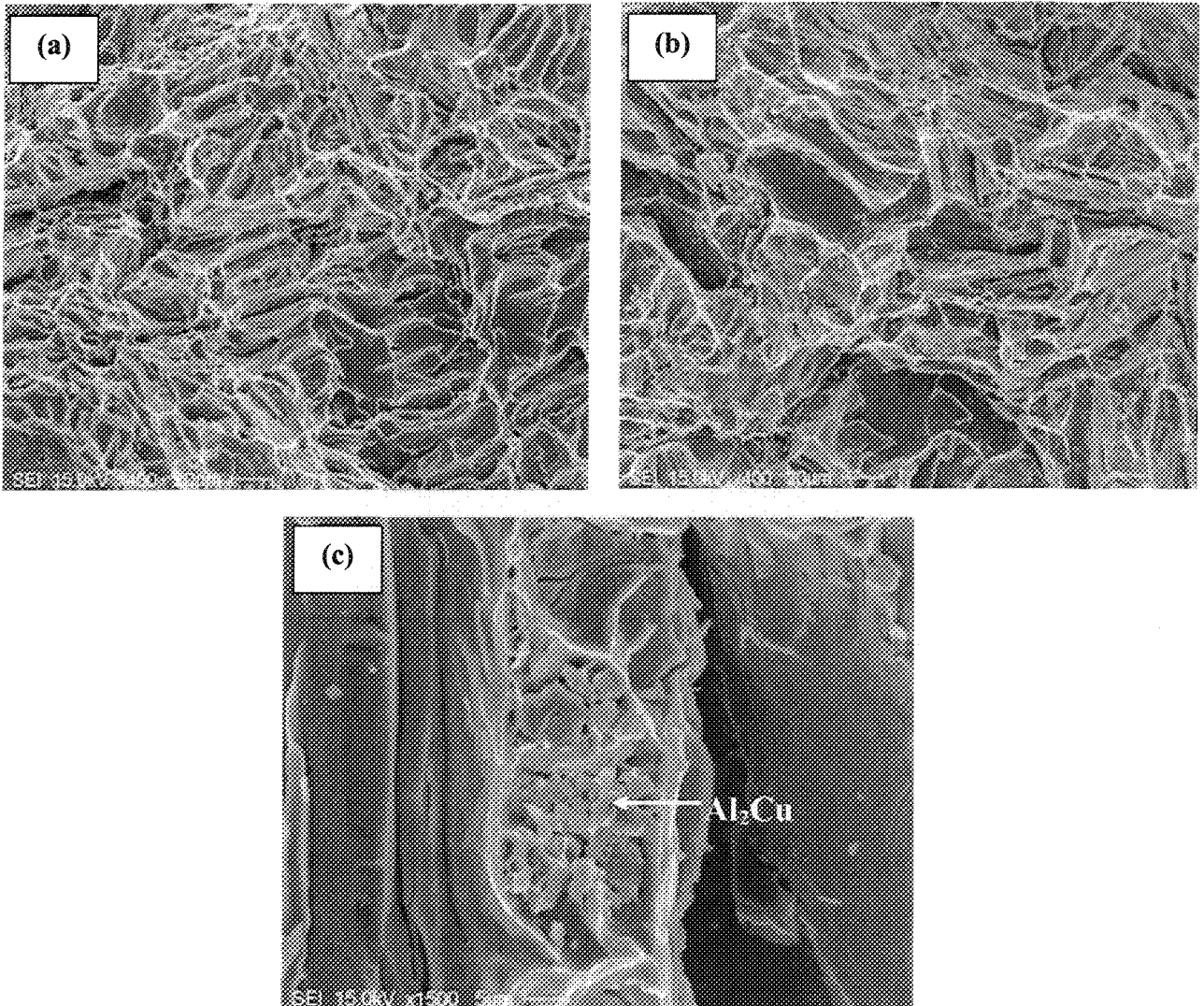


Figure 5.17 Fracture surface of : (a) D1 alloy, (b) LD1 alloy, and (c) LD1 alloy at high magnification.

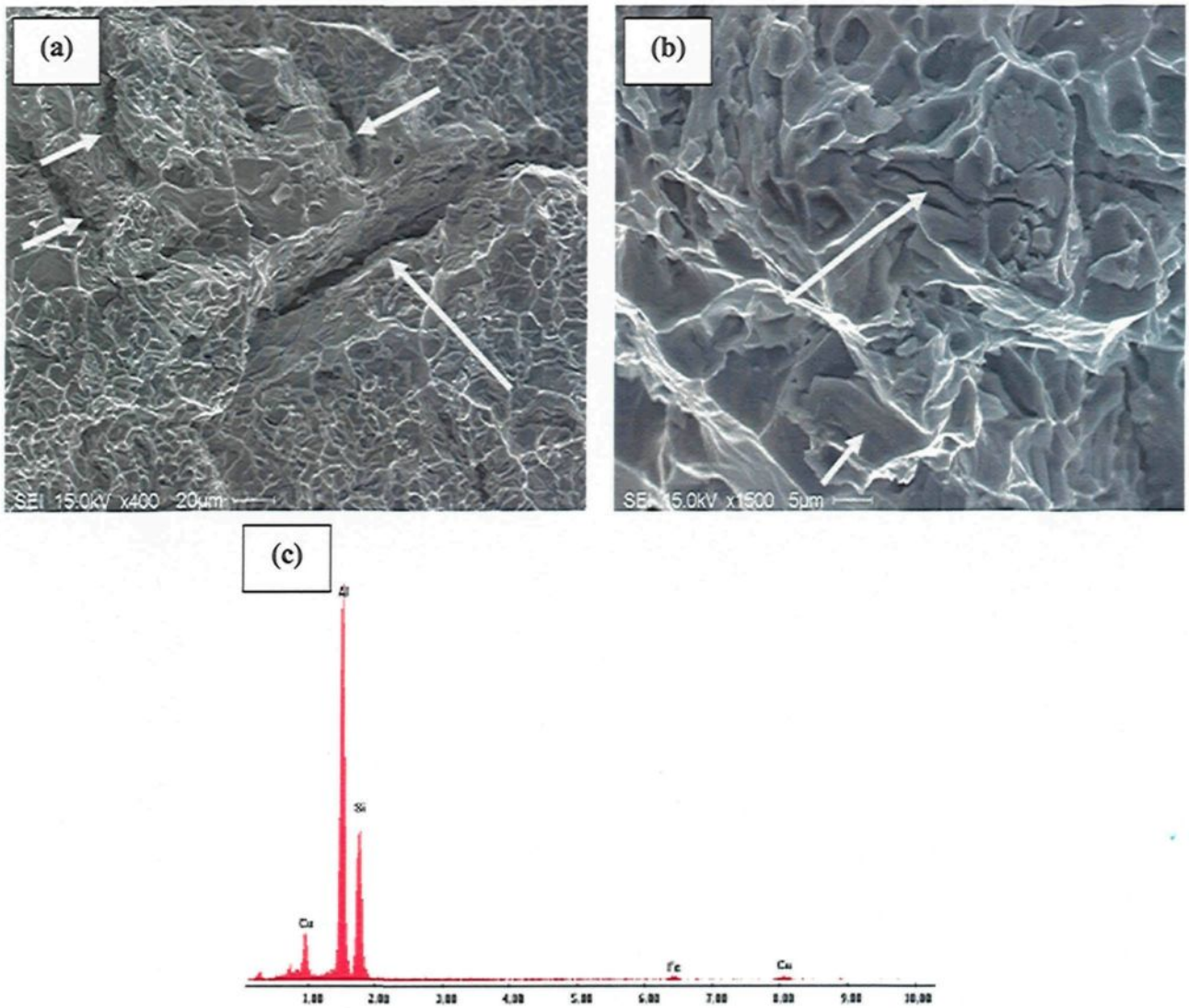


Figure 5.18 Fracture surface of DS1 alloy: (a) general view, (b) high magnification view, and (c) EDS spectrum corresponding to (b).

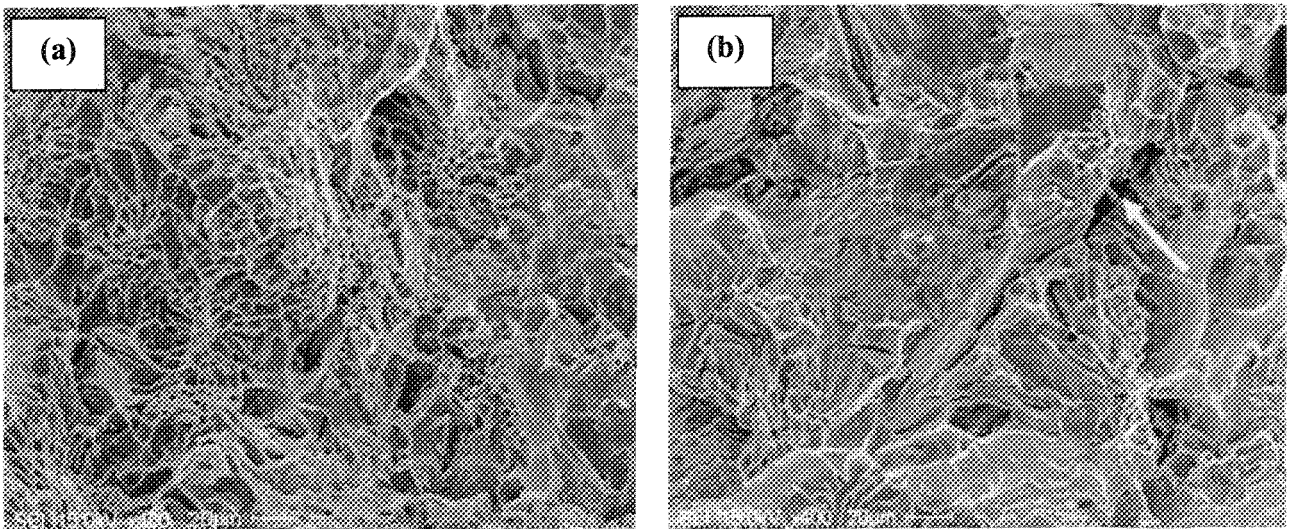


Figure 5.19 Fracture surface of LDS1 alloy showing: (a) crack initiation area, and (b) crack propagation across the sample surface. Note the presence of the secondary crack (arrowed) in (b).

The addition of 0.6% Mg to the D1 alloy (coded D6) results in the appearance of cleavage fracture in a number of places on the fracture surface of D6 alloy samples indicated by the arrows shown in Figure 5.20 (a) and (b). The high magnification micrograph presented in Figure 5.20(c) shows the fracture of an Al_2Cu particle into several parts as a result of crack propagation. It is interesting to note that decreasing the cooling rate of this alloy did not affect the appearance of a network of dimple structures, as may be seen from Figure 5.21(a) corresponding to the LD6 alloy sample; also, to be noted is the presence of a step-like fracture in the fractograph. Attention should also be drawn here to the cleavage-fracture observed in Figure 5.21(b) (arrowed). The propagation of the crack was associated with the fracture of the $\text{Q-Al}_5\text{Mg}_8\text{Cu}_2\text{Si}_6$ phase as shown in Figure 5.21(c).

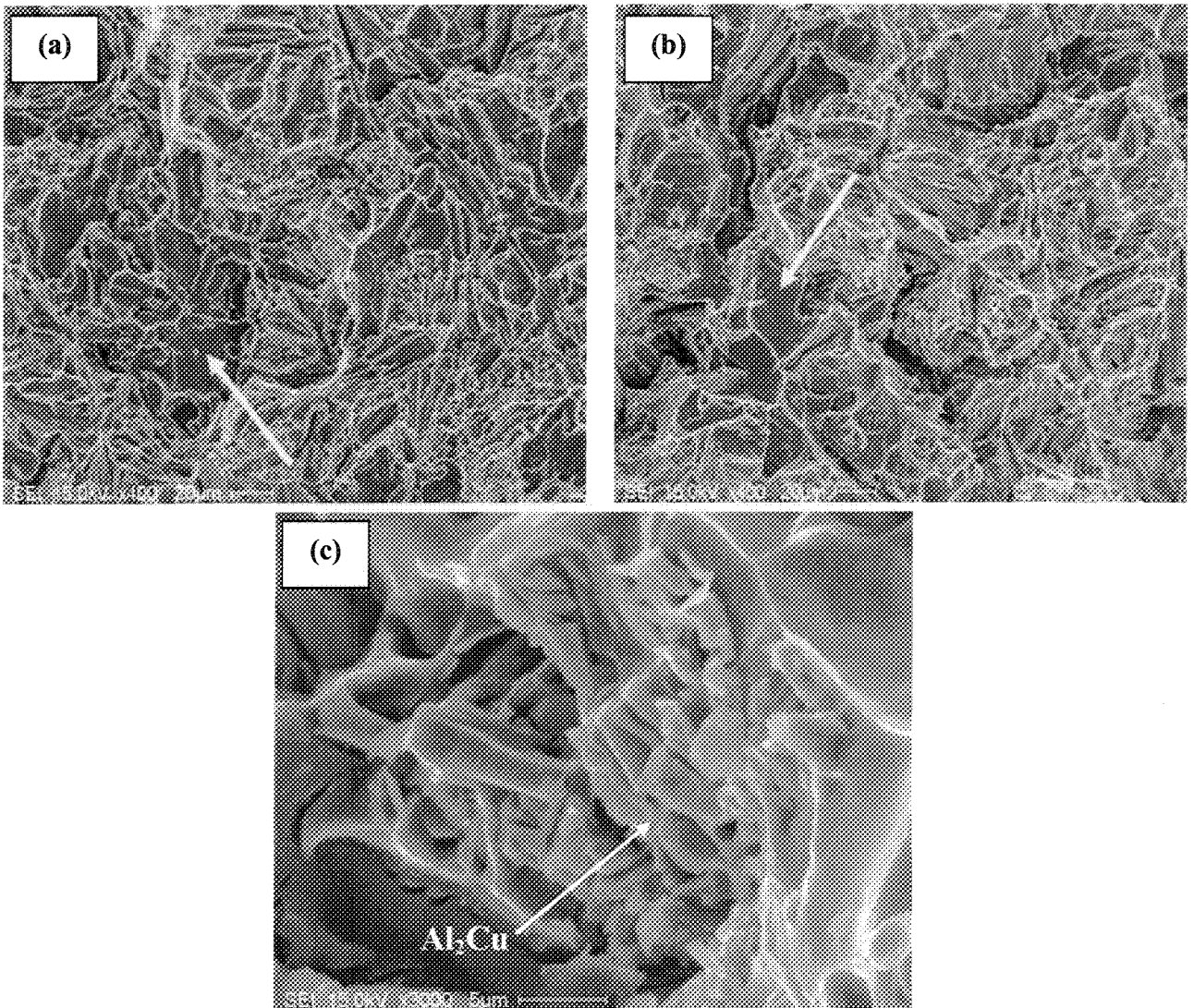


Figure 5.20 Fracture surfaces of D6 alloy showing: (a) crack initiation area, (b) crack propagation across the sample, and (c) fracture of an Al_2Cu particle.

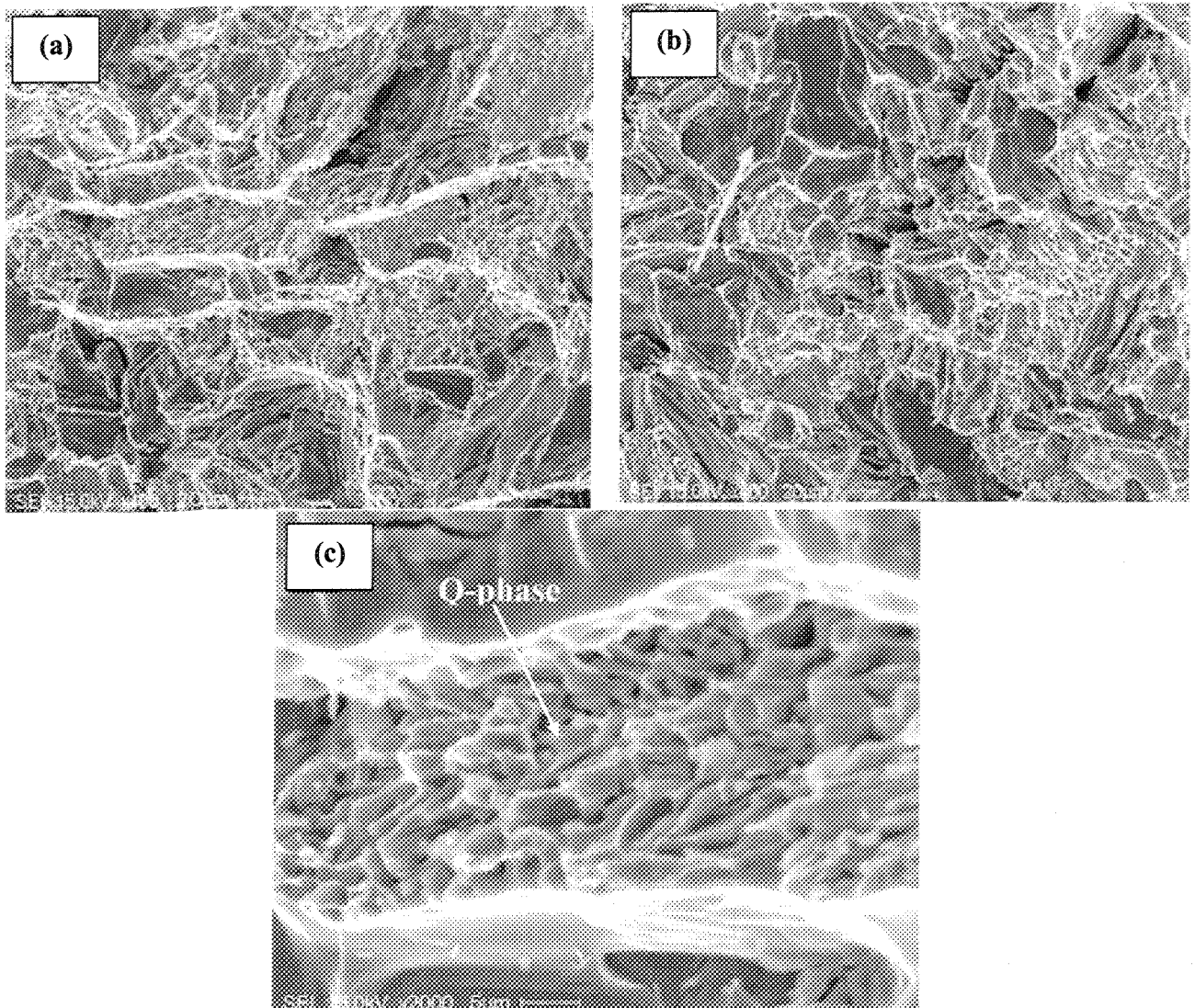


Figure 5.21 Fracture surface of LD6 alloy showing: (a) crack initiation area, (b) crack propagation across the sample, and (c) fracture of Q-phase.

Introduction of 200 ppm Sr to the D6 alloy (coded DS6) resulted in a uniform dimple structure throughout the fracture surface of the DS6 alloy sample shown in Figure 5.22(a). As in the previous cases, the crack propagates through the fracture of the precipitated intermetallics, mainly $Q\text{-Al}_5\text{Mg}_8\text{Cu}_2\text{Si}_6$ and $\pi\text{-Al}_8\text{Mg}_3\text{FeSi}_6$ as shown in Figure 5.22(b) and the corresponding EDS spectrum in Figure 5.22(c), where, the presence of the

Fe peak is also noted. Similar observations were made for the LDS6 alloy sample obtained at the low cooling rate i.e. the dimple structure shown in Figure 5.23(a), and frequent occurrence of fractured Q- $\text{Al}_5\text{Mg}_8\text{Cu}_2\text{Si}_6$, and π - $\text{Al}_8\text{Mg}_3\text{FeSi}_6$ phase particles, as shown in Figure 5.23(b) and confirmed by the associated EDS spectrum presented in Figure 5.23(c), exhibiting Cu and Fe peaks in addition to those of Al, Mg and Si.

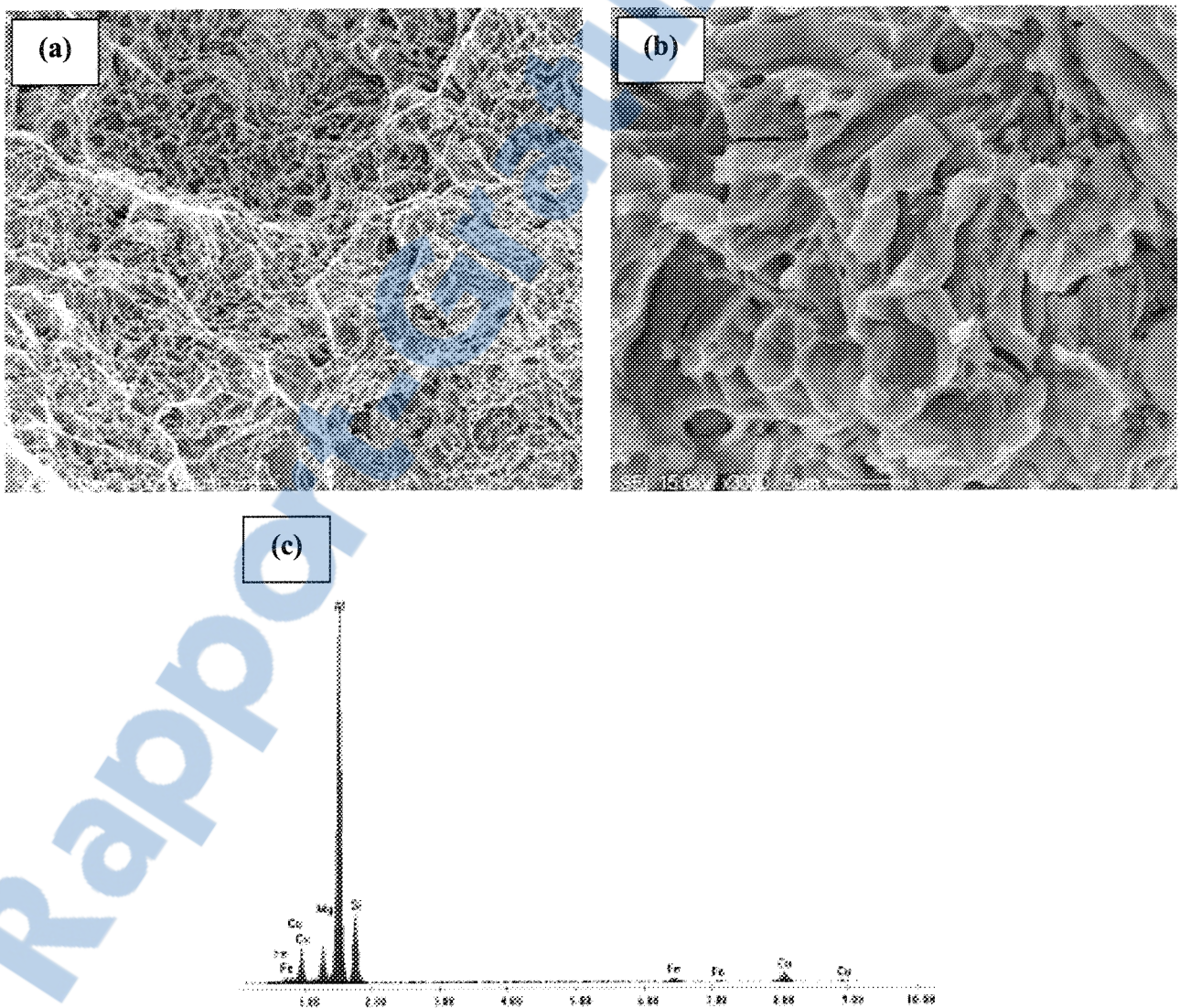


Figure 5.22 Fracture surface of D6 alloy showing: (a) crack initiation area, (b) fracture of Q-phase, and (c) EDS spectrum corresponding to (b).

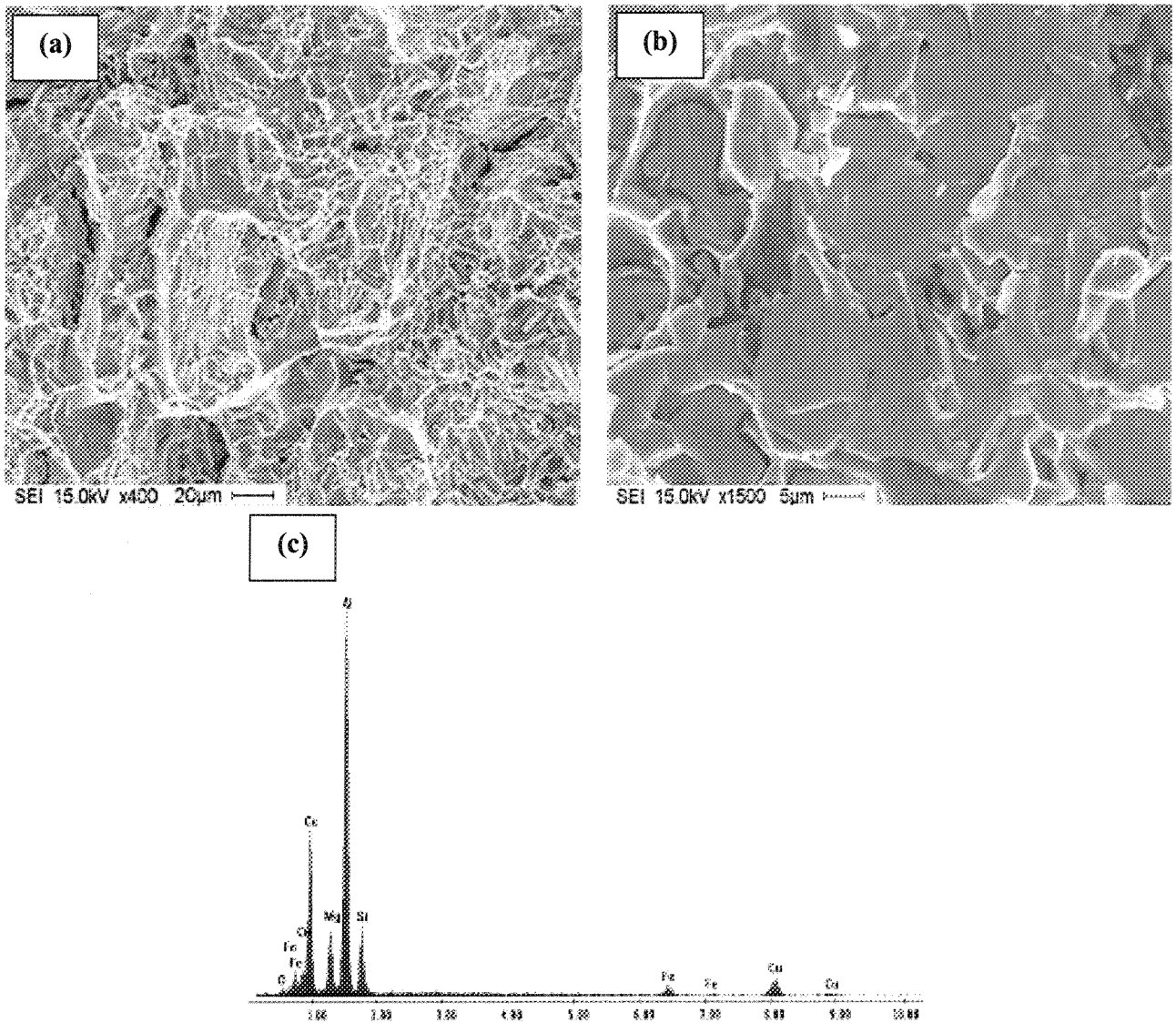


Figure 5.23 Fracture surface of LDS6 alloy showing: (a) crack initiation area, (b) fracture of a mixture of Q- and π - phase particles, and (c) EDS spectrum corresponding to (b).

Increasing the aging temperature from 180°C to 220°C, *i.e.* applying a T7 heat treatment, results mainly in the development of a dimple structure in non-modified alloys, as shown in Figure 5.24(a) and (b), and a relatively finer dimple size in Sr-modified alloys, as shown in Figure 5.24(c) and (d); this, however, caused significant changes to be

observed in the main fracture mechanism with respect to the cooling rate, compared to the features reported for the previous figures. Similar observations were also noted for high Mg containing T7-treated alloys, *i.e.* D6 and LDS6 alloys, as shown in Figure 5.25.

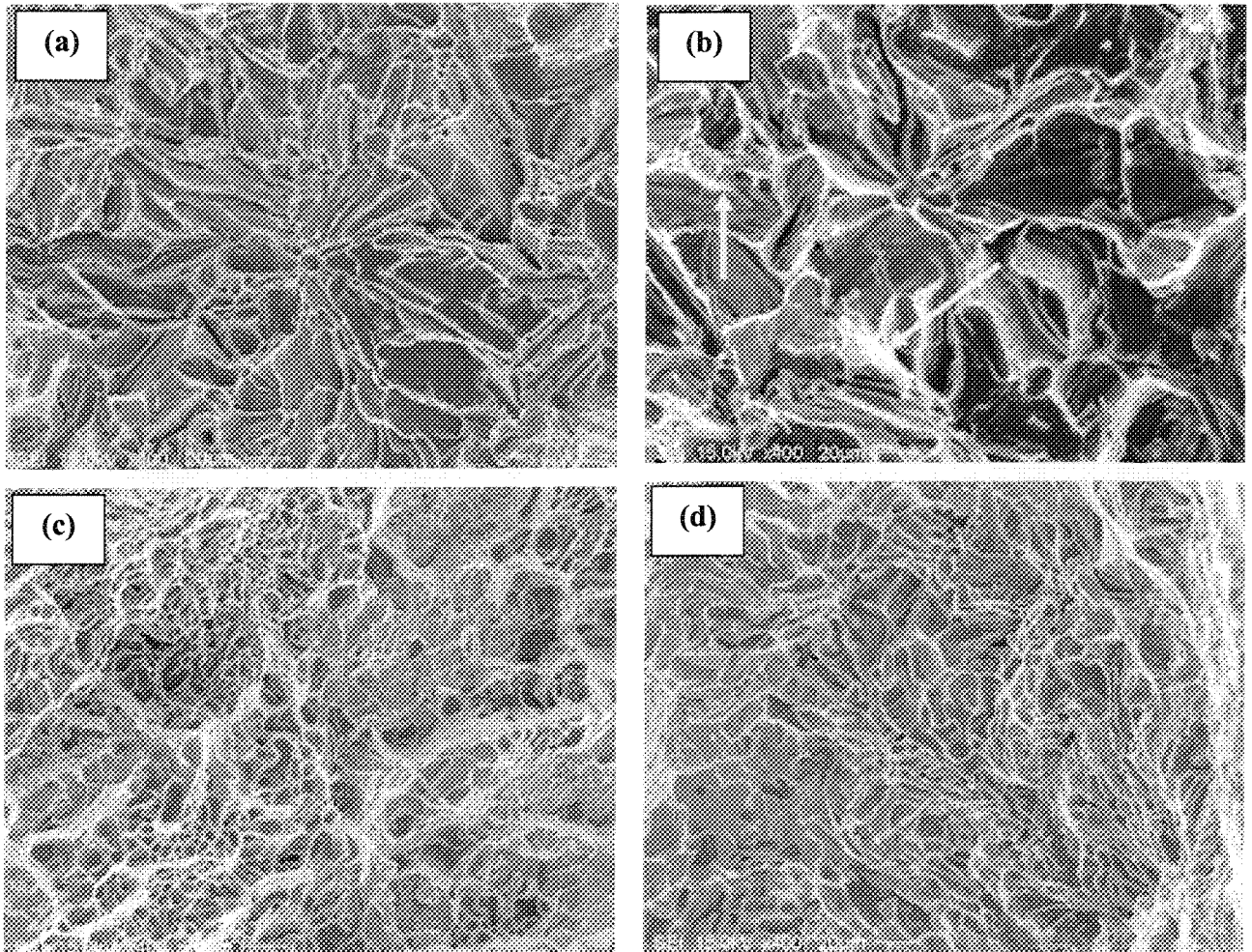


Figure 5.24 Fracture surfaces of T7-tempered alloys: (a) D1, (b) LD1, (c) DS1, and (d) LDS1 alloys.

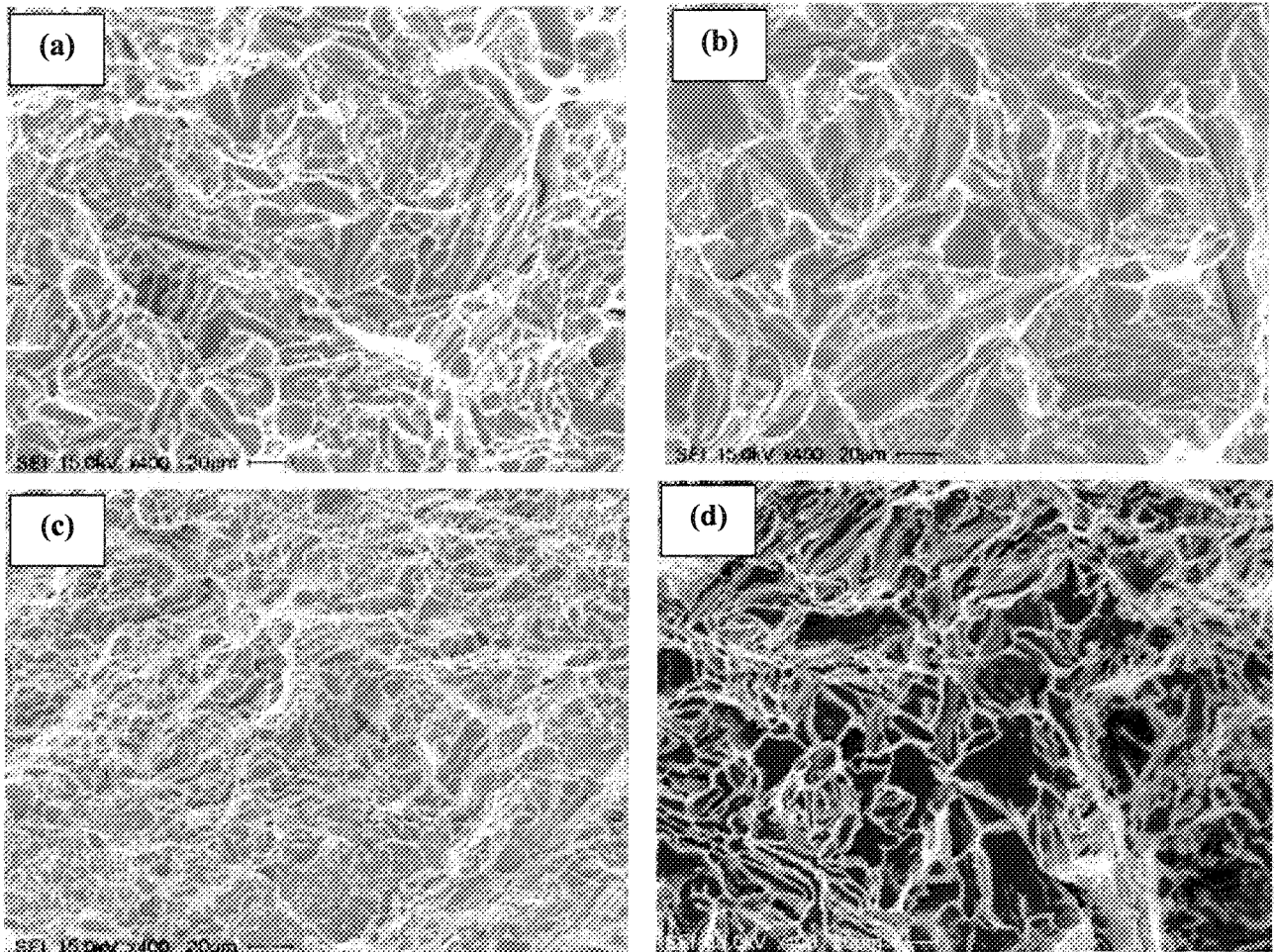


Figure 5.25 Fracture surfaces of T7-tempered alloys: (a) D6, (b) LD6, (c) DS6, and (d) LDS6 alloys. Note the difference in the size of Si particles in (a) and (b), corresponding to high and low cooling rates.

5.10.2 Backscattered Imaging

Figure 5.26(a) reveals scattered fractured particles of the Al_2Cu copper phase in the D1 alloy sample. The presence of an Fe peak in the corresponding EDS spectrum, shown in Figure 5.26(b), indicates that some of these particles could as well be the Al_7FeCu_2 phase. In the Sr-modified DS1 alloy sample, shown in Figure 5.27, large proportions of Al_2Cu were frequently observed on the fracture surface near the side where crack initiation

occurred because of the segregation effect of the Al_2Cu particles caused by the presence of Sr.

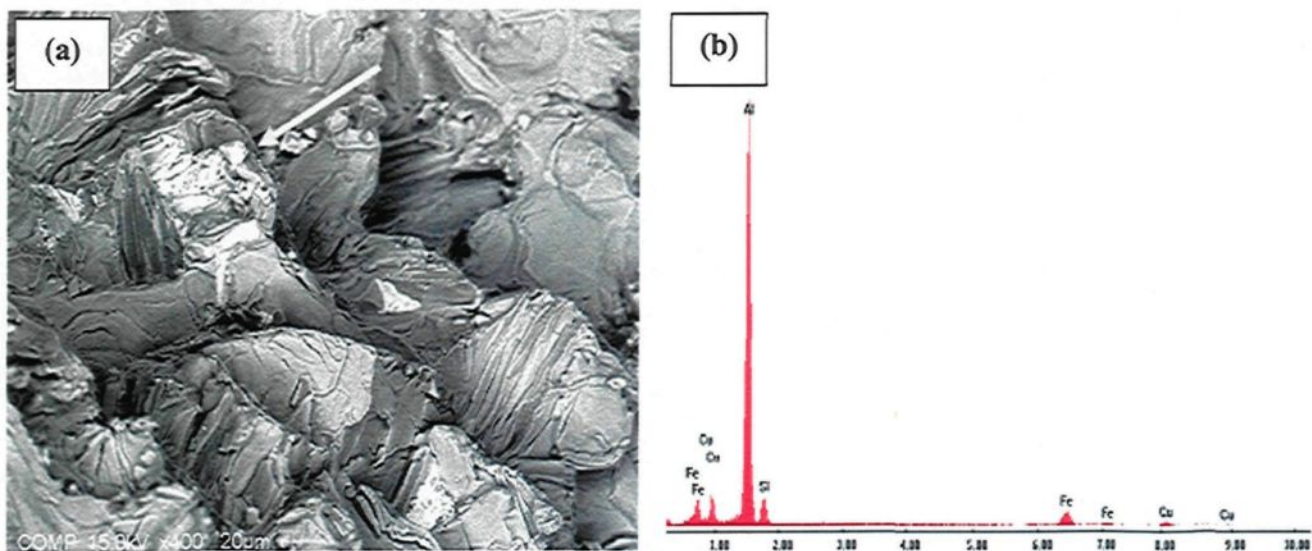


Figure 5.26 Backscattered image of the fracture surface of the D1 alloy sample: (a) general view; arrow points the presence of Al_2Cu particles, and (b) corresponding EDS spectrum.

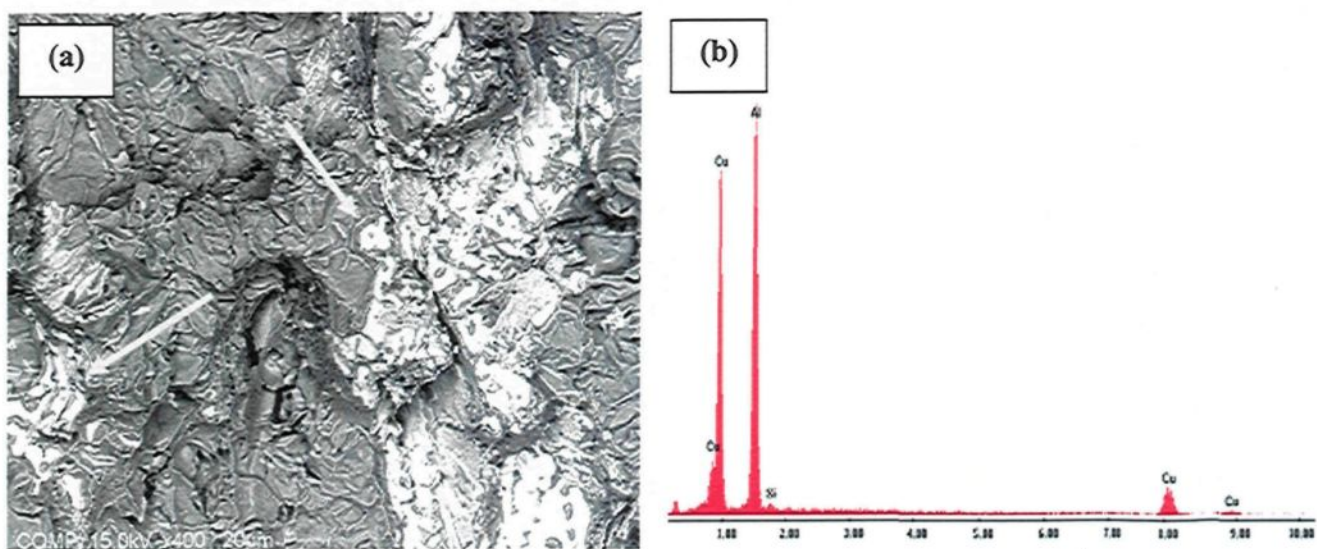


Figure 5.27 Backscattered image of the fracture surface of the DS1 alloy sample: (a) general view; arrows point to massive areas of Al_2Cu , and (b) corresponding EDS spectrum.

Increasing the Mg content to 0.6%, *i.e.* D6 alloy, led to the formation of the Q- $\text{Al}_5\text{Mg}_8\text{Cu}_2\text{Si}_6$ phase (light grey), in addition to the Al_2Cu phase (white), as shown in Figure 5.28. Modification of the D6 alloy by adding 200 ppm Sr leads to the formation of massive particles of Al_2Cu as shown in Figure 5.29(a), in addition to the $\pi\text{-Al}_8\text{Mg}_3\text{FeSi}_6$ phase, Figure 5.29(b), as is evident from the corresponding EDS spectra shown in Figure 5.29(c) and (d), respectively.

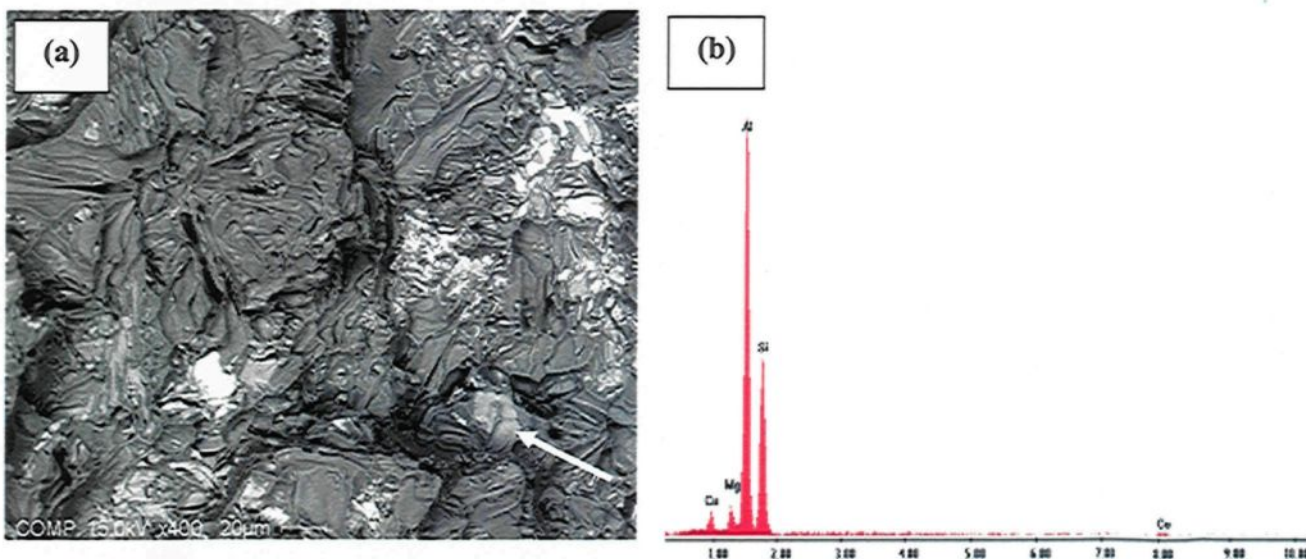


Figure 5.28 Backscattered image of the fracture surface of the D6 alloy sample: (a) general view, and (b) EDS spectrum of Q-phase particle (arrowed) observed in (a).

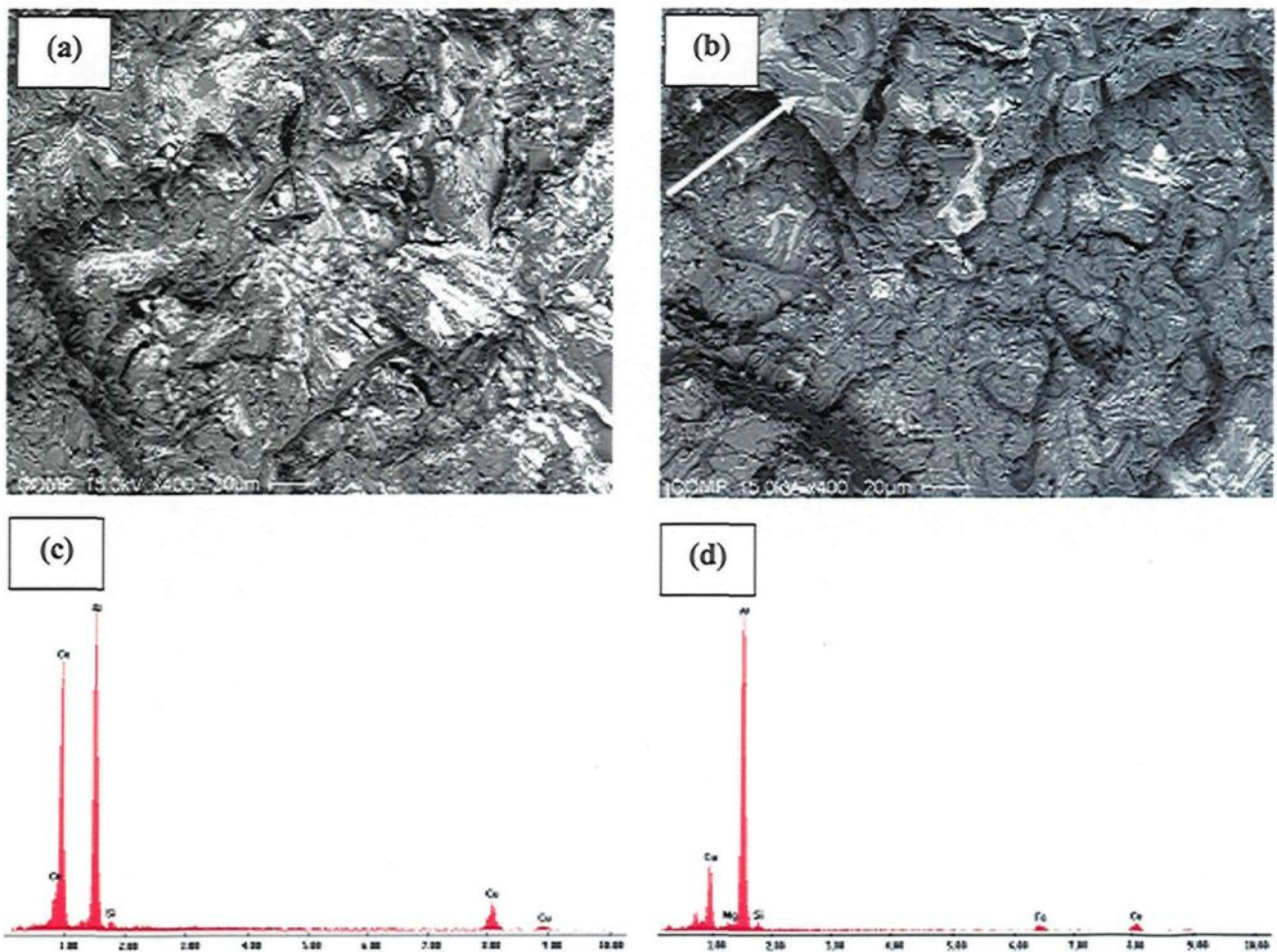


Figure 5.29 Backscattered images of the fracture surface of the DS6 alloy sample showing: (a) crack initiation area, (b) crack propagation; arrow shows the fracture of the π -phase, (c) EDS spectrum corresponding to (a), and (d) EDS spectrum corresponding to (b).

Decreasing the cooling rate of the D6 and DS6 alloys by using the L-shaped mold, results in the precipitation of coarse intermetallics in the LD6 and LDS6 alloy samples. Figure 5.30(a) shows the presence of β -Fe platelets which contributes to the crack formation, as indicated by the arrows. In the LDS6 alloy, shown in Figure 5.30(b), precipitation of the π - $\text{Al}_8\text{Mg}_3\text{FeSi}_6$ phase is clear from the indication of the solid arrow. The EDS spectrum shown in Figure 5.30(c) reveals the presence of undissolved Mg_2Si

particles, as indicated by the broken arrows.

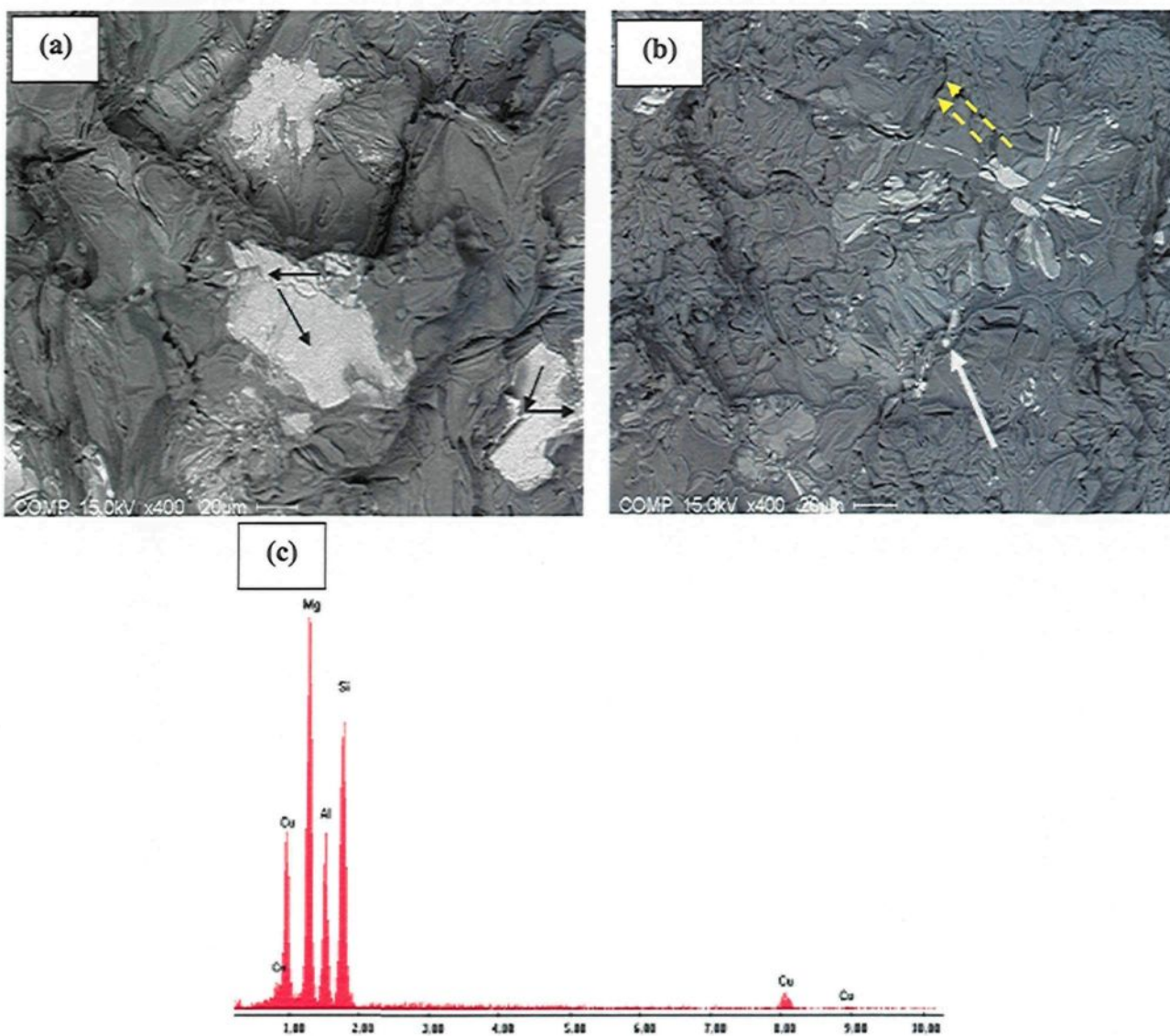


Figure 5.30 Backscattered images of the fracture surface of the: (a) LD6 alloy sample showing β -Fe platelets, (b) LDS6 alloy sample showing precipitation of π -phase (solid arrow) together with undissolved Mg_2Si (broken arrows), and (c) EDS spectrum corresponding to Mg_2Si .

The results and observations from the analysis of the fracture surfaces of 319 alloys, as investigated here, are in satisfactory agreement with the studies carried out by other researchers on Al-Si-Cu-Mg alloys.^[82,104,107,108,109,110,111]

CHAPTER 6
CONCLUSIONS

CHAPTER 6

CONCLUSIONS

This study was undertaken to investigate the effects of magnesium content and aging conditions on the impact toughness and hardness of 319-type Al-Si-Cu-Mg alloys in the as-cast and heat-treated conditions. Based on the results presented in Chapters 4 and 5, the following conclusions may be drawn.

1. The porosity parameters were greater in the industrial alloys than in the experimental alloys, in both the non-modified and Sr-modified conditions. These parameters increased greatly with Sr modification and the application of a low cooling rate in all alloys studied. When up to 0.6wt% Mg was added to the 319 alloys, both the area percent porosity and pore length increased noticeably.
2. Strontium modification increased the eutectic Si particle count per unit area in the as-cast condition, indicating a refinement of the microstructure; both the size and shape parameters of the eutectic Si particles were also affected. The addition of Sr also led to the segregation of the copper phase in areas away from the modified eutectic Si and at the dendrite boundaries, leading to the precipitation of the Al₂Cu phase in a block-like form, which, in turn, was more difficult to dissolve than the finer eutectic-like form of the phase.
3. The addition of Mg, especially at 0.6wt%, to the 319 alloys modified the Si particle morphology, as well as lowered the Al-Al₂Cu eutectic temperature, where this

temperature depression increased with further Mg additions. Additionally, Mg caused a segregation of the copper phases, which then led to the precipitation of the block-like Al_2Cu phase.

4. An increase in Mg content in the Sr-containing alloys resulted in an increase in the Si particle size (area, length, and aspect ratio) and a decrease in the roundness ratio. In effect, this diminished the modifying influence of Sr. The addition of Mg to the Fe-containing 319 alloys resulted in the precipitation of the Mg_2Si , Q- $\text{Al}_5\text{Mg}_8\text{Cu}_2\text{Si}_6$ and π - $\text{Al}_8\text{Mg}_3\text{FeSi}_6$ phases, where Q- and π -phases were in a script-like form rather than irregularly-shaped particles.
5. Magnesium slightly refined the Si phase and had a negative effect on Sr modification, as a change in the microstructure from a well modified one to a partially modified one was observed.
6. The eutectic Al_2Cu phase particles were nearly fully dissolved in the aluminum matrix after solution heat treatment in all alloys studied. Ultrafine Si particles could be noticed after dissolving the eutectic Al_2Cu particles. These small Si particles precipitated at the end of solidification. The block-like Al_2Cu , Q- $\text{Al}_5\text{Mg}_8\text{Cu}_2\text{Si}_6$, and α - $\text{FeAl}_{15}\text{Fe}_3\text{Si}_2$ intermetallics were insoluble, the plate-like β - FeAl_5FeSi and π - $\text{Al}_8\text{Mg}_3\text{FeSi}_6$ phases dissolved partially, and the Mg_2Si phase dissolved completely during solution heat treatment at $495^\circ\text{C}/8\text{hrs}$.
7. For the range of cooling rates used in the present study (corresponding to dendrite arm spacings of $24\ \mu\text{m}$ and $50\ \mu\text{m}$), the higher cooling rate ($24\ \mu\text{m DAS}$) was the

- dominant parameter in controlling the size and distribution of the Si particles, intermetallic phases and porosity in both the non-modified and Sr-modified alloys.
8. Magnesium and copper improved the hardness of the alloy samples tested, especially in the T6 heat-treated condition. The higher cooling rate also produced an increase in the hardness, especially for the non-modified Mg-containing alloys. However, the addition of Sr decreased the hardness of both the Mg-free and Mg-containing alloys, which most likely arose from a retardation of the Mg_2Si precipitation during the aging process for the Mg-containing alloys.
 9. The T7 heat-treated alloys displayed lower values of hardness and, consequently, higher values of impact toughness than those which were T6 heat-treated. In both T6 and T7 heat-treated conditions and for both the non-modified and Sr-modified alloys, the experimental alloys demonstrated higher values of hardness and impact energy than the industrial alloys.
 10. Aging of the Mg-containing 319 alloys at 180°C (T6 heat treatment conditions) as well as of the Mg-containing experimental 319 alloys at 220°C (T7 heat treatment conditions) produced a sharp rise in hardness during the first two hours of aging. At 180°C, this initial rise was then followed by a plateau from 2 to 12 hours, with a noticeable period of over-aging after 12 hours. At 220°C, this initial rise was followed by an aging peak, as well as a noticeable period of over-aging after 2 hours.
 11. Magnesium and copper decreased the impact toughness of the alloy samples tested, especially under T6 heat treatment conditions. The high cooling rate also displayed

an increase in the impact properties, especially for the non-modified Mg-containing alloys. The addition of Sr, however, decreased the toughness values of both the Mg-free and Mg-containing alloys. This decrease is most likely the result of a segregation of the block-like Al_2Cu phase.

12. Aging of the Mg-containing 319 alloys either at 180°C (T6 treatment) or at 220°C (T7 treatment) produced a sharp drop in impact toughness during the first two hours of aging. For both 180°C and 220°C, this initial drop was subsequently followed by a plateau occurring between 2 and 24 hours, with a noticeable period of over-aging beyond 24 hours.
13. The impact properties of 319 alloys are influenced by the microstructure which depends strongly on the solidification conditions and alloy composition. High cooling rates improve the impact toughness of both the experimental and industrial alloys investigated. The presence of copper significantly lowers the impact properties which are determined mainly by the Al_2Cu phase and not by the eutectic Si particles.
14. Increasing the Mg content produces intermetallic phases which cause a noticeable deterioration of the impact properties; Mg also leads to the segregation of Al_2Cu in a brittle block-like form thereby decreasing alloy toughness, particularly for Sr-modified alloys, although the addition of Mg enhances the response of the alloy to artificial aging.
15. A greater part of the total absorbed energy is used for crack initiation, *i.e.* crack initiation energy is greater than crack propagation energy, reflecting the high

ductility of the 319 alloys investigated. This ductility may be enhanced by alloy homogeneity and such strengthening intermetallic phases as Mg_2Si , Al_2CuMg , and $Q-Al_5Mg_8Cu_2Si_6$. The alloy homogeneity may be increased by eutectic Al_2Cu .

16. The fracture surfaces of non-modified alloys consisted of long Si particles with cracks at their interiors. Addition of Sr resulted in a dimple structure throughout the matrix. Increasing the Mg content up to 0.6% resulted in the appearance of fractured particles of $Q-Al_5Mg_8Cu_2Si_6$ and $\pi-Al_8Mg_3FeSi_6$ phases. Decreasing the cooling rate or increasing the aging temperature did not alter the fracture mechanism with respect to the alloy composition.
17. The tendency of Sr to segregate the Al_2Cu phase away from Al-Si eutectic regions causes sluggishness of the dissolution of Al_2Cu during solution heat treatment. The presence of relatively large proportions of undissolved Al_2Cu compromise the beneficial effect of the soft Al matrix, leading to lower toughness.

RECOMMENDATIONS FOR FUTURE WORK

In order to arrive at a complete understanding of the effects of Mg addition, cooling rate, and aging conditions studied in the present work on the performance of 319 alloys, the following may be suggested:

1. Carrying out a study on tensile testing using test bars prepared from experimental and commercial alloys, using different permanent molds to obtain the required cooling rate.
2. Studying the effects of reducing the copper content from the traditional 3.5% in 319 alloys to 2% in order to minimize the amount of undissolved Al_2Cu during solution heat treatment, and thereby improve the mechanical properties of the alloy (tensile and impact toughness).
3. Controlling the segregation of the Al_2Cu phase which causes a deterioration in alloy toughness by regulating the amount of Sr added to the alloy.

REFERENCES

- [1] J.E. Gruzleski and B.M. Closset, "The Treatment of Liquid Aluminum-Silicon Alloys," American Foundrymen's Society, Inc., Des Plaines, IL, 1990.
- [2] J.R. Davis, ASM Special Handbook, "Aluminum and Aluminum Alloys," ASM International, The Materials Information Society, Materials Park, OH, 1994, pp. 1-30.
- [3] Jerry H. Sokolowski, Mile B. Djurdjevic, Christopher A. Kierkus, and Derek O. Northwood, "Improvement of 319 Aluminum Alloy Casting Durability by High Temperature Solution Treatment," *Journal of Materials Processing Technology*, 2001, Vol. 109, pp. 174-180.
- [4] Jerry H. Sokolowski, X-C. Sun, G. Byczynski, D.E. Penord, R. Thomas, and A. Esseltine, "The Removal of Copper-Phase Segregation and the Subsequent Improvement in Mechanical Properties of Cast 319 Aluminum Alloys by a Two-Stage Solution Heat-Treatment," *Journal of Materials Processing Technology*, 1995, Vol. 53, pp. 385-392.
- [5] J.L. Jorstad, "Hypereutectic Al-Si Casting Alloys: 25 Years, What's Next?," Silver Anniversary Paper, AFS Transactions, Vol. 104, 1996, pp. 669-671.
- [6] F. Paray and J.E. Gruzleski, "Factors to Consider in Modification," AFS Transactions, Vol. 102, 1994, pp. 833-842.
- [7] L. Bäckerud, G. Chai and J. Tamminen, "Solidification Characteristics of Aluminum Alloys," Vol. 2: Foundry Alloys, AFS/Skanaluminium, Des Plaines, IL, 1990, pp. 71-84.
- [8] J.E. Hatch (Ed.), "Aluminum: Properties and Physical Metallurgy", American Society for Metals, Metals Park, OH, 1984, pp. 320-350.
- [9] D.O. Northwood, X-C. Sun, G.E. Byczynski and J.H. Sokolowski, "A Metallurgical Study of the Heat Treatment of Aluminum Alloy 319 (Al-6Si-3.5Cu) Castings," Proceedings of the International Symposium on Recent Metallurgical Advances in Light Metals Industries, 34th Annual Conference of Metallurgists of CIM, Vancouver, British Columbia, August 20-24, 1995, pp. 355-365.
- [10] J.E. Davis (Ed.), "Aluminum and Aluminum Alloys," ASM Specialty Handbook,

ASM International, Materials Park, OH, 1993.

- [11] H. Baker, "Alloy Phase Diagrams," ASM Handbook, Vol. 3, ASM International, Materials Park, OH, 1992, pp. 2-86.
- [12] A.M. Samuel and F.H. Samuel, "Modification of Iron Intermetallics by Magnesium and Strontium in Al-Si Alloys," International Journal of Cast Metals Research, Vol. 10, 1997, pp. 147-157.
- [13] M.F. Hafiz and T. Kobayashi, "A Study on the Microstructure-Fracture Behavior Relations in Al-Si Casting Alloys," Scripta Metallurgica et Materialia, Vol. 30, 1994, pp. 475-480.
- [14] E.N. Pan, Y.C. Cherng, C.A. Lin, and H.S. Chiou, "Roles of Sr and Sb on Silicon Modification of A356 Aluminum Alloys," AFS Transactions, Vol. 102, 1994, pp. 609-629.
- [15] D. Apelian, G.K. Sigworth, and K.R. Whaler, "Assessment of Grain Refining and Modification of Al-Si Foundry Alloys by Thermal Analysis," AFS Transactions, Vol. 92, 1984, pp. 297-307.
- [16] Pacz Aladar, United States Patent 1,387,900 (August 16, 1921).
- [17] L.M. Hogan and M. Shamsuzzoha, "Crystallography of the Flake-Fibre Transition in the Al-Si Eutectic," Materials Forum, Vol. 10, 1987, pp. 270-277.
- [18] S.Z. Lu and A. Hellawell, "The Mechanism of Silicon Modification in Aluminum-Silicon Alloys: Impurity Induced Twinning," Metallurgical Transactions, Vol. 18A, 1987, pp. 1721-1733.
- [19] P.D. Hess and E.V. Blackmun, "Strontium as a Modifying Agent for Hypoeutectic Aluminum Silicon Alloys," AFS Transactions, Vol. 83, 1975, pp. 87-90.
- [20] M. Garat, G. Laslaz, S. Jacob, P. Meyer, P.H. Guerin, and R. Adam, "State of the Art of the Use of Antimony, Sodium, and Strontium-Modified Aluminum Silicon Casting Alloys," AFS Transactions, Vol. 100, 1992, pp. 549-562.
- [21] C.B. Kim and R.W. Heine, "Fundamentals of Modification in the Aluminum-Silicon System," Journal of the Institute of Metals, Vol. 92, 1964, pp. 367-376.
- [22] J. Gobrecht, "The Influence of Alloying Elements on the Duration of Modification of Na and Sr in Al-Si Cast Alloys," Giesserei, Vol. 65, 1975, pp. 87-90.
- [23] J.E. Gruzleski, M. Pekguleryuz, and B. Closset, "Strontium Addition to Al-Si Alloy

- Melts,” in Proceedings of the Third International Solidification Conference, Institute of Metals, Sheffield, UK, September 1987, pp. 52-54.
- [24] G-Q. Wang, X-F. Bian, W-M. Wang, and J-Y. Zhang, “Influence of Cu and Minor Elements on the Solution Treatment of Al-Si-Cu-Mg Cast Alloys,” *Materials Letters*, Vol. 57, Issues 24-25, August 2003. pp. 4083-4087.
- [25] L. Heusler and W. Schneider, “Influence of Alloying Elements on the Thermal Analysis Results of Al-Si Cast Alloys,” *Journal of Light Metals*, Vol. 2, 2002, pp. 17-26.
- [26] Jerry H. Sokolowski, Mile B. Djurdjevic, Christopher A. Kierkus, and Derek O. Northwood, “Improvement of 319 Aluminum Alloy Casting Durability by High Temperature Solution Treatment,” *Journal of Materials Processing Technology*, Vol. 109, Issues 1-2, 1 February 2001, pp. 174-180.
- [27] N. Crowell and S. Shivkumar, “Solution Treatment Effects in Cast Al-Si-Cu Alloys,” *AFS Transactions*, Vol. 103, 1995, pp.721-726.
- [28] M. Djurdjevic, T. Stockwell, and J. Sokolowski, “The Effect of Strontium on the Microstructure of the Aluminium-Silicon and Aluminium-Copper Eutectics in the 319 Alloys,” *International Journal of Cast Metals Research*, Vol. 12 (2), 1999, pp. 67-73.
- [29] G. Sigworth, “Theoretical and Practical Aspects of the Modification of Al-Si Alloys,” *AFS Transactions*, Vol. 91, 1983, pp. 7-16.
- [30] F.H. Samuel, P. Ouellet, A.M. Samuel, and H.W. Doty, “Effect of Mg and Sr Additions on the Formation of Intermetallics in Al-6 Wt Pct Si-3.5 Wt Pct Cu-(0.45) to (0.8) Wt Pct Fe 319-Type Alloys,” *Metallurgical and Materials Transactions A*, Vol. 29A, 1998, pp. 2871-2884.
- [31] H. de la Sablonnière and F.H. Samuel, “Solution Heat Treatment of 319 Aluminium Alloy Containing ~ 0.5 wt% Mg,” *International Journal of Cast Metals Research*, Vol. 9, 1996, pp. 151-225.
- [32] F.H. Samuel, “Incipient Melting of $Al_5Mg_8Si_6Cu_2$ and Al_2Cu Intermetallics in Unmodified and Strontium-Modified Al-Si-Cu-Mg (319) Alloys During Solution Heat Treatment,” *Journal of Materials Science*, Vol. 33, 1998, pp. 2283-2297.
- [33] L. Bäckerud, G. Chai, and J. Tamminen, “Solidification Characteristics of Aluminium Alloys,” Vol. 2: Foundry Alloys, AFS/Skanaluminium, Des Plaines, IL, USA, 1990, pp. 71-84.

- [34] Z. Li, A.M. Samuel, F.H. Samuel, C. Ravindran, S. Valtierra, and H.W. Doty, "Factors Affecting Dissolution of Al₂Cu Phase in 319 Alloys," AFS Transactions, Vol. 111, 2003, Paper 03-100, pp. 1-14.
- [35] F.H. Samuel, A.M. Samuel, and H.W. Doty, "Factors Controlling the Type and Morphology of Cu-Containing Phases in 319 Al Alloy," AFS Transactions, Vol. 104, 1996, pp. 893-901.
- [36] Z. Li, "Parameters Controlling the Precipitation and Dissolution of Al₂Cu Phase in 319 Alloys and Their Influence on the Alloy Performance," Master's Thesis, Université du Québec à Chicoutimi, Chicoutimi, Canada, 2003.
- [37] L.F. Mondolfo, "Manganese in Aluminum Alloys," The Manganese Center, Neuilly-sur-Seine, France, 1990, pp. 1-35.
- [38] W. Bonfield and B.K. Dutta, "Precipitation Hardening in an Al-Cu-Si-Mg Alloy at 130 to 220° C," Journal of Materials Science, Vol. 11, 1976, pp. 1661-1666.
- [39] J. Gauthier, P.R. Louchez, and F.H. Samuel, "Heat Treatment of 319.2 Aluminium Automotive Alloy: Part 1, Solution Heat Treatment," Cast Metals, Vol. 8, 1994, pp. 91-114.
- [40] J. Gauthier, P.R. Louchez, and F.H. Samuel, "Heat Treatment of 319.2 Aluminium Automotive Alloy: Part 2, Aging Behavior," Cast Metals, Vol. 8, 1995, pp. 107-114.
- [41] Jerry H. Sokolowski, X-C. Sun, G. Byczynski, D.E. Penrod, R. Thomas, and A. Esseltine, "The Removal of Copper-Phase Segregation and the Subsequent Improvement in Mechanical Properties of Cast 319 Aluminum Alloys by a Two-Stage Solution Heat Treatment," Journal of Materials Processing Technology, Vol. 53, 1995, pp. 385-392.
- [42] J.E. Hatch (Ed.), "Aluminum: Properties and Physical Metallurgy," American Society for Metals, Metals Park, OH, 1984, p. 157.
- [43] S. Shivkumar, C. Keller, and D. Apelian, "Aging Behavior in Cast Al-Si-Mg Alloys," AFS Transactions, Vol. 98, 1990, pp. 905-911.
- [44] A.M.A. Mohamed, F.H. Samuel, A.M. Samuel, and H.W. Doty, "Influence of Additives on the Microstructure and Tensile Properties of Near-eutectic Al-10.8%Si Cast Alloy," Journal of Materials and Design, 2009, pp. 3943-3957.
- [45] A.M. Samuel and F.H. Samuel, "Review: Various Aspects Involved in the

- Production of Low Hydrogen Aluminum Castings," *Journal of Materials Science*, Vol. 27, 1992, pp. 6533-6563.
- [46] J. Campbell, "The Solidification of Metals," Iron and Steel Institute, Publication No. 110, London, 1967, pp. 18-26.
- [47] K. Kubo and R.D Pehlke, "Mathematical Modeling of Porosity Formation in Solidification," *Metallurgical Transactions B*, Vol. 16B, 1985, pp. 359-366.
- [48] M. Tsukuda and S. Koike, "The Heat Treatment of Al-7%Si-0.3%Mg Alloy," *Journal of Japan Institute of Light Metals (in Japanese)*, 1978, Vol. 28(3), pp. 109-115.
- [49] O. Vorren, J.E. Evensen, and T.B. Pederson, "Microstructure and Mechanical Properties of AlSi(Mg) Casting Alloys," *AFS Transactions*, 1984, Vol. 93, pp. 459-466.
- [50] J. Espinoza-Cuadra, G. Garcia-Garcia, and H. Mancha-Molinar, "Influence of Defects on Strength of Industrial Aluminum Alloy Al-Si-Cu 319," *Materials and Design*, 2007, Vol. 28, pp. 1038-1044.
- [51] B. Closset and J.E. Gruzleski, "Structure and Properties of Hypoeutectic Al-Si-Mg Alloys Modified with Pure Strontium," *Metallurgical Transactions A*, 1982, Vol. 13, pp. 945-951.
- [52] B. Closset and J.E. Gruzleski, "A Study on the Use of Pure Metallic Strontium in the Modification of Al-Si Alloys," *AFS Transactions*, 1981, Vol. 89, pp. 801-808.
- [53] N. Roy, A.M. Samuel, and F.H. Samuel, "Porosity Formation in Al-9%Si-3%Cu Alloy Systems: Metallographic Observations," *Metallurgical and Material Transactions A*, 1996, Vol. 27, pp. 415-429.
- [54] N. Roy, L. Zhang, P.R. Louchez, and F.H. Samuel, "Porosity Formation in Al-9%Si-3%Cu-X Alloy Systems: Measurements of Porosity," *Journal of Materials Science*, 1996, Vol. 31, pp. 1243-1254.
- [55] Y. Awano and Y. Shimizu, "Non-equilibrium Crystallization of AlFeSi Compound in Melt-Superheated Al-Si Alloy Castings," *AFS Transactions*, 1990, Vol. 98, pp. 889-895.
- [56] M.M. Haque, "Strontium Modification of Aluminum-Silicon Eutectic Alloy and the Factors Affecting It," *Metals Forum*, 1983, Vol. 6(1), pp. 54-56.
- [57] M. Garat and R. Scalliet, "A Review of Recent French Casting Alloy

- Developments,” AFS Transactions, 1978, Vol. 86, pp. 549-562.
- [58] R.X. Li, R.D. Li, Y.H. Zhao, L.Z. He, Li, H. Guan, and Z. Hu, “Age-Hardening Behavior of Cast Al-Si Base Alloy,” *Materials Letters*, 2004, Vol. 58, pp. 2096-2101.
- [59] A.M.A. Mohamed, “Effect of Additives on the Microstructure and Mechanical Properties of Al-Si Alloys,” Ph.D. Thesis, Université du Québec à Chicoutimi, Chicoutimi, Canada, 2008, pp. 26-37.
- [60] <http://www.bikepro.com/products/metals/hardness.html>
- [61] <http://www.wargamer.org/GvA/background/hardness1.html>
- [62] N. Komatsu, M. Nakamura, and Y. Yamamoto, “Relationship between Si Crystallized Form and Impact Strength of Al-Si Alloys, Observations of Impact Strength of Al-Si Alloys,” *Japanese Journal of Light Metals*, 1997/1998, Vol. 43, pp. 398-408.
- [63] G.E. Dieter, Jr., “Mechanical Metallurgy,” 2nd edition, Metallurgy and Metallurgical Engineering Series, McGraw-Hill, New York, 1976.
- [64] R.A. Wullaert, “Application of the Instrumented Charpy Impact Test,” *Impact Testing of Metals*, ASTM-STP 466, American Society for Testing and Materials, 1970, pp. 148-164.
- [65] N. Komatsu, M. Nakamura, and Y. Yamamoto, “Metallurgical Structure and Impact Strength of Al-Si Alloys,” Technical Report of Toyota RD Center (in Japanese), TR-11, 1975, pp. 1-46.
- [66] F. Paray, B. Kulunk, and J. E. Gruzleski, “Impact Properties of Al-Si Foundry Alloys,” *International Journal of Cast Metals Research*, Vol. 13, 2000, Issue 1, pp. 17-37.
- [67] S. Hotta, K. Saruki, and M. Nakamura, “Effects of T6 Heat Treatment on the Impact Strength of AC4C and AC2B Aluminum Alloy Castings Solidified for a Long Time,” *Journal of Japan Institute of Light Metals* (in Japanese), Vol. 37, No. 7, July 1987, pp. 478-482.
- [68] E. Kato, Y. Ueda, and A. Matumoto, “Effect of Various Modification Elements on Fatigue and Impact Properties of Al-Si System Casting Alloys,” *Journal of the Japan Foundrymen 's Society* (in Japanese), Vol. 63, No. 4, 1990, pp. 283-288.

- [69] M. Tsukuda, S. Koike, and M. Harada, "The Heat Treatment of Al-7%Si-0.3Mg Alloy," *Journal of Japan Institute of Light Metals (in Japanese)*, Vol. 28, No. 1, pp. 8-14.
- [70] M. Richard, "La résilience des alliages d'aluminium moulés," *Fonderie*, Vol. 404, December 1980, pp. 397-400.
- [71] ASTM Designation: E23-94b, "Standard Test Methods for Notched Bar Impact Testing for Metallic Materials," *ASTM Standards*, Vol. 03.01, pp. 137-157.
- [72] S. Shivkumar, L. Wang, and C. Keller, "Impact Properties of Al-Si-Cu Alloys," *Zeitschrift für Metallkunde*, Vol. 85, No. 6, 1994, pp. 394-399.
- [73] S. Shivkumar, L. Wang, and C. Keller, "Impact Properties of A356-T6 Alloys," *Journal of Materials Engineering and Performance*, Vol. 3, February 1994, pp. 83-90.
- [74] D. Apelian, "Aluminum Cast Alloys: Enabling Tools for Improved Performance," *Worldwide Report, NADCA*, Wheeling, Illinois, 2009, p. 59.
- [75] A.T. Joenoes and J.E. Gruzleski, "Magnesium Effects on the Microstructure of Unmodified and Modified Al-Si Alloys," *Cast Metals*, 1991, Vol. 4, No. 2, pp. 62-71.
- [76] A.M. Samuel, P. Ouellet, F.H. Samuel, and H.W. Doty, "Microstructural Interpretation of Thermal Analysis of Commercial 319 Al Alloy with Mg and Sr Additions," *AFS Transactions*, 1997, Vol. 105, pp. 951-962.
- [77] A.M. Samuel and F.H. Samuel, "Porosity Factor in Quality Aluminum Castings," *AFS Transactions*, Vol. 100, 1992, pp. 657-666.
- [78] D. Yang, "Role of Magnesium Addition on the Occurrence of Incipient Melting in Experimental and Commercial Al-Si-Cu Alloys and its Influence on the Alloy Microstructure and Tensile Properties," *Master's Thesis, Université du Québec à Chicoutimi, Chicoutimi, Canada*, 2006, pp. 57-116.
- [79] M.B. Durdjevic, B. Duric, A. Mitrasinoniv, and J.H. Sokolowski, "Modeling of Casting Processes Parameters for the 3xx Series of Aluminum Alloys Using the Silicon Equivalency Algorithm," *Association of Metallurgical Engineers Serbia and Montenegro*, 2003, Vol. 9, No. 2, pp. 91-106.
- [80] J. Barresi, M.J. Kerr, H. Wang, and M.J. Couper, "Effect of Magnesium, Iron and Cooling Rate on Mechanical Properties of Al-7Si-Mg Foundry Alloys," *AFS Transactions*, 2000, Vol. 117, pp. 563-570.

- [81] C.H. Caceres, C.J. Davidson, J.R. Griffiths, and Q.G. Wang, "The Effect of Mg on the Microstructure and Mechanical Behavior of Al-Si-Mg Casting Alloys," *Metallurgical and Materials Transactions A*, 1999, Vol. 30A, pp. 2611-2618.
- [82] Q.G. Wang, "Microstructural Effects on the Tensile and Fracture Behavior of Aluminum Casting Alloys A356/357," *Metallurgical and Materials Transactions A*, 2003, Vol. 34A, pp. 2887-2899.
- [83] J.A. Taylor, D. H. StJohn, L. H. Zheng, G. A. Edwards, J. Barresi, and M.J. Couper, "Solution Treatment Effects in Al-Si-Mg Casting Alloys: Part 1 - Intermetallic Phases," *Aluminium Transactions*, 2001, Vol. 45, pp. 95-110.
- [84] T.O. Mbuya, B.O. Odera, and S.P. Ng'ang'a, "Influence of Iron on Castability and Properties of Aluminium Silicon Alloys: Literature Review," *International Journal of Cast Metals Research*, 2003, Vol. 16, No. 5, pp. 451-465.
- [85] J.A. Taylor, "The Effect of Iron in Al-Si Casting Alloys," 35th Australian Foundry Institute National Conference, Adelaide, South Australia, 31 Oct - 3 Nov 2004, pp. 148-157.
- [86] Q.G. Wang, "Solidification and Precipitation Behaviour of Al-Si-Mg Casting Alloys," *Journal of Materials Science*, Vol. 36, 2001, pp. 739-750.
- [87] M.A. Moustafa, C. Lepage, F.H. Samuel, and H.W. Doty, "Metallographic Observations on Phase Precipitation in Strontium-Modified Al-11.7% Si Alloys: Role of Alloying Elements," *International Journal of Cast Metals Research*, 2003, Vol. 15, pp. 609-626.
- [88] M.A. Moustafa, F.H. Samuel, and H.W. Doty, "Effect of Solution Heat Treatment and Additives on the Microstructure of Al-Si (A413.1) Automotive Alloys," *Journal of Materials Science*, Vol. 38, 2003, pp. 4507-4522.
- [89] M.A. Moustafa, F.H. Samuel, and H.W. Doty, "Effect of Solution Heat Treatment and Additives on the Hardness, Tensile Properties and Fracture Behaviour of Al-Si (A413.1) Automotive Alloys," *Journal of Materials Science*, Vol. 38, 2003, pp. 4523-4534.
- [90] M. Tash, F.H. Samuel, F. Mucciardi, and H.W. Doty, "Effect of Metallurgical Parameters on the Hardness and Microstructural Characterization of As-Cast and Heat-Treated 356 and 319 Aluminum Alloys," *Materials Science and Engineering A*, Vol. 443, 2007, pp. 185-201.
- [91] M. Tash, F.H. Samuel, F. Mucciardi, H.W. Doty, and S. Valtierra, "Experimental

- Correlation between Metallurgical Parameters and Hardness in Heat-Treated 319 Alloys: A Quantitative Study Using Factorial Analysis,” AFS Transactions, Vol. 114, 2006, pp. 6-14.
- [92] W. Reif, S. Yu, J. Dutkiewicz, R. Ciach, and J. Krol, “Pre-Aging of AlSiCuMg Alloys in Relation to Structure and Mechanical Properties,” *Materials and Design*, Vol. 18, No. 4, 1997, pp. 253-256.
- [93] R.K. Mishra, G.W. Smith, W.J. Baxter, A.K. Sachdev, and V. Franetovic, “The Sequence of Precipitation in 339 Aluminum Castings,” *Journal of Materials Science*, Vol. 36, No. 2, 2001, pp. 461-468.
- [94] S. Morin, “Effet du magnésium, des traitements thermiques et de la porosité sur les propriétés mécaniques de traction et de fatigue de l’alliage sous pression A380.1,” Master’s Thesis, Université du Québec à Chicoutimi, Chicoutimi, Canada, 2002, pp. 137-144.
- [95] B.L. Gabriel, “SEM: A User's Manual for Materials Science,” American Society for Metals, Metals Park, OH, 1985, p. 97.
- [96] The ASM Committee on Fractography by Electron Microscopy, “The Scanning Electron Microscope and Its Application to Fractography,” in *Metals Handbook*, 8th Edition, Vol. 9: Fractography and Atlas of Fractographs, American Society for Metals, Metals Park, OH, 1978, pp. 49-53.
- [97] W.W. Gerberich, “Microstructure and Fracture,” in *Metals Handbook*, 9th Edition, Vol. 8: Mechanical Testing, American Society for Metals, Metals Park, OH, 1985, pp. 476-491.
- [98] http://www.metallurgicalaluminium.com/Downloads/tech_paper_pdfs/Guide_Modif_AlSi_Alloys.pdf
- [99] M. Hafiz and T. Kobayashi, “Mechanical Properties of Modified and Non-modified Eutectic Al-Si Alloys,” *Journal of Japan Institute of Light Metals*, Vol. 44, No. 1, Jan. 1994, pp. 28-34.
- [100] M. Tsukuda, T. Suzuki, I. Fukui, and M. Harada, “Problems on Modification of Al-7%Si-0.8%Mg Alloy by Sb,” *Journal of Japan Institute of Light Metals*, Vol. 30, No. 2, 1980, pp. 65-71.
- [101] M.F. Hafiz, T. Kobayashi, and N. Fat-Halla, “Role of Microstructure in Relation to the Toughness of Hypoeutectic Al-Si Casting Alloy,” *Cast Metals*, Vol. 7, No. 2, pp. 103-111.
- [102] M. Tsukuda, M. Harada, T. Suzuki, and S. Koike, “The Effect of Si, Mg, Fe on the

- Mechanical Properties of Al-Si-Mg Alloys for Casting,” Journal of Japan Institute of Light Metals (in Japanese), Vol. 28, No. 3, 1978, pp. 109-115.
- [103] S. Nishi and T. Kobayashi, “A Study on the Toughness of Aluminum Alloy Castings,” Journal of the Japan Foundrymen’s Society (in Japanese), Vol. 46, No. 10, Oct. 1974, pp. 905-912.
- [104] Z. Ma, “Effect Fe-Intermetallics and Porosity on Tensile and Impact Properties of Al-Si-Cu and Al-Si-Mg Cast Alloys,” Ph.D. Thesis, Université du Québec à Chicoutimi, Chicoutimi, Canada, 2002, pp. 158-211.
- [105] F.J. Tavitas-Medrano, “Artificial Aging Treatment of 319-Type Aluminum Alloys,” Ph.D. Thesis, McGill University, Montreal, Canada, 2007, pp. 76-196.
- [106] N.R. Andrade-González, “Aging Effects in 319-Type Alloys,” Ph.D. Thesis, McGill University, Montreal, Canada, 2006, pp. 159-166.
- [107] N. Fat-Halla, “Structural Modification of Al-Si Eutectic Alloy by Sr and Its Effect on Tensile and Fracture Characteristics,” Journal of Materials Science, Vol. 24, 1989, pp. 2488-2492.
- [108] M. Hafiz and T. Kobayashi, “Fracture Toughness of Eutectic Al-Si Casting Alloy with Different Microstructural Features,” Journal of Materials Science, Vol. 31, 1996, pp. 6195-6200.
- [109] G. Mrówka-Nowotnik, “The Effect of Intermetallics on the Fracture Mechanism in AlSi1MgMn alloy,” Journal of Achievements in Materials and Manufacturing Engineering, Vol. 30, No. 1, 2008, pp. 35-42.
- [110] D.S. Jiang, T.S. Lui, and L.H. Chen, “Crack Propagation Behavior of A356 Aluminum Alloy under Resonant Vibration,” Scripta Materialia, Vol. 36, No. 1, 1997, pp. 15-20.
- [111] A. Thirugnanam, K. Sukumaran, U.T.S. Pillai, K. Raghukandan, and B.C. Pai, “Effect of Mg on the Fracture Characteristics of Cast Al-7Si-Mg Alloys,” Materials Science and Engineering A, Vol. 445-446, 2007, pp. 405-414.